(56)

DEVELOPMENT OF A POTENTIAL BIOARTIFICAL LIVER: SELECTIVE ADHESION OF HEPATOCYTES

by

Sangeeta N. Bhatia

B. Sc., Biomedical Engineering
Brown University, 1990

Submitted to the Department of Mechanical Engineering in Partial Fulfillment of the Requirements for the Degree of

Master of Science
in Mechanical Engineering
at the

Massachusetts Institute of Technology

June 1993

Signature of Author Signature redacted
Department of Mechanical Engineering
May 7, 1993

Certified by Signature redacted
Mehmet Toner
Thesis Supervisor

Certified by Signature redacted
Martin L. Yarmush
Thesis Supervisor

Accepted by Signature redacted
Ain. A. Sonin
Chairman, Department Graduate Committee

DEVELOPMENT OF A POTENTIAL BIOARTIFICIAL LIVER: SELECTIVE ADHESION OF HEPATOCYTES

by

Sangeeta Bhatia

Submitted to Department of Mechanical Engineering on May 7, 1993 in partial fulfillment of the requirements for the degree of Master of Science in Mechanical Engineering

ABSTRACT

Liver disease is the cause of death for 30,000 Americans every year. For those who suffer from acute liver failure, transplantation is rarely a viable option. Bioartificial liver devices address this problem by combining live cells, performing an array of liver-specific functions, with extracorporeal machinery. Most conventional approaches to bioartificial liver support suffer from two problems: (1) unstable culture configurations and (2) mass transport limitations. Micropatterning technology can hope to address both of these issues by sandwiching hepatocytes aligned in rows, to preserve phenotypic function. Rows of cells would alternate with hepatocyte-free areas, creating channels for fluid flow and an efficient transport system. To achieve this goal, hepatocytes must first be selectively adhered to a single, solid substrate.

The experimental portion of this study focused on obtaining reproducible, selective adhesion of hepatocytes on a glass substrate with large regions of adhesive and non-adhesive coatings . The 'banded', circular surfaces of 5 cm diameter were entirely non-adhesive except for a band of adhesive coating approximately 2 cm wide. Surface coatings of entirely adhesive or non-adhesive regions were first characterized for their hepatocyte-surface interaction after exposure to various aqueous solutions (bovine serum albumin, poly-L-lysine, and collagen type I). The adhesive surface has hydrophilic characteristics allowing adsorption of collagen molecules from an aqueous solution, and subsequent hepatocyte adhesion, whereas the non-adhesive surface has hydrophobic properties and remains hepatocyte-free. A reproducible processing technique for obtaining patterns of hepatocytes was developed and optimized. This was achieved by spin-coating an aqueous collagen type I solution [0.1 mg/ml] on a 'banded' surface at 500 rpm for 25 seconds. Finally, the morphology and long-term function of the hepatocytes in this configuration was assessed by overlaying the patterned hepatocytes with a top layer of collagen gel to mimic sandwich culture. The hepatocytes in the patterned configuration with a gel overlay were found to function as well as stable, differentiated sandwich cultures. The creation of micropatterns utilizing this technology can now be attempted.

The actual creation of a micropatterned flow chamber is dependent on some critical design criteria which can be explored through mathematical modeling. The oxygen distribution and viscous pressure drop were modeled along a typical microchannel. Furthermore, by limiting these parameters to *in vivo* values, an optimal channel length of 0.7 cm and a flow rate of 2.2×10^{-6} ml/s were obtained. These values are reasonable in terms of practical implementation.

Therefore, the creation of micropatterned flow device can now be attempted utilizing spin-coating for selective adhesion of hepatocytes to micropatterns and the results of the mathematical model to approximate design parameters.

Thesis supervisors:

Mehmet Toner, Ph.D.
Assistant Professor of Surgery (Bioengineering)
Massachusetts General Hospital and Harvard Medical School
Lecturer, Department of Mechanical Engineering
Massachusetts Institute of Technology

Martin L. Yarmush, M.D., Ph. D.
Professor of Chemical Engineering and Biochemical Engineering
Rutgers University

ACKNOWLEDGEMENTS

I would like to thank Dr. Mehmet Toner. He has been an inspiration to me in his ability to combine engineering with cell biology. I am grateful for all the time he spent with me, patiently coaching me in research, presentations, technical writing, and how to survive through qualifying exams. I am also grateful to Drs. Martin Yarmush and Ron Tompkins for their direction and support. Their expertise was invaluable.

Many thanks to Dr. Jim Brown for the time, effort, and expense he devoted to this project. In addition, I thank him for his patience with a novice in the world of surface chemistry.

I have enjoyed working with all the various members of our Surgical Research team. I would like to thank François Berthiaume, Inne Borel Rinkes, John Bischof, Brent Foy, Joe Horowitz, Howard Matthews, Avi Rotem, Peter Stefanovich, and Bill Thorpe for the many informative conversations as well as Yogesh Pancholi and Kristin Hendricks for their technical assistance and friendship.

Financial support came from the Department of Defense and Shriners's Burns Institute for Crippled Children.

Emotional support came from everywhere. I thank all of the Beantown crew, including Theresia Gouw who has recently migrated to the west coast, and the latest Canadian addition, Jagesh Shah. Finally, I thank my family for helping me keep things in perspective and for their love.

TABLE OF CONTENTS

NOMENCLATURE

A	cross-sectional area of channel [cm^2]
c	oxygen concentration [nmol / ml]
c_i	inlet oxygen concentration [nmol / ml]
$\hat{c}$	dimensionless concentration
D	diffusivity of oxygen in liquid [cm^2/s]
D_h	hydraulic diameter [cm]
h	channel height [cm]
k	solubility of oxygen in liquid [nmol/ ml/ mm Hg]
K_m	P_{O_2} at which half-maximal oxygen uptake rate occurs [mm Hg]
L	half channel width [cm]
L_c	channel length in axial direction [cm]
ρ	cell density [cells/cm^2]
P	mechanical pressure [mm Hg]
P_{O_2}	partial pressure of oxygen [mm Hg]
Q	volumetric flow rate [cm^3/s]
R	constant oxygen uptake rate [nmol/ ml / cm]
Re	Reynolds Number = $\frac{D_h u_m}{\nu}$
Sc	Schmidt Number = $\frac{\nu}{D}$
μ	viscosity [g/cm/s]
u	velocity [cm / s]
$\hat{u}$	dimensionless velocity
u_m	mean velocity [cm / s]
ν	kinematic viscosity [cm^2/s]

V oxygen uptake rate [nmol / s / 10^6 cells]

V_m maximal oxygen uptake rate [nmol / s / 10^6 cells]

w channel width [cm]

x axial coordinate [cm]

$\hat{x}$ dimensionless axial coordinate

y radial coordinate [cm]

$\hat{y}$ dimensionless radial coordinate

CHAPTER I

INTRODUCTION

1.1 Background

The liver has a variety of metabolic and anabolic functions: detoxification, aiding digestion, regulating blood clotting, protein synthesis, and regenerating its own damaged tissue. Failure of the liver is the eighth leading cause of disease-related death in the United States and is responsible for the deaths of 25,000 Americans annually. Those who suffer from acute liver failure confront an 80% mortality rate whereas those suffering from chronic liver failure face the third major cause of death between the ages of 25 and 59. The significant forms of liver disease include viral hepatitis, cirrhosis, gallstones, alcohol-related disorders, cancer of the liver, and more than 100 different types of liver disorders in children (Yarmush et al., 1992B).

Liver transplantation is currently the most effective treatment for liver failure. 7 out of 10 recipients survive the first year; however, organ scarcity is a major limitation. In 1991, approximately 3000 liver transplants were performed and it is estimated that 375 prospective recipients died while waiting for a transplant. Alternative treatments have been attempted utilizing a variety of biological, non-biological, and hybrid approaches. Hemodialysis, hemoperfusion, immobilized enzyme systems, and ion exchange resins have been employed by a number of investigators with limited beneficial results (Yarmush et al., 1992B). This mainly because non-biological approaches generally focus on only a few of the many liver functions. In contrast, biological approaches such as xenograft cross circulation, exchange transfusion, plasma exchange, and liver tissue hemoperfusion encounter another class of difficulties related to donor response, immunological reactions, and surgical complications. Clearly, the necessity of harnessing a full range of liver functions for patient support exists. To this end, a number of hybrid or bioartificial

approaches have been proposed. The potential solutions can be broadly classified as hepatocyte-based (i) transplantable and (ii) extracorporeal devices. A variety of approaches to hepatocyte transplantation have been developed. Cells have been directly injected in the liver or spleen (Matas et al., 1976, and Mito et al., 1978), microencapsulated (Dixit et al., 1990), or implanted on some support structure. These substrates include microcarriers (Demetriou et al., 1986B), and biodegradable polymers (Vacanti et al., 1988). Although these transplantable devices have had some success in animal models, the clinical applicability still faces the problems of immunological host response and transport limitations due to inadequate perfusion. Cyclosporin has eased the immunological problems at the expense of lifetime immunosuppression and a large financial burden. Even so, transplantation is unlikely to be a viable solution for acute liver failure patients. The livers of these patients are undergoing a regenerative process where the pace of regeneration cannot compete successfully with that of the injury. If the patients were sustained during this regenerative period, their own livers would fully regenerate thereby eliminating the necessity for any lifelong treatment. Therefore, the most viable alternative for these acute liver failure patients is temporary liver support using an hepatocyte-based extracorporeal device to sustain a full range of liver functions. In addition, this device would be useful as a bridge to transplantation for potential transplant recipients. Furthermore, 25 % of liver transplant recipients undergo post-surgical complications and require a second surgical procedure; these patients are also candidates for an extracorporeal device.

Extracorporeal devices confront a variety of obstacles which are discussed below in more detail. In particular, the hybrid device is most dependent on its cellular components and their performance. Therefore, stable, differentiated cell cultures are critical to the success of an extracorporeal bioartificial device.

1.2 Hepatocyte Culture

The development of an extracorporeal device requires a stable culture system. Hepatocytes, the most abundant cells in the liver, are responsible for a large portion of the liver-specific functions. They are, however, notoriously difficult to maintain *in vitro*. When cultured in monolayer cultures they dedifferentiate rapidly and lose adult liver phenotype within one week of isolation. The hepatocytes detach from the underlying substrate and die. To address this problem, investigators have developed a number of methods to sustain differentiated function of primary hepatocytes *in vitro*. One approach utilizes a matrix known as Matrigel, derived from Engelbroth-Holm-Swarm tumors, as an underlying substrate. This culture configuration induces the formation of spherical aggregates which maintain long-term liver functions (Bissell et al., 1987); however the introduction of tumor-derived compounds in a clinical setting is unacceptable. In addition, Matrigel is prohibitively expensive. Other nonadherent substrates also seem to produce multicellular spheroids with high liver-specific activity (Koide et al., 1990). The clinical applicability of the latter culture configuration is severely limited because the formation of these spheroids is completely reversed by the addition of serum to the culture. Other investigators have attempted to utilize hormonally-defined medium (Dich et al., 1988) and medium supplemented with high concentrations of dimethyl sulfoxide (Isom et al., 1985). Both of these approaches are severely limited in their applicability to extracorporeal devices by the potential toxic effects of systemic patient exposure to the components of the media. Yet another approach has included co-culture with a liver-derived epithelial cell line (Gugen-Guillouzo et al., 1983). Like Matrigel, it is unlikely to be practically implemented because of its tumorigenic origins.

Recently, in our laboratory, sandwich culture of a monolayer of hepatocytes between two layers of collagen gel, mimicking the *in vivo* environment of hepatocytes, have also been shown to preserve adult liver phenotypic functions *in vitro* (Dunn et al., 1991). The sandwich culture configuration is depicted in Figure 1.1. Hepatocytes *in vivo*

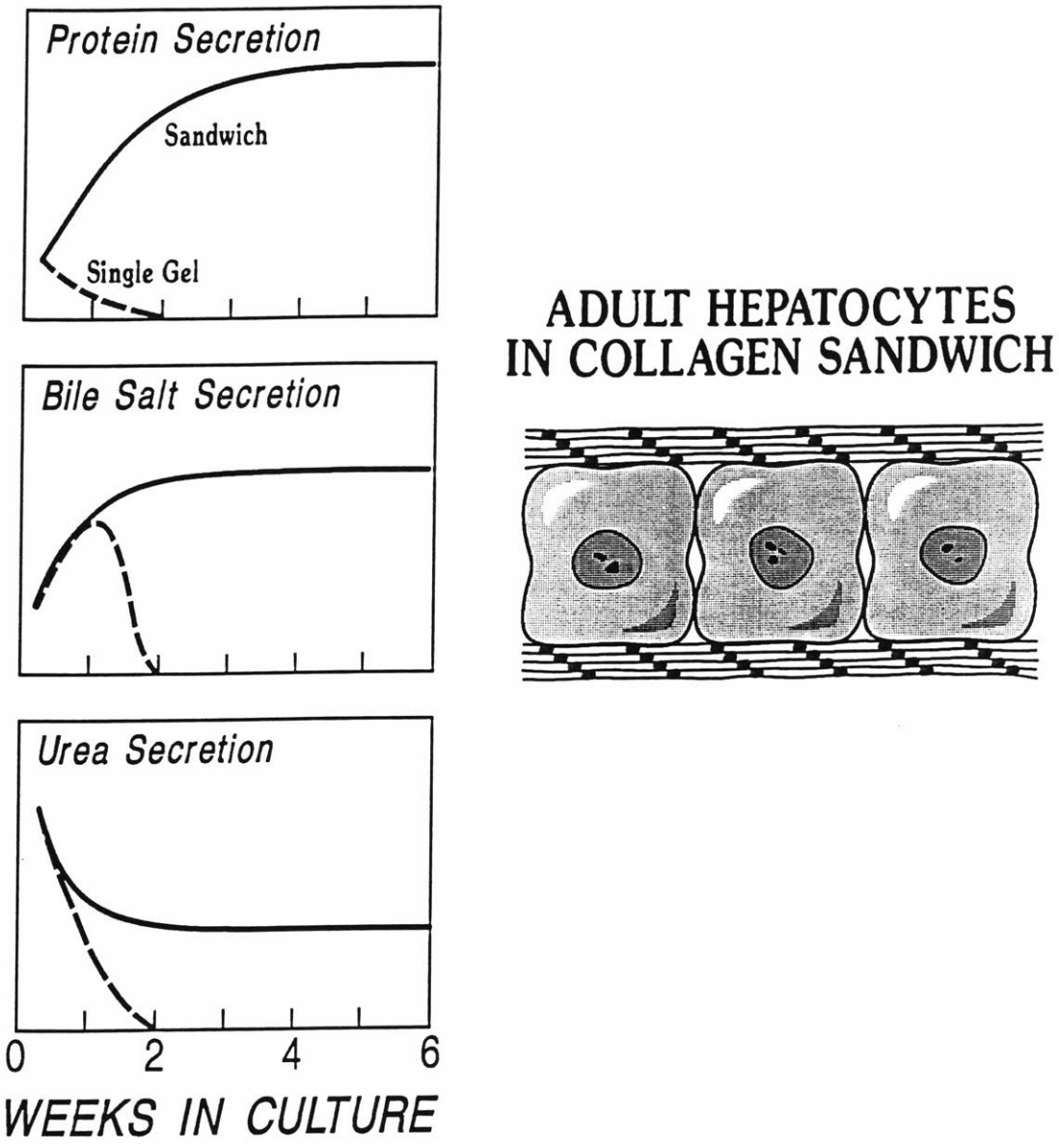

Figure 1.1. Hepatocytes cultured in collagen gel sandwich configuration. Schematic of typical protein secretion, bile salt secretion, and urea secretion stability as compared to cells cultured on single, underlying layers of collagen gel.

have a belt of apical (bile canilucular) surface that surrounds each cell and divides two basolateral (sinusoidal) surfaces, each of which is in contact with extracellular matrix (Yarmush et al., 1992A). The sandwich system introduces the normal cellular polarity *in vitro* and produces maintained differentiated function of the cells. Thus, the sandwich system provides a defined, non-tumoriginic, non-toxic, and relatively simple approach to the maintaining stable hepatocyte cultures for use in an extracorporeal bioartificial device. This culture configuration combined with an efficient mass exchanger could then provide the basis for the development of an extracorporeal bioartificial liver.

1.3 Conventional Approaches to Bioartificial Extracorporeal Liver Assist Devices

Not only does the development of a bioartificial device require a stable culture system, but efficient mass transport is also essential to its performance. In fact, the design of most bioartificial extracorporeal devices is focused on optimal configurations for exchange of nutrients and proteins. Because of the large metabolic requirements of the liver, specifically its oxygen uptake, and the low solubility of oxygen in liquids, mass transport limitations in bioartificial extracorporeal liver devices are especially critical. A variety of approaches have been taken to maximizing mass transport between hepatocytes, the functional unit of the liver, and the perfused liquid, including microcarriers, hollow fibers, monolayer cultures, and cell suspensions. Microcarriers are spherical support structures with dimensions on the order of 200 μm. Approximately 100 hepatocytes are attached to each microcarrier (Foy et al., 1993). Microcarriers also provide a large surface area in a relatively small volume and can be configured either in packed arrays or fluid beds. Packed arrays are hollow column shells filled with microcarriers, whereas fluid beds are created by fluidizing a bed of microcarriers with fluid flow from below. Hollow fibers, on the other hand, consist of a shell traversed by a large number of small diameter tubes. The cells may be placed within the fibers in the intraluminal space or on the shell side in the

Table 1.1A. *In Vitro* and Animal Studies Utilizing Extracorporeal Bioartificial Livers[a]

Author, yr	Reactor Configuration	Cell Source	Number of Cells	Dead Volume	Animal Model	Duration of culture	Perfusion Schedule	Control Experiment	In vitro Functions	In vivo Functions
Nyberg, '93	h.f. (100kD cutoff) contracted collagen gel intraluminal	rat	N/R	N/R	N/A	7 days	N/A	none	Vital dye (42%) FACS (66%) V (12-16 μmol/hr) albumin production(20 μg/h) insulin uptake (50μg/h) arginine, urea, orthinine prod. morphology	N/A
Rozga,'93 [b]	h.f. (0.2μm pore) collagen- coated microcarriers plasmapheresis extraluminal	dog cryopreserved	60×10^6	5 ml	dog end-to-side portocaval shunt	none	6-h	without hepatocytes porcine hepatocytes	trypan blue (90%) after cryopreservation (80%) increased cyclosporine metabolites	reduced ammonia, lactate LDH increased blood pressure
Sussman, '92	h.f. (70kD cutoff) extraluminal	C3A human-derived cell line	$15\text{-}40 \times 10^9$ [c]	N/R	dog acetominophen	3-4 wk	42-48 h	none	none	reduced prothrombin time, to normal human albumin accumul. (0.5 - 6 g/ml/h)
Shatford, '92	h.f. (100D cutoff) contracted collagen gel intraluminal	rat	50×10^6	N/R	N/A	7 days	N/A	without hepatocytes	V (0.09 nmol/10^6 cells/s) albumin production (0.6 μg/10^6 cells/h) amino acid clearance lidocaine clearance (0.74 pg/cell/h)	N/A
Takahashi, '92	cultured monolayers collagen coated plates	pig	500×10^6	200 ml	anhepatic rabbit	1-7 days	15-36 h	none without hepatocytes	trypan blue (>90%) gluconeogenesis (6 - 10μg/ 10^6 cells/ h) urea synthesis (1 μg/ 10^6 cells/ h) ammonia removal (2.3 μg/ 10^6 cells/h)	survival time (24.5 vs 15.5 h)

[a] h.f. = hollow fiber; N/R = not reported; N/A = not applicable, V= oxygen uptake rate

[b] Demetriou, 1986A

[c] 200 g ; assuming (10-13 $\times 10^9$ g/ cell) or cell diamerter 20 μm and ρ= 1.4 g/ml

Shnyra, '91 Shnyra, '90	microcarrier fibronectin-coated packed column pre-oxygenated with perfluorodecalin	rat	50×10^6	1.6 ml [d]	rat D-galactosamine	1-5 days	3-h	without hepatocytes	trypan blue (80%) albumin production (4-5 μg/10^6 cells/h) bilirubin	survival (60% vs 5%) decreased GOT, GPT, bilirubin
Yanagi, '89	rotating disks cells embedded in alginate hydrogel with DMSO no plasmapheresis	rat, rabbit	1.7×10^9	80 ml	cat portojugular shunt, ligation of hepatic artery	none	4-h	without hepatocytes	trypan blue (20-50%) ammonium removal urea synthesis	ammonium removal
Arnaout, '90	h.f. (0.2 μm pore) collagen-coated microcarriers extraluminal	rat [e] cryopreserved	$30\text{-}40 \times 10^6$	7 ml	Gunn rat	none	3-4 h	without hepatocytes	trypan blue (30-85%)	conjugation of 5 μM bilurubin
Uchino, '88	cultured monolayers collagen-coated borosilicate multiplated plasmapheresis	dog	6×10^9 [f]	not reported	anhepatic dog	1-14 days	24-65 h	no treatment without hepatocytes	glyconeogenesis (110 ng/ug DNA/min) urea synthesis (3.6 ng/ug DNA/min) albumin production (0.12 or 1.2 μg/10^6 cells/h) ammonia removal	survival (55 vs 27.8h) albumin decline reduced ammonia normal bilirubin maintained at amino acids not elevated decreased bleeding
Demetriou, '86	microcarriers (packed column) collagen coated	rat cryopreserved	160×10^6	10 ml	N/A	none	N/A	N/A	trypan blue (55-60%) increased ratio of conjugated/ unconjugated bilirubin albumin production	N/A
Jauregui, '84	h.f. (50 kD cutoff) collagen-coated extraluminal	rat	not reported	N/A	N/A	1-18 days	N/A	N/A	LDH leakage glucose uptake total protein (30% drop) P450	N/A

[d] 40% of 4 ml column volume
[e] Demetriou et al., 1986A
[f] approximately 80 g

Kasai, '84	h.f. (40 kD cutoff) hepatocyte suspensions plasmapheresis	dog	21×10^9 [g] (viable cells)	not reported	dog D-galactosamine	none	1-h on, 1-h off 6-h total	none	trypan blue (85-60%) ammonia removal BUN production (2.15μg/10^6 cells/h) [h] glucose production (36.8 μg/g 10^6 cells/h)	ammonia removal. 0.083 pg/ 10^6 cells/h BUN maintenance glucose maintenance
Hager, '83	h.f. (50 kD cutoff) extraluminal	mice	10×10^6	N/R	N/A	1-58 days	N/A	N/A	protein synthesis (0.23 mg/ml/day) urea accumulation deamination of cytidine	N/A
Shatford, '91	h.f.; 100 kD cutoff contracted collagen gel	rat	38×10^6	N/R	N/A	1-6 days	N/A	none	V (0.09 - 0.03 nmol / 10^6 cells/s) Albumin production (0.28 - 0.45 μg /10^6 cells/h) lidocaine clearance (1 pg/cell/h)	N/A
Hager, '78	h.f. (50 kD cutoff) extraluminal	neonatal mice	N/R	N/R	N/A	6-8 wks	N/A	none	diazepam metabolism uridine (65.9 pM/h) urea (increased 13% in 15 days)	N/A
Olumide, '77	dialysis against hepatocyte suspension (5-10 kD cutoff)	pig	N/R	N/R	anhepatic pig	none	2- 4h	without hepatocytes	trypan blue (95-100%) pyruvate metabolism: (decreased 70% in 1 h) V (0.25-0.01 ml/g of liver/min)	survival (34.8 vs 35 h) lightened coma glucose maintenance BUN decrease (2.4 mg % in 36 h) bilirubin conjugation
Wolf, '75	h.f. (30-50 kD cutoff) extraluminal	hepatoma Reuben-H4-II-E	$10 - 15 \times 10^6$	N/R	Gunn rat	1-43 days	N/R	none	conjugated bilirubin total bilirubin glucosen consumption LDH, GOT, GTP accumulation	bilirubin conjugation

[g] approximately 40 g

[h] assuming 10×10^{-9} g/cell and therefore 100 million cells /g

Table 1.1B. Clinical Findings from the Utilization of Extracorporeal Bioartificial Livers

Author, year	Reactor Configuration	Cell Source	Number of Cells	Dead Volume	Duration of culture	Treatment Schedule	Control Experiment	Findings
Neuzil, '93	h.f. (0.2μm pore) collagen-coated microcarriers extraluminal	pig cryopreserved	1×10^9	N/R	none	6-h	none	increased mental status after 2 h; began to deteriorate 12 h post support patient's liver function and mental status improved over 3 weeks and patient received orthotopic liver transplantation after 6 mo. ammonia (120 to 32 μM/L) increased clotting factors; oozing recurred 15 h post support twofold increase in most amino acids Porcine hepatocyte viability post support(90%)
Sussman, '92	h.f.	C3A-human derived cell line	$15\text{-}40 \times 10^9$ [i]	N/R	3-4 wk	144-h new cartridge every 5-36 h	none	increased mental status in 1 h patient died 132 h post support decreased bilirubin (20 mg/dL) decreased alkaline phophatase increased α-fetoprotein demonstrates recovery of native liver function
Margulis, '89	hemoperfusion through a cell suspension with actived charcoal	porcine	N/R	20 ml	none	1-h per cartridge, 6-h total	67 patients (30 in coma, 37 in precoma) treated with commonly used curative measures	59 patients (20 in coma , 39 in precoma) survival (63% vs 41%) coma lightened free bilirubin decreased 45.5% ammonium decreased 50.3% EEG increased in normalcy
Matsumara,'87	hemodialysis against cell suspension plasmapheresis	rabbit cryopreserved	10×10^9	325 ml	none	5.2-h on , 2 days off, 4.5-h on	heat-deactivated control	mentation, appetite returned patient discharged decreased bilirubin (25 to 16.8 mg/dL) morphology nonpolygonal in vitro (urea synthesis, lactate to glucose conversion)

[i] 200 g ; assuming $(10\text{-}13 \times 10^9$ g/ cell) or d=20 μm and ρ= 1.4 g/ml

extraluminal compartment and transport takes place through the membrane of each fiber (Berthiaume et al., 1993). In addition, some investigators have coated the fibers to promote hepatocyte attachment or pre-attached cells to microcarriers which were subsequently inserted in a hollow fiber device. Table 1.1 displays the range of bioartificial extracorporeal devices that have been reported. Table 1.1A summarizes *in vitro* and animal studies whereas Table 1.1B contains clinical data.

Two classes of limitations become apparent in the examination of Table 1.1A: transport issues and problems with culture stability. Hollow fiber devices, are prone to transport limitations because of the relatively large distance between the perfused fluid and the peripheral cells. In addition, the interfiber distance is difficult to control, creating variations in transport distance, thereby limiting the efficiency of extraluminal seeded devices. Studies by Nyberg et al. (1993) and Wolf et al. (1975) have included data indicating necrotic cell masses. Microcarriers, in contrast, suffer from transport limitations in their scale-up. The two studies which utilized packed columns have a small cell number of 50- 160 $\times 10^6$ (Shnyra et al., 1991 and Demetriou et al., 1986B). The scale-up of these devices will be hampered by transport limitations as the column height increases. All nutrients being provided at the entrance must traverse the entire device. If one increases the flow rate to ameliorate this problem, packed bed configurations generate large shear stresses associated with a greater fluid velocity through small pathways. Furthermore, the amount by which the column diameter can be increased to reduce the fluid velocity, has a practical upper limit in relation to the column height. In fact, the aspect ratio (height/diameter) is limited to 1:1 by the practicality of evenly distributing the liquid over the entire column cross section (Berthiaume et al., 1993). Other bioreactor configurations, such as vertical disks rotating in a bath of fluid, face limitations from the low hepatocyte viability and the dissolution of the embedding gel (Yanagi et al., 1989). Finally, monolayer culture configurations necessitate a large dead volume which is clinically impractical (Takahashi et al., 1992).

Table 1.1A also elucidates a number of problems with the stability of hepatocyte cultures in these devices. All investigators who measure cell viability in primary hepatocyte systems found cultures were stable for less than 7 days. Hepatocyte suspensions, in fact, fair even worse with a cell viability on the order of hours. Furthermore, some investigators utilized freshly thawed, cryopreserved, primary hepatocytes even though other studies indicate that cryopreserved hepatocytes to not regain stable, differentiated function for several days while the cells recover from freezing stresses (Borel Rinkes et al., 1992). Finally, the device which included a C3A human-derived cell line is difficult to assess (Sussman et al., 1992). This device may potentially have problems due to the utilization of transformed cells, cell growth, or maintenance of liver-specific functions.

The aforementioned transport and culture stability limitations have hindered the progress of any large scale clinical trials. A few studies have been reported as seen in Table 1.1B. The primary effect of the extracorporeal bioartificial devices was an increase in mental status in the treated patients with a drop in serum ammonia and bilirubin concentrations. The treatments are difficult to assess because of the general lack of any controlled studies. One study did compare hemoperfusion through a cell suspension with active charcoal in addition to conventional acute liver failure treatment as compared to acute liver failure treatment alone (Margulis et al., 1989). They found a 63% survival rate as compared to a 41% survival rate in the controlled group. On closer inspection of the data, it should be noted that only 33% of the hemoperfused group were initially comatose whereas 45% of the conventionally treated group were already comatose, therefore, the margin of increased survival with hemoperfusion through a cell suspension may be effectively decreased.

In general, it is obvious that the current bioartificial extracorporeal liver support devices suffer from transport and culture stability limitations. These problems can perhaps be addressed by a new application of micropatterning technology.

1.4 Micropatterning

Micropatterning techniques rely on creating surfaces with selective adhesiveness on which cells can be organized into microstructures. This technology may also be used in designing a bioartificial liver system which mimics the sandwich culture configuration (Figure 1.1) as well as the efficient transport properties of the liver. A liver lobule, the functional unit of the liver is shown schematically in Figure 1.2. Cells are aligned in rows and stacked vertically in plate-like structures. The blood flows along the sinusoids, on both sides of the hepatocytes, where it comes in contact with the cells and mass exchange takes place. Figure 1.3 shows a schematic of a micropatterning approach to mimicking the liver geometry in hopes of preserving differentiated cell function and facilitating mass transfer between the perfused fluid and the hepatocytes. This figure depicts hepatocytes aligned in rows with dimensions on the order of 50-200 μm. These micropatterned hepatocytes are sandwiched between two layers of collagen and perfused on both sides by fluid flow through the microchannels. Rows of hepatocytes, in the sandwich configuration, alternate with channels of fluid flow allowing for efficient mass transfer and preservation of differentiated function. The sites to which the hepatocytes adhere may be a biocompatible, adhesive surface (AS), whereas the hepatocyte-free sites for fluid flow may be created using some non-adhering surface (NAS). Creation of such a micropatterned device in the sandwich configuration will requires selective adhesion of hepatocytes on a single underlying substrate.

Although there have been no attempts to use selective adhesion to create a liver support device, investigators have been interested in the ordered arrays of cells *in vitro* for a variety of reasons: tumor invasion, wound healing, embryogenesis, mechanisms of cell locomotion and orientation, synapse formation and the creation of bioelectric circuits in culture. Weiss (1945), seeking to find support for his theory of contact guidance, first

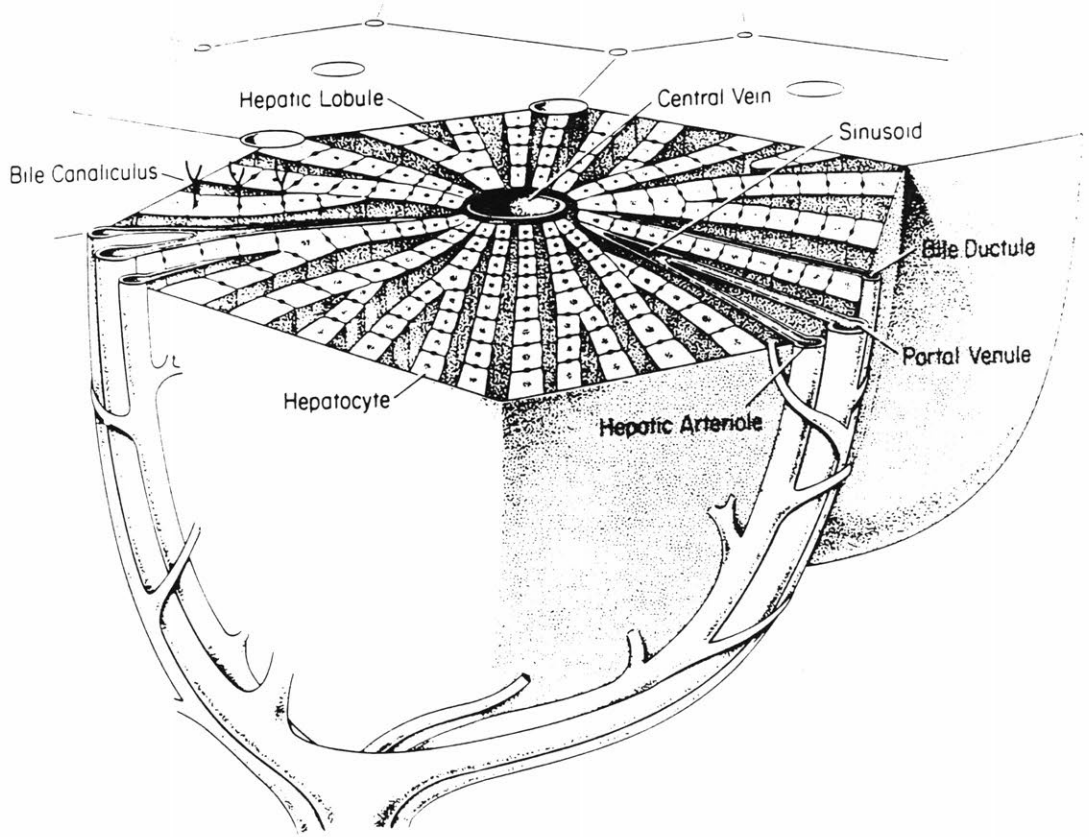

Figure 1.2. Schematic of the liver lobule. Blood flows inward from the portal triad (i.e. portal venule, hepatic arteriole, and bile ductule) along the sinusoid and to the central vein (Yarmush et al., 1992B).

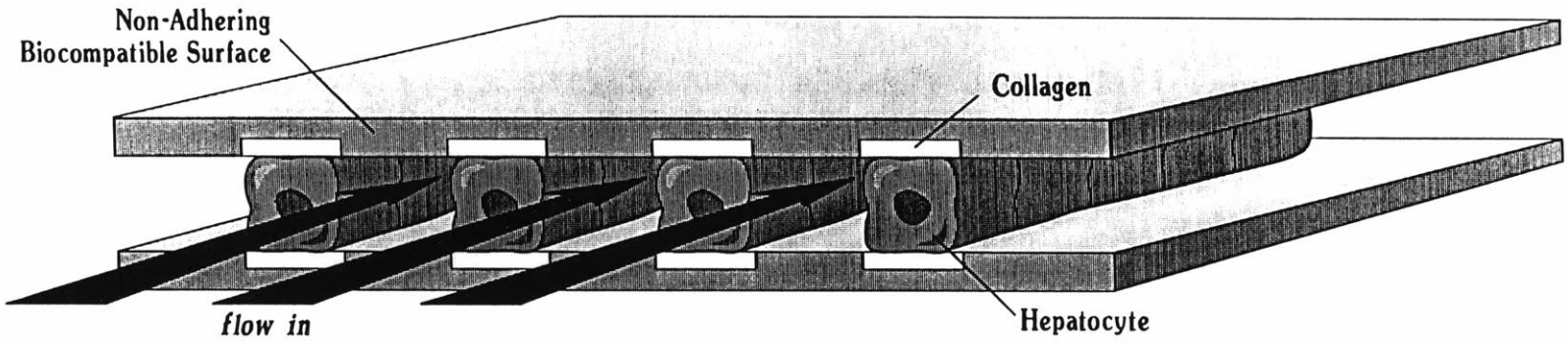

Figure 1.3. Schematic of a hypothetical micropatterned device. Hepatocytes are sandwiched and aligned along a collagen-coated adhesive surface in alternating rows. The intermediate rows are composed of a non-adhesive, biocompatible surface and are perfused with fluid.

plated a suspension of cells on a glass substrate ruled with fine parallel grooves. Later, Carter (1965) coined the term haptotaxis [1] to describe passive cell movement directed by the relative strength of its peripheral adhesions. Since then many studies have reported different types of cellular patterning (see Table 1.2). Most recently, with the advent of photolithography, a number of groups have published results indicating selective adhesion of cells can be obtained on the order of 20 to 150 μm. Britland et al. (1992B) describe patterning of Baby Hamster Kidney (BHK) cells whereas Stenger et al. (1992) demonstrate the selective adhesion of porcine aortic endothelial cells and fetal rat hippocampal neurons directly to a photochemically modified substrate. In contrast, Matsuda et al. (1992) achieved selective adhesion of rat-derived PC-12 cells and neuroblastoma C6 glial cells to a collagen treated substrate. None of these studies examined the toxic effects of the surfaces or the function of the adhered cells over time. Furthermore, none of these studies utilized selective adhesion for potential use in a bioreactor configuration.

1.5 Scope of This Study

Our overall goal is to create the micropatterned device shown in Figure 1.3. for use in bioartificial liver development. The critical experimental parameter in obtaining this goal is the creation of ordered arrays of hepatocytes. Thus, the specific aim of this study was to obtain selective adhesion of hepatocytes to a single substrate with the ultimate goal of creating a micropattern. The critical design parameters for the construction of the device can be approximated by mathematical modeling of the oxygen distribution and viscous pressure drop along the channels.

The experimental portion of the study utilized collagen as an adhesive molecule. As an abundant component of the extracellular matrix, it is known to promote

[1]Greek: haptein, to fasten; taxis, arrangement

Table 1.2. Studies Utilizing Cellular Patterning[a]

Investigator, year	Application	Material	Pattern	Resolution [μm]	Cells
Aizawa, '92	bioelectric circuits	indium tin oxide, glass	lines	not reported	neuron like PC-12
Stenger, '92	range	organosilanes	lines outlined polygons	W,τ = 100 W=1-20 τ = 200	porcine endothelial rat hippocampal
Matsuda, '92	neurocircuits	copolymer with collagen	outlined hexagons	not reported	neuron like PC-12
Britland, '92A,B	biosensors	depostition of bioactive peptides	lines	W=1-2 τ= 1-2	baby hamster kidney
Baier, '92	retinal nerve cell guidance in development	glyco-protein suspensions,glass	lines	W=90	embryonic chick retinal nerve cells
Corey, '91	synapse formation	polylysine, glass	lines	W=3-10 τ = 80-160	hippocampal neurons
Matsuda, '90	neurocircuits	copolymer with phenylazide	lines	W=20-200	bovine endothelial
Hammarback, '88	contact guidance and density	laminin, fibronectin	lines	W= 7-10	range
Klebe, '88	deposition of fibronectin	collagen fibronectin, agar	letters	W=25-100	fibroblasts
Kleinfeld, '88	cytoarchitecture and elect. activity of nerv. tissue	silane derivatives-quartz	squares grids	W=50-100 τ = 50-100	mouse spinal and rat cerebellar
Ireland, '87	limiting spreading and intercellular contact	poly (HEMA)- Palladium	circles	D= 22.5- 80	fibroblasts
Dow, '87	alignment, electron microlithography	glass	step grooves spirals	range >0.3	baby hamster kidney, chick myocytes
Gundersen, '87	biological substrata	IV collagen, laminin, fibronectin	circles	D= 300	dorsal root ganglia
Dunn, '86	migration and orientation	quartz	lines	W=1-9 τ =3-32	chick heart fibroblasts
Brunette, '86	dentistry	silicone	lines	D= 5-92 W=36-162	human gingivial fibroblasts
Hammarback, '86	guidepost theory	agarose-albumin, laminin	squares lines	D=100 W=40-50	dorsal root ganglia
Gundersen, '85	growth cone age and guidance	adsorbed NGF on collagen	circles	300	dorsal root ganglia
Hammarback, '85	neurite outgrowth	laminin	lines	W=1	dorsal root ganglia
Turner, '83	fibronectin	fibronectin, urea, glass	fibrils of fibronectin	W=0.7-8 τ = 5-10	range
Dunn, '82	contact guidance	cell. acetate-glass	lines	W=10-50	chick heart fibroblasts
Albrecht-Buehler, '79	immune response, cancer, development	gold, albumin, glass	lines	W=17	3T3 fibroblasts
Cooper , '76	synapses in culture	silicon monoxide	radial lines	W=40	mouse clonal neuroblastoma
Letourneau, '75	embryogenesis	collagen, polystyrene, Palladium	squares lines	D=80 W=30	chick embryo
Harris, '73	locomotion	cell. acet- Palladium, glass	squares, lines	D=50-85 W=33	range
Rovensky, '71	locomotion / orientation	PVC, nickel	circles	D=5-65 W=100-200	fibroblasts
Carter, '67	cytokinesis	cellulose acetate- Palladium	squares	100-400	mouse fibroblasts
Carter, '65	cancer/ contact inhib	cellulose acetate- Palladium	lines	not reported	mouse fibroblasts
Weiss, '45	contact guidance	glass. mica	lines	not reported	rat Schwann cells

[a] W = width of line, D = diameter of circle or width of square, τ = spatial frequency

differentiated function of hepatocytes. Surface coatings with adhesive and non-adhesive properties after exposure to an aqueous collagen solution were characterized for their hepatocyte-surface interaction. The adhesive surface (AS) has hydrophilic characteristics allowing adsorption of collagen molecules from an aqueous solution, and subsequent hepatocyte adhesion, whereas the non-adhesive surface (NAS) has hydrophobic properties and remains hepatocyte-free. Furthermore, the combination of AS and NAS results in preliminary patterns on a large grid with dimensions on the order of centimeters. A reproducible processing technique for obtaining these patterns was developed and optimized. The selective adhesion was shown to correlate with preferential protein deposition on the AS. Finally, the morphology and long-term function of hepatocytes was assessed by overlaying the patterned hepatocytes with a top layer of collagen gel to mimic sandwich culture. They were found to be normal as compared to stable, differentiated sandwich cultures.

The modeling portion of this work provided optimal channel lengths and associated flow rates for a typical microchannel in the hypothetical micropatterned device. The creation of a micropatterned flow chamber can now be attempted: first, by the application of the selective adhesion process to micropatterns on a single substrate, and then by the design and construction of a sandwich-type device.

CHAPTER II

SELECTIVE ADHESION OF HEPATOCYTES

2.1 Introduction

The experimental portion of this study was directed towards obtaining reproducible, selective adhesion of hepatocytes to a solid substrate. This approach will ultimately be applied to the design and construction of a microchannel device, as described previously. The microchannel device will potentially have application as an extracorporeal bioartificial liver.

The theory behind achieving the selective adhesion of hepatocytes is based upon the process depicted in Figure 2.1. Polymer coated glass substrates are exposed to a collagen solution. The polymer coatings have differential wettability. The wettable, hydrophilic coating has a small contact angle whereas the non-wettable, hydrophobic coating has a much larger contact angle. Exposing these coatings to a water-based collagen type I solution causes wetting and subsequent deposition of collagen molecules on the hydrophilic surface whereas the hydrophobic surface remains bare. Collagen, known to be an adhesive molecule with corresponding integrin receptors on the cell surface, causes hepatocytes seeded on the two individual surfaces to preferentially adhere to the collagen-coated surface.

Combining the hydrophobic and hydrophilic coatings onto a patterned grid on the same glass substrate would create the base of a microchannel device. The patterned substrate can be manufactured by standard photolithographical techniques. The surface is then treated with a collagen solution and seeded with hepatocytes. Subsequent agitation of the hepatocyte-substrate complex causes removal of any loosely bound hepatocytes from the hydrophobic coating while hepatocytes remain adhered to the collagen-coated,

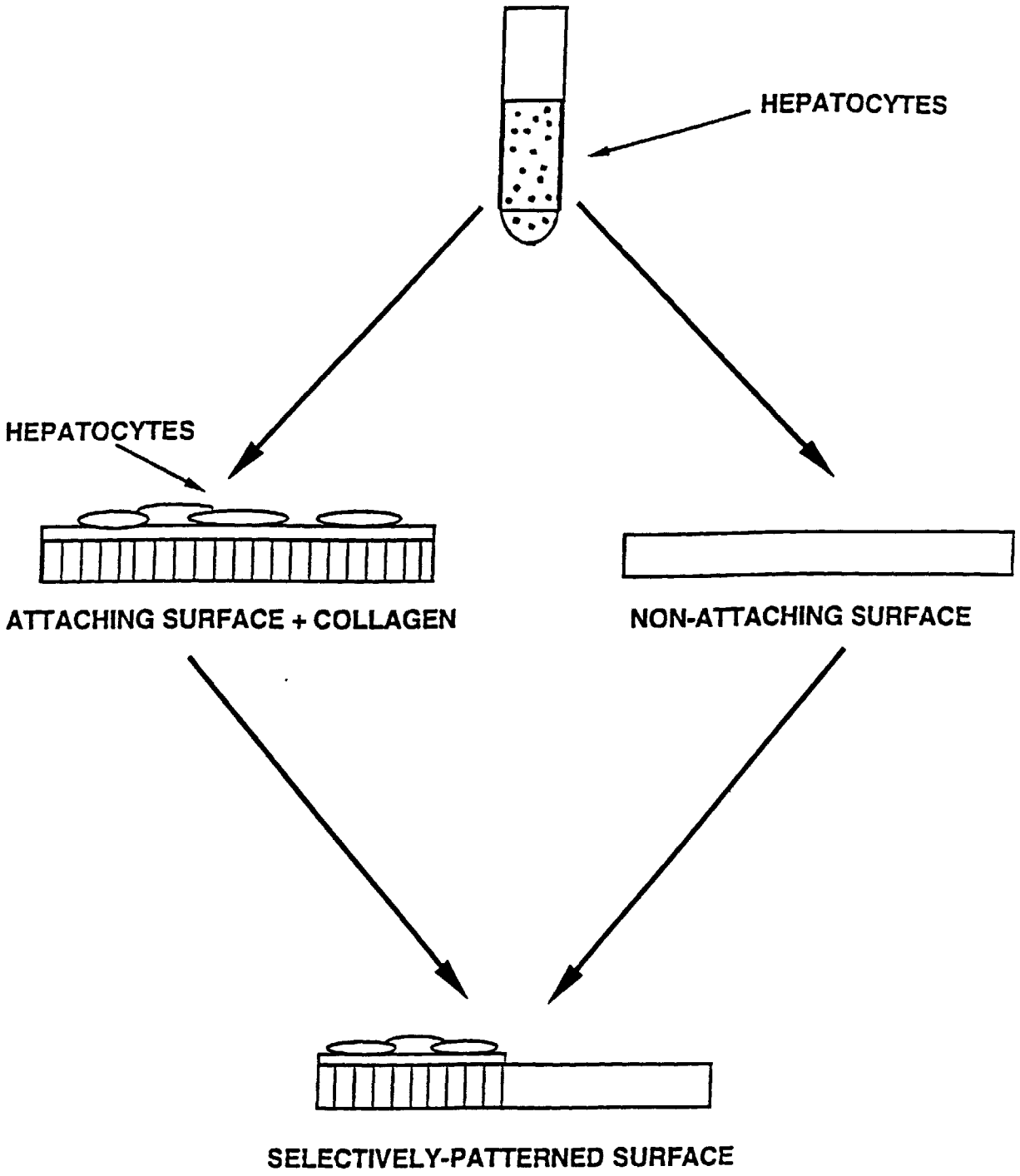

Figure 2.1. Schematic of selective adhesion of hepatocytes.

hydrophilic polymer regions. Finally, the patterned base of the microchannel device is obtained with hepatocytes aligned in regular, alternating rows.

This study focused on the characterization and optimization of selective adhesion of hepatocytes on a *large*-scale pattern of the two coatings prior to applying the technology to smaller 'micropatterns'. Specifically, attachment efficiency, spreading and toxicity were investigated on individual surfaces. A reproducible process was developed and optimized for obtaining selective adhesion on a large grid substrate. Finally, differentiated, sustained function of hepatocytes in the selectively adhered configuration was demonstrated.

2.2 Materials and Methods

2.2.1 Preparation of Hepatocytes

Hepatocytes were isolated from 2-3 month-old female Lewis rats (Charles River, MA), weighing 180-220 g, by a modified procedure of Seglen (1976) and as described in detail elsewhere (Dunn et al, 1991). Figure 2.2 depicts a schematic diagram of the procedure used for isolating rat hepatocytes. Animals were anesthetized in a chamber containing saturated ether. The liver, weighing 7-8 g, was first perfused through the portal vein in situ with 400 mL of perfusion buffer with 1mM ethylenediaminetetraacetic acid (EDTA) at 45 mL/min. Perfusion buffer is 154 mM sodium chloride, 5.6 mM potassium, 5.5 mM glucose, 25 mM sodium bicarbonate, and 20 mM N-(2-hydroxyethyl)piperazine-N'-2-ethanesulfonic acid (Hepes), pH 7.4 (see Figure 2.2A).[1] The perfusate was equilibrated with 5 L/min 95% O_2 and 5% CO_2 through 5 m of silicone tubing (inner diameter 0.058 in., outer diameter 0.077 in.) and was maintained by a 100-mm heat exchanger (reflux

[1]Unless specified, chemicals were purchased from Sigma (St. Louis, MO), Aldrich (Milwaukee, WI), EM Science (Gibbstown, NJ), JT Baker (Phillipsburg, NJ), and Mallinckrodt (Paris, KY).

A

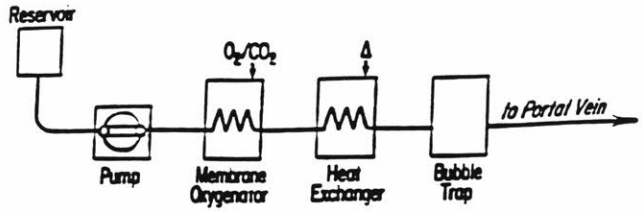

B

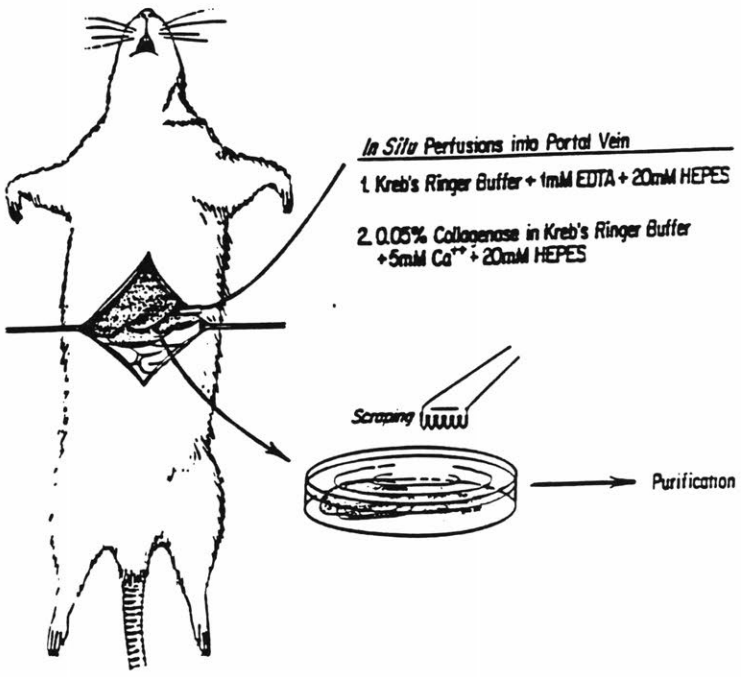

Figure 2.2. Procedure for hepatocyte isolation A. In vivo perfusion B. In vitro isolation

condenser 283000, Kontes, Vineland, NJ) at 37 °C before entering the liver. The liver was subsequently perfused with 200 mL of 0.05% type IV collagenase (Sigma) in perfusion buffer with 5 mM calcium chloride at the same flow rate. During this time, the liver swelled to about twice the original size. The swollen liver was dissected away from ligaments and the diaphragm and was transferred to a 100-mm dish with 20 mL of ice-cold perfusion buffer (see Figure 2.2B). The liver capsule was teased apart, and the resulting cell suspension was filtered through two nylon meshes with grid sizes 250 and 62 μm (Small Parts, Miami, FL). The cell pellet was collected by centrifugation at 50*g* for 5 min.

Cells were further purified by a modified procedure of Kreamer et al. (1986). The cell pellet was resuspended to 50 mL, and 12.5 mL of cell suspension was added to 10.8 mL of Percoll (Pharmacia, Piscataway, NJ) and 1.2 mL of 10x HBSS. Hanks' balanced salt solution (1X HBSS) is 138 mM sodium chloride, 5.4 mM potassium chloride, 0.33 mM sodium phosphate, 0.33 mM potassium phosphate, 0.8 mM magnesium sulfate, and 5.6 mM glucose, pH 7.4. The mixture was centrifuged at 500*g* for 5 min, and the cell pellet was washed twice with Dulbecco's modified Eagle's medium (DMEM) with 4.5 g/L glucose (Gibco, Grand Island, NY). Routinely, 200-300 million cells were isolated with viability between 92% and 99% as judged by trypan blue exclusion. Nonparenchymal cells, as judged by their size (less than 10μm in diameter) and morphology (nonpolygonal or stellate), were less than 1%.

2.2.2 Preparation of Rat Tail Collagen

Type I collagen was prepared from Lewis rat tail tendons by a modified procedure of Elsdale and Bard (1972). Four tendons were dissected from each rat tail and stirred in 200 mL of 3% (v/v) acetic acid overnight at 4°C. The solution was filtered through four layers of cheesecloth and centrifuged at 12000*g* for 2 h. The supernatant was precipitated with 40 mL of 30% (w/v) sodium chloride, and the pellet was collected by centrifugation at 4000*g* for 30 min. The pellet was dissolved in 50 mL of 0.6% (v/v) acetic acid, and the

solution was dialyzed against 500 mL of 1mM hydrochloric acid five times. For sterilization, 0.15 mL of chloroform was added to the solution. The solution was stirred for 2 days loosely capped to allow evaporation of chloroform. A 5-mL aliquot was lyophilized and weighed to determine the yield of collagen. Generally 100 mg was isolated per rat tail. This preparation yields type I collagen molecules mostly in its native, not cross-linked, triple-helical form (Elsdale and Bard, 1972).

2.2.3 Hepatocyte Culture

Hepatocyte culture was performed on a variety of collagenous and non-collagenous substrates. Standard single gel refers to a gel consisting of 9 parts collagen solution at 1.11 mg/ml, and 1 part 10X DMEM, pH 7.4, chilled on ice, mixed just prior to use. Collagen forms a gel at physiological pH and ionic strength at room temperature, but the rate of gelation is accelerated at higher temperature. Standard sandwich culture utilizes an overlay of the same collagen gel solution on top of the hepatocytes.

Some collagen gels were formed without the use of DMEM. Gels were formed by utilizing a salt solution consisting of six times the inorganic salt concentration found in DMEM. This salt solution had the following composition: 5.5 mM sodium phosphate, 10.8 mM calcium chloride, 4.9 mM magnesium sulfate, 32.3 mM potassium chloride, 0.264 M sodium bicarbonate, and 0.657 M sodium chloride brought to pH 7.4. Dilute collagen gels of 0.5 mg/ml collagen (1/2 as concentrated as standard collagen gel) were formed by mixing 5 parts of 1.11 mg/ml collagen gel solution, 3.3 parts of distilled deionized water, and 1.67 parts of the salt solution. Collagen gels of higher concentrations (i.e., greater than standard gel concentration) were prepared by lyophilizing 40 mL of 1.11 mg/mL collagen gel solution in a FTS Systems lyophilizer (Model FD-3-55A-MP, Stone Ridge, NY). The collagen was weighed and dissolved in 10 mL of 1mM hydrochloric acid to obtain a highly concentrated stock solution of 4 mg/ml. This stock

solution was then used in conjunction with 1.67 parts salt solution and distilled deionized water to obtain intermediate collagen gel concentrations.

Collagen gels were applied by distributing 1 mL of the appropriate collagen gel solution evenly over a 60-mm tissue culture dish (Falcon, Lincoln park, NJ) and incubated at 37°C at least 1 h before use. Two million viable cells were seeded in 2 mL of medium, consisting of DMEM supplemented with 10% (v/v) fetal bovine serum (Hazleton, Lenexa, KS), 0.5 unit/mL insulin (Squibb, Princeton, NJ), 7 ng/mL glucagon (Lilly, Indianapolis, IN), 20 ng/mL epidermal growth factor (Collaborative Research, Bedford, MA), 7.5 μg/mL hydrocortisone (Upjohn, Kalamazoo, MI), 200 units/mL penicillin (Hazleton), and 200 μg/mL streptomycin (Hazleton). This constituted the underlying, single gel, system. For the sandwich systems, an additional 1 mL of collagen gel solution was distributed over the cells after 1 day of culture at 37 °C and 10% CO_2. Culture medium was first removed and care was taken to ensure that the second layer of collagen gel was evenly spread over the entire dish. Thirty minutes of incubation at 37°C was allowed for gelation and attachment of the second gel layer before the medium was replaced. Culture medium was changed daily. The collected media samples were stored at 4°C prior to analyses.

2.2.4 Surface Specifications

Disks of glass (5.08 cm diameter) with various coatings were obtained from Cytonix (Beltsville, MD). Adhesive surfaces (AS) were formed by spin-coating with urethane epoxy and curing in ultraviolet light. Non-adhesive surfaces (NAS) were formed by overcoating with a solution of a perfluorinated polymer. 'Banded' patterns were created by masking the urethane epoxy coated surface with a single strip of adhesive tape of 1.9 cm width. Disks were then overcoated with a perfluorinated polymer followed by removal of the adhesive tape. A banded surface is depicted in Figure 2.3.

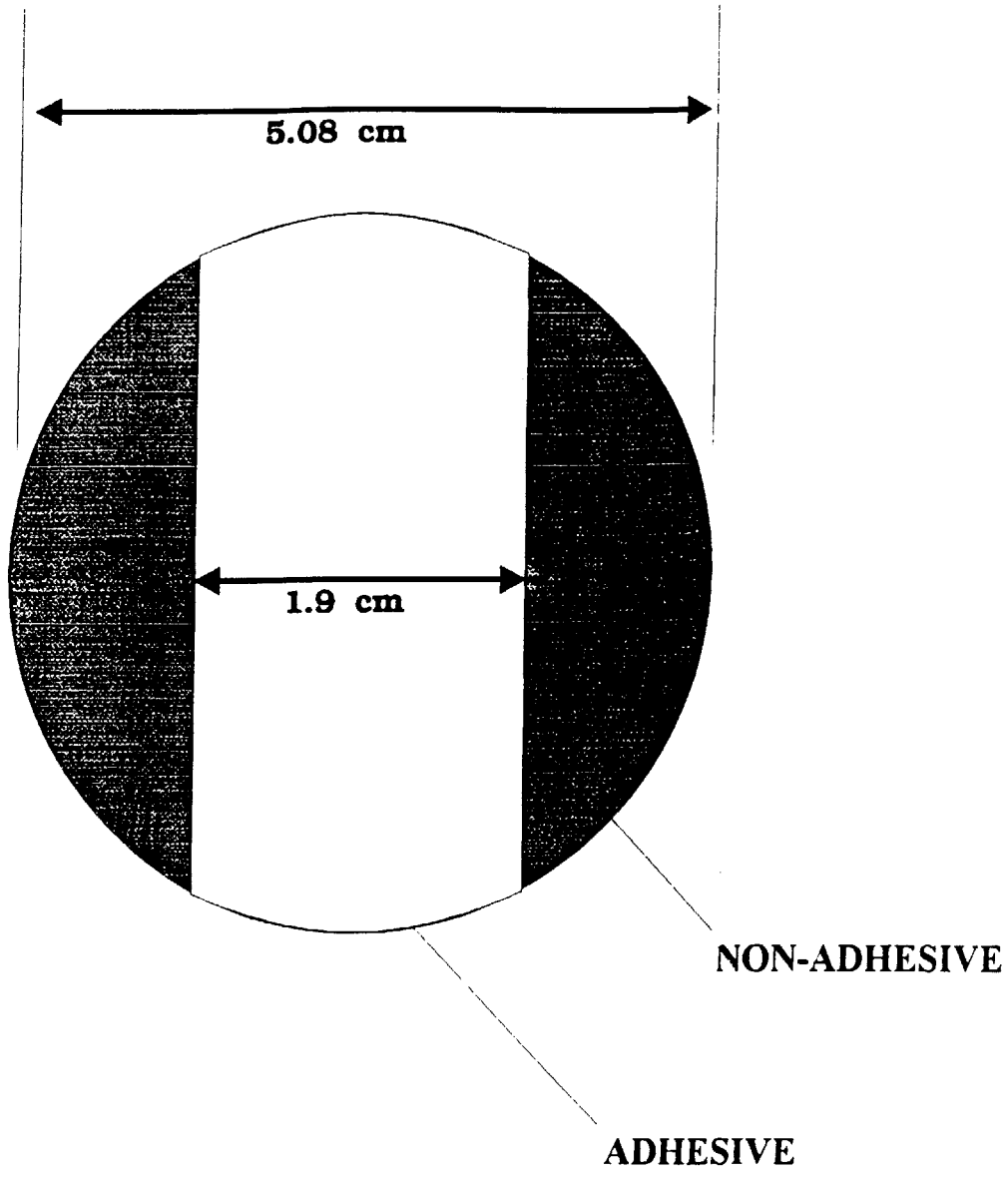

Figure 2.3. A banded surface with adhesive (AS) and non-adhesive (NAS) regimes.

2.2.5 Processing of Surfaces

All surfaces were washed for 2 min in 3 mL of distilled, deionized water by shaking at 400 RPM on a shaker (Model R-2, New Brunswick Scientific, Edison, NJ).

For patterning, dilute (non-gelling) collagen solutions (0.01% (w/v)) were prepared by mixing 1 part of 1.11 mg/ml collagen solution with 9 parts of distilled, deionized water. 0.01% (w/v) bovine serum albumin (Sigma, Lot Number 118F005) solution and 0.01% (w/v) PL (Sigma) were prepared in distilled, deionized water.

Surfaces were coated with various solutions, described in section 2.2.3, by immersion into 300 mL of the appropriate solution at a 90° angle and a rate of 1mm/s by a modified Harvard Syringe pump (Cambridge, MA) at 4°C. Surfaces were then placed in 60-mm tissue culture dishes. In addition, some surfaces were spin-coated at 4°C by utilizing the following procedure. Surfaces were clamped to the center of a modified centrifuge rotor (Dynac, Cat # 0101, Parsippany, NJ). The technical drawing of the machined accessory is depicted in Figure 2.4. A fixed volume of solution (2 ml) was pipetted onto the center of the surface over 5 seconds. Solution was allowed to spread for 5 s prior to spinning. Spinning was done at 500 RPM (centrifuge setting of 18) for 20s. The brake was applied for a duration of approximately 5 s until rotation had ceased. Surfaces were then unclamped, and placed in a 60-mm tissue culture dish (Falcon).

Following processing, all surfaces were incubated at 37 °C and 10% CO_2 for 30 min. Dilute collagen coatings evaporated during this time whereas gelation occurred in the salt-based collagen solutions. Surfaces that were analyzed for differentiated, long-term function were pre-treated by ethylene oxide gas sterilization.

MATERIAL: STAINLESS STEEL
DIMENSIONS: IN MM

BASE PIECE:

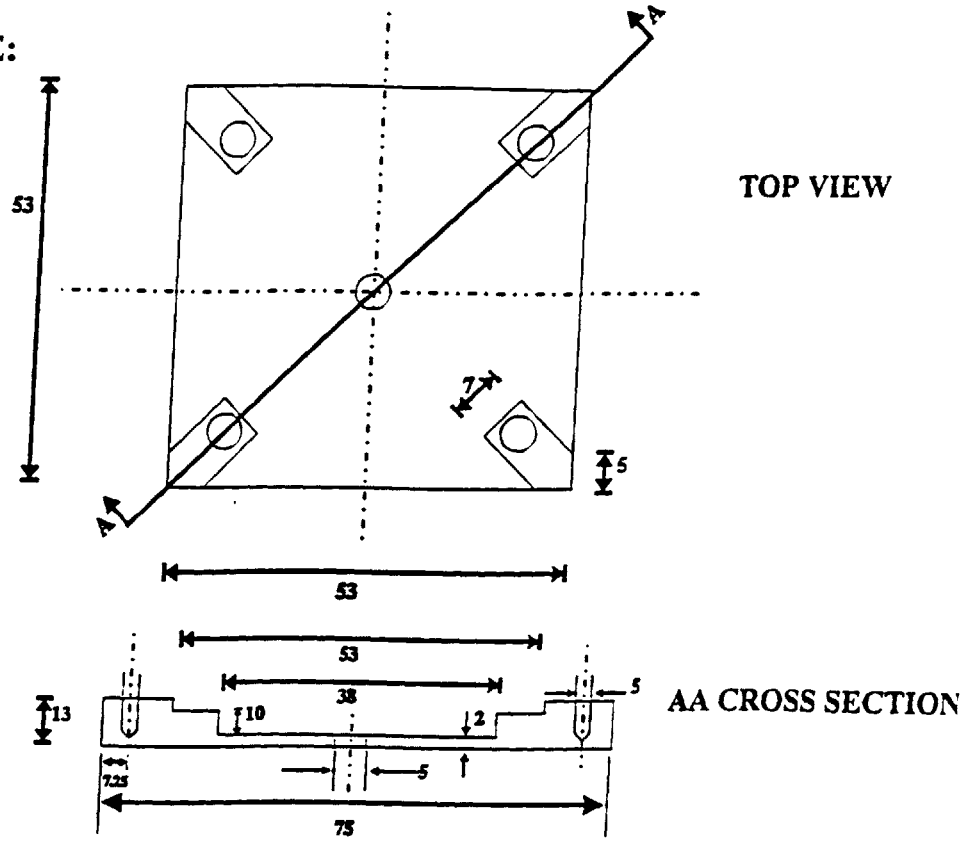

CORNER PIECE:

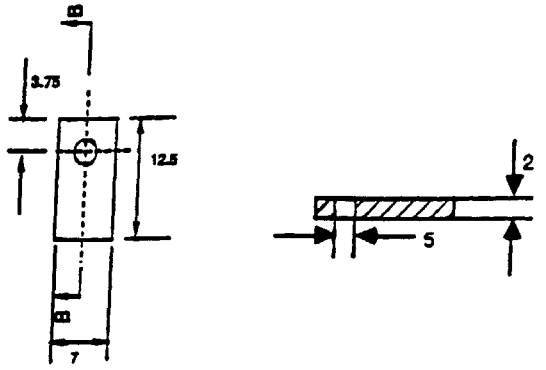

TOP VIEW **BB CROSS SECTION**

Figure 2.4. Technical drawing of machined accessory to modify a centrifuge for spin-coating.

2.2.6 Attachment Assay and Morphological Measurements

As described above, two million freshly isolated, viable cells were seeded in 2 mL of medium on the appropriate pre-treated surface or single layer of collagen gel in a 60-mm tissue culture dish (Falcon). Cells were spread evenly and incubated for 45 minutes at 37°C and 10% CO_2. The following washing procedure was repeated twice. Unattached cells and medium were then aspirated and 3 mL of medium was added to each dish. Dishes were agitated at 200 RPM on a shaker (New Brunswick Scientific) for 4 minutes. After 2 minutes, the orientation of the dishes was changed by rotating each dish 90 °and shaking was resumed for the remaining 2 minutes. Finally, media was aspirated and 2 mL of media was added to each dish. Cells were recorded at 50X original magnification using a video system consisting of an Olympus microscope (CK2, Japan), camera (Hamamatsu C-2400, Japan), monitor (Sony PVM1343MD, Japan), and VCR (Panasonic, AG-6750, Japan) as described in detail elsewhere (Rotem et al., 1992). The number of remaining cells in 10 random fields were counted from the recorded images using an image analysis system (Argus 10, Hamamatsu) and compared to the number of remaining cells on a single layer of collagen gel which had been similarly treated. Morphological measurements were made by recording the cells at 200X magnification after 24 h of incubation at 37 °C and 10% CO_2. The projected surface area (PSA) of the cells was analyzed from the recorded images using an image analysis system (Argus 10) which had been previously calibrated using a hemocytometer grating.

2.2.7 Biochemical Analysis

Collected media samples were analyzed for rat albumin content by enzyme-linked immunosorbent assays (ELISA). Chromatographically purified albumin was purchased from Cappel (Cochranville, PA). The 96-well plates (NUNC-Immuno Plate, Maxisorp, Newbury Park, CA) were coated with 100 μL of rat albumin in 25 mM carbonate buffer, pH 9.6, overnight at 4 °C. The wells were washed four times with PBS plus 0.5% (v/v)

Tween 20 (PBS-Tween). Fifty microliters of sample was mixed with an equal volume of antibody (800ng/mL in PBS-Tween) before it was transferred to the wells. After overnight incubation at 4 °C, the wells were washed four times with PBS-Tween and were developed with 100 μL of 25 mM citrate and 50mM phosphate, pH 5, containing 0.4mg/mL o-phenylenediamine by the conjugated peroxidase. The absorbance was measured at 490 nm with the a Dynatech (Chantilly, VA) MR600 microplate reader. Positive controls included known concentrations of purified rat albumin added to the culture medium and negative controls included the culture medium and PBS-Tween. Concentrations of standards were calibrated by their absorbances at 280 nm, by using 0.6 as an extinction coefficient for 1mg/mL solutions of albumin. Concentrations of samples were determined from a standard curve generated for each ELISA plate. Absolute rates of secretion were calculated from the concentration by multiplying the total volume of the medium and dividing by the elapsed time. Results were given in micrograms per hour per 2×10^6 cells .

2.2.8. Atomic Force Microscopy

Two banded surfaces with regions of AS and NAS were analyzed by Imaging Services (Santa Barbara, CA). Both disks were washed by agitation and 500 rpm for 1 minute in distilled, deionized water. One disk was imaged without any further treatment whereas the other sample was spin-coated with 2 ml of 0.1 mg/ml collagen solution at 500 rpm for 25 seconds.

2.2.9 Statistics and Data Analysis

Generally, two duplicate wells were averaged for each ELISA sample. Experiments were repeated two to three times. The absolute secretion rate of the control culture on the second to last day of culture was used to normalize all data in an experiment. Combining data from experiments with different sampling schedules was done by linearly interpolating

missing data points. Attachment data was quantified by dividing number of cells attached by the number of cells attached to a single layer of collagen gel (control) and expressed as a percentage. Each data point represents the average of 10-20 fields. Error bars indicate standard deviation of the mean. Morphological measurements were quantified by analyzing the projected surface area for 5 random cells in 10 random fields, per condition. Error bars indicate standard deviation of the mean.

2.3 Results

Hepatocyte Culture

Albumin secretion is typically utilized as a marker for differentiated hepatocyte function because it involves many complex cellular functions such as transcription, translation, intracellular packaging and transport, and secretion. Figure 2.5 shows the albumin secretion of cells cultured in two different collagen gel configurations, namely; a single layer of collagen gel and sandwich culture. In the sandwich configuration, albumin secretion shows a marked increase followed by a plateau at day 8 at approximately 3 $\mu g/h/2\times 10^6$ cells. In contrast, single gel culture shows a maximum at day 2 at 0.89 ± 0.1 $\mu g/h/2\times 10^6$ cells followed by a steady decline in albumin secretion and differentiated function. In the original study by Dunn et al (1991), similar trends were reported for albumin and other proteins. These results indicate the importance of utilizing a sandwich configuration to create a stable, differentiated culture system.

The aforementioned experiments were done using a collagen gel concentration of 1 mg/ml. In order to test the effect of varying the collagen concentration in the extracellular matrix on the differentiated function of hepatocytes, a series of experiments were performed where the collagen gel concentration was varied between 3 and 0.5 mg/ml. Figure 2.6 shows the albumin secretion of hepatocytes sandwiched between two gels of varying concentrations. Altering the collagen concentrations within the examined range

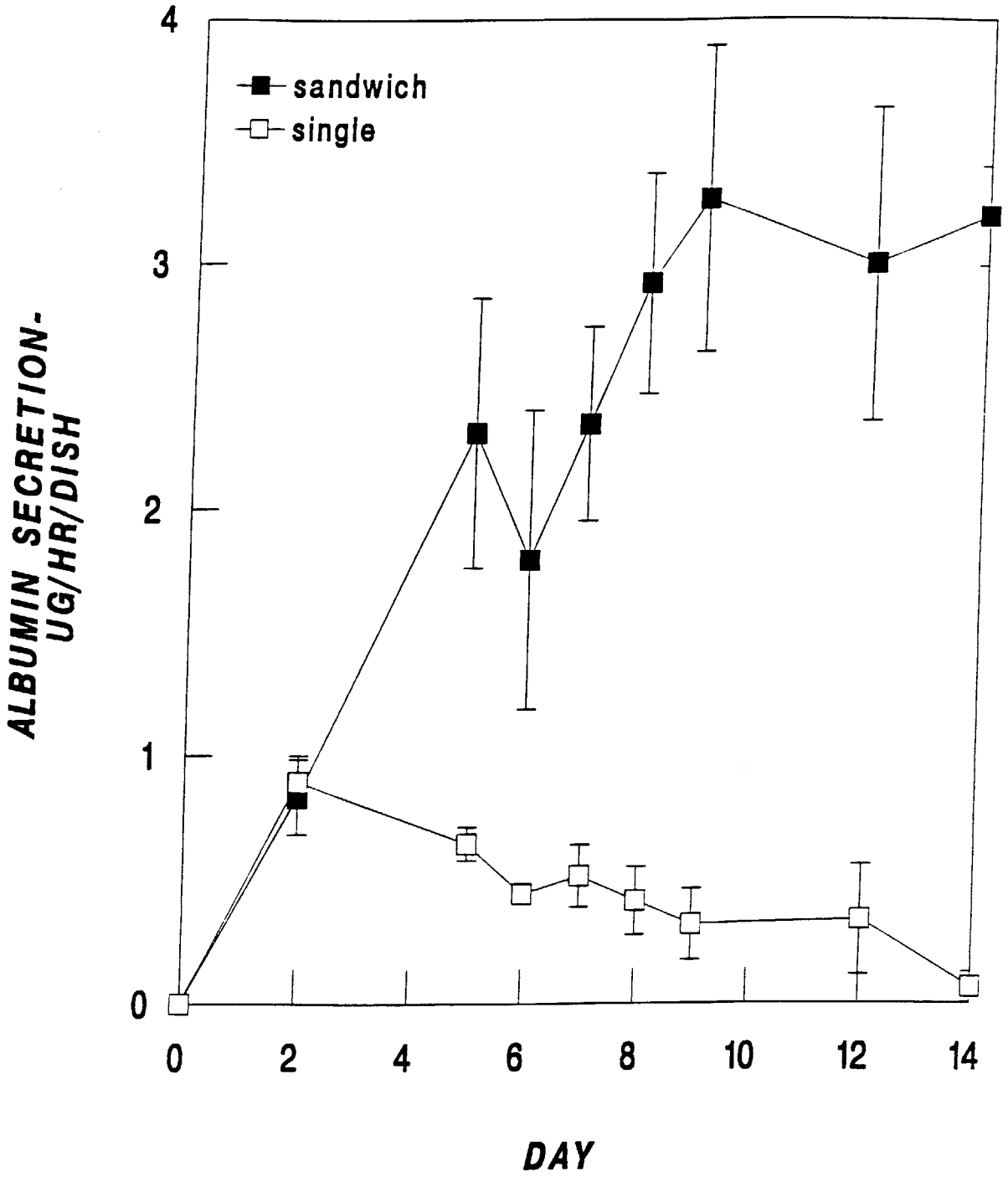

Figure 2.5. Albumin secretion of hepatocytes cultured in sandwich and single gel configurations.

seemed to have no effect on albumin secretion. All cultures showed an increase in albumin secretion to a maximal level around day 8. Lower collagen gel concentrations were not investigated because a stable gel does not form below a concentration of 0.4 mg/ml.

Surface Characterization

Adhesive (AS) and non-adhesive surfaces (NAS) were characterized before and after surface coating utilizing atomic force microscopy (AFM). The methodology for surface coating with collagen is described in the previous section. Figure 2.7 shows 3-dimensionally rendered AFM images of untreated and treated (by spin-coating with a collagen solution), AS and NAS, on a banded surface. The term 'banded surface' refers to circular 5.08 cm diameter surfaces with a 1.9 cm strip of AS in the center flanked by NAS as depicted in Figure 2.3. As seen in Figure 2.7, spin-coating a banded surface resulted in selective adsorption of collagen to the AS with no observable change in the NAS. Table 2.1 summarizes the roughens of the four surfaces.

Table 2.1. Comparison of surface roughness for various sites on a banded surface.[a]

	UNTREATED [nm]		TREATED [nm]	
ADHESIVE	0.190	(0.240)	0.350	(0.382)
NON-ADHESIVE	0.303	(0.459)	0.304	(0.382)

Clearly, the roughness of the AS increases after collagen treatment whereas the surface of the NAS is unchanged. Figure 2.8 shows the interface of the two coating regions after

[a] Data in parentheses represents rms.

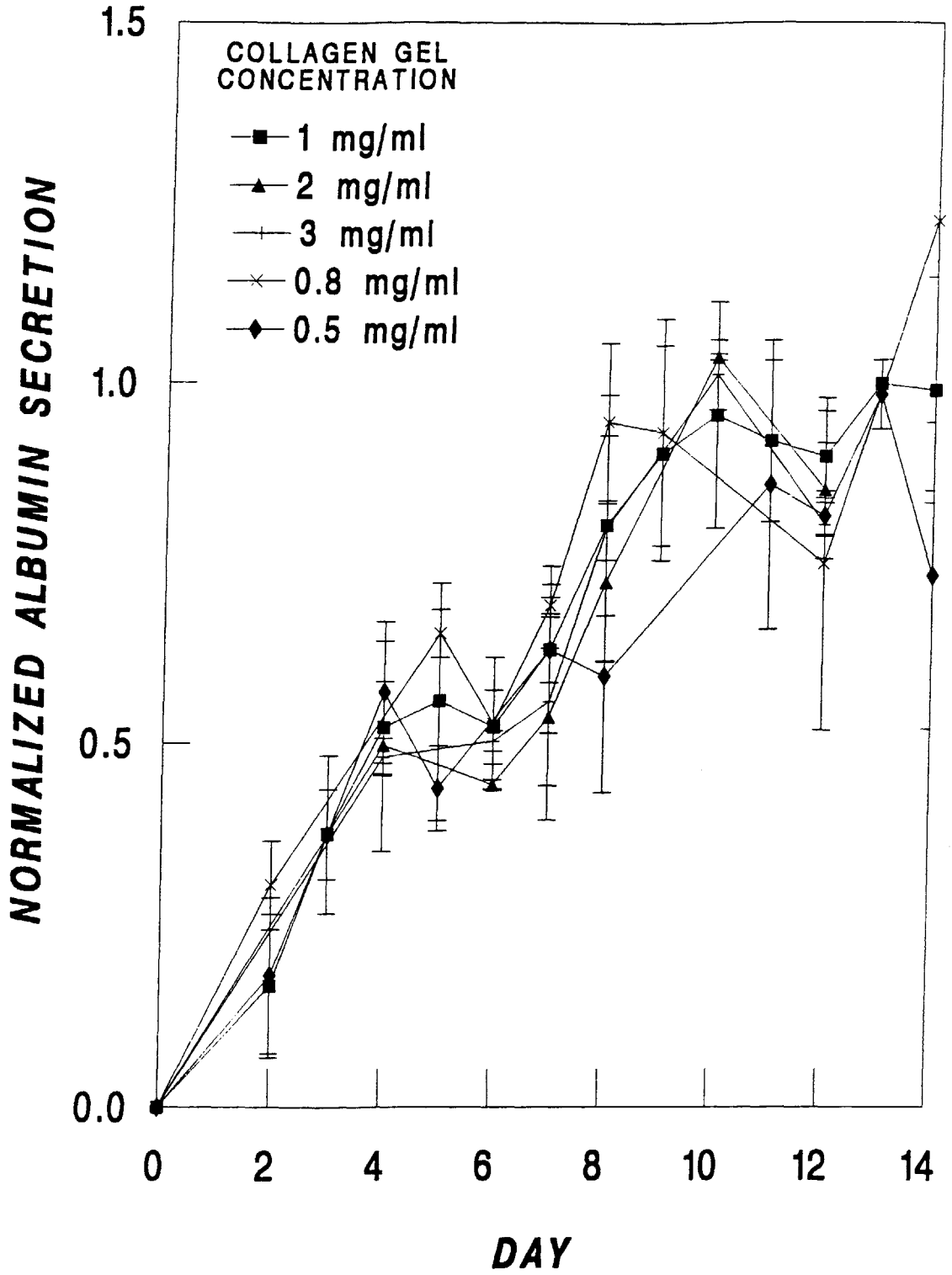

Figure 2.6. Normalized albumin secretion of hepatocytes cultured in sandwiches of varying collagen concentration. All samples were normalized to their own control cultures. (A normalized value of 1.0 corresponds to 4.4 $\mu g / h / 2 \times 10^6$ cells and represents the average of the control values.)

UNTREATED TREATED

ADHESIVE

NON-ADHESIVE

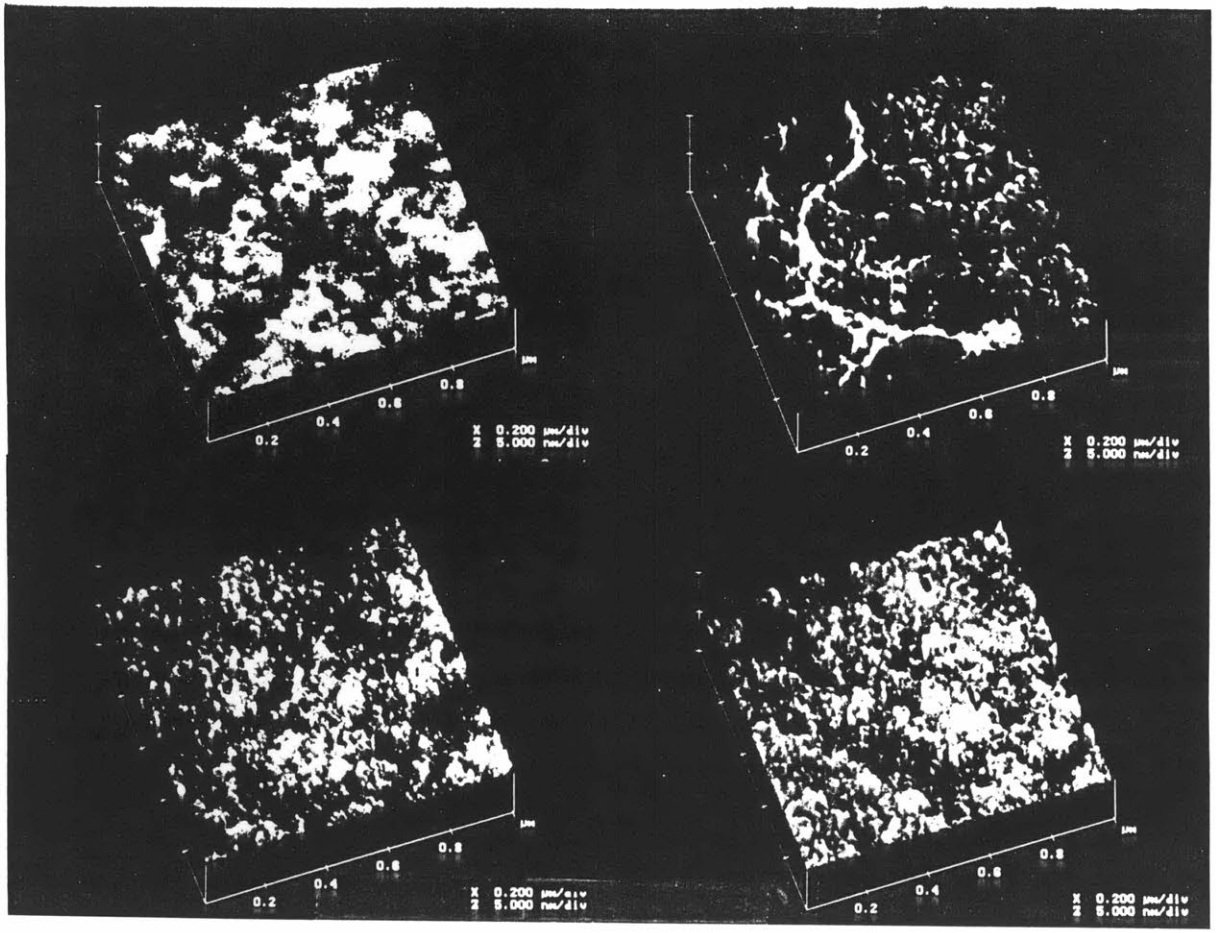

Figure 2.7. Atomic Force Microscopy image of (going clockwise from upper left) A. adhesive surface (AS) untreated, B. AS treated by spin-coating with aqueous collagen [0.1 mg/ml], C. non-adhesive surface (NAS) treated D. NAS untreated by spin-coating with aqueous collagen [0.1 mg/ml].

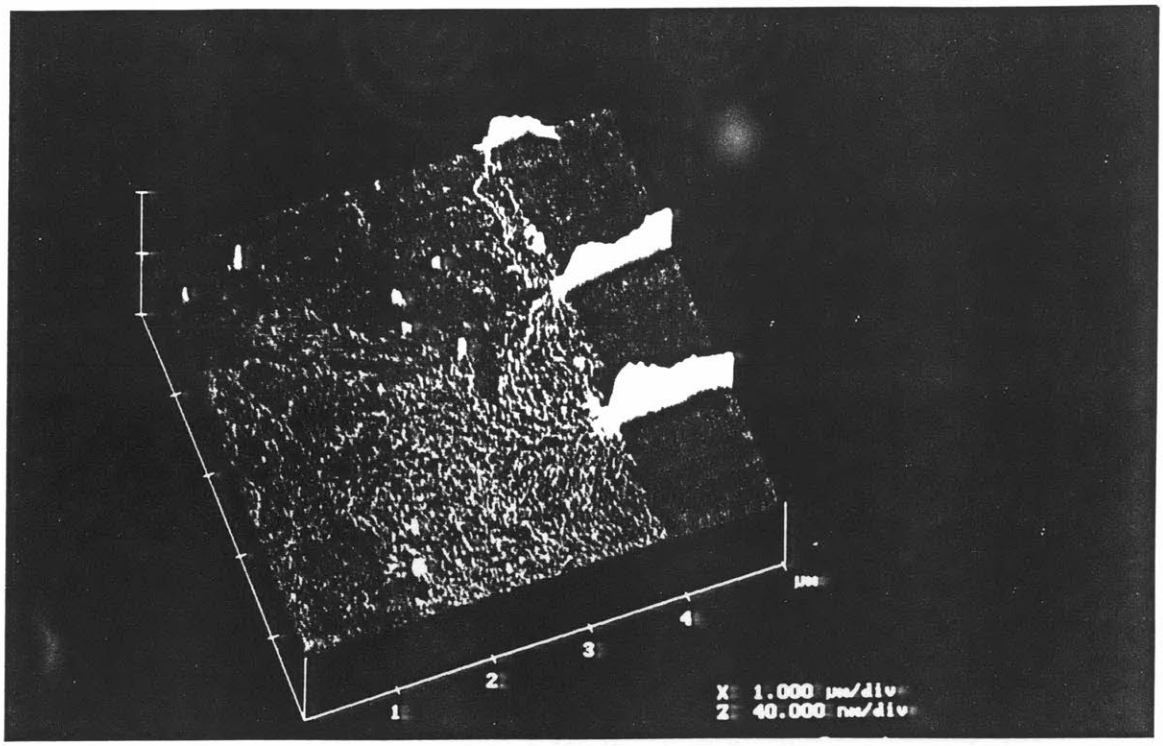

Figure 2.8. Atomic Force Microscopy image of interface between adhesive (on the left) and non-adhesive regions of a banded surface after treatment by spin-coating with aqueous collagen [0.1 mg/ml]. The adhesive region is covered with a matte coating of collagen whereas the non-adhesive region exhibits the beginning of striations resulting from drying during spin-coating.

collagen treatment. A matte layer of protein is visible on the AS region. In contrast, the NAS portion of the image displays striations of 10-100 nm in height. In addition, other images taken at lower magnification show that the NAS-associated striations begin approximately 5 μm before the NAS interface begins, possibly indicating a resolution limitation to this processing technique.

Hepatocyte-Surface Interactions

The hepatocyte-surface interaction was assessed separately for both AS and NAS. Surfaces were evaluated for the level of hepatocyte attachment, spreading, and differentiated function. Attachment to various processed surfaces was expressed as a percent of the cells that attached to a similarly processed standard collagen gel. PSA was used to quantify the hepatocyte-substrate interaction at later time points following the early attachment phase. Analysis of the preservation of differentiated function was done by seeding cells on a pre-treated AS with a collagen gel overlay to mimic the sandwich culture described in the previous section. This sandwich culture was compared to the conventional sandwich culture by measuring albumin secretion. Finally, preservation of differentiated function in the presence of the NAS was evaluated by culturing cells in the sandwich configuration with media that had been incubated with NAS.

2×10^6 cells were seeded on AS and NAS treated as described previously by immersion into a 300 ml bath of 0.01% (w/v) collagen solution, 0.01% (w/v) BSA, 0.01% (w/v) PL solution, or distilled, deionized water. The NAS should tend to discourage wetting by a water-based solution because of its hydrophobic properties. Conversely, the AS is wettable and thereby should promote adhesion of the water-based protein solution. Figure 2.9 compares adhesion of hepatocytes to a variety of pre-treated surfaces after 45 minutes. Collagen-treated AS showed the largest levels of attachment at 82 $\pm$ 15 % of control. AS treated with a PL solution and water alone also displayed small

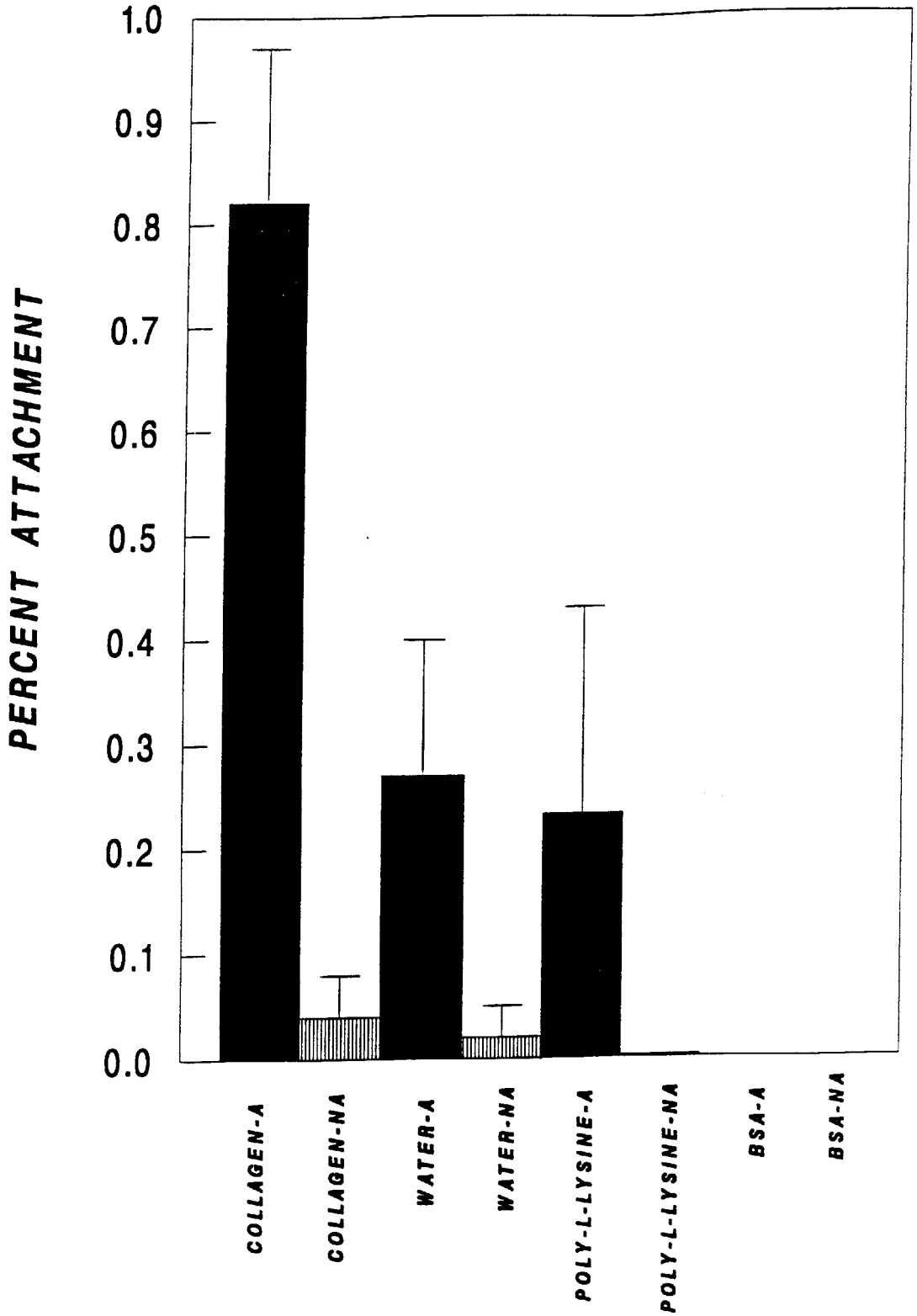

Figure 2.9. Attachment of hepatocytes to various treated substrates as percentage of hepatocytes attached to collagen gel after 45 minutes. A signifies adhesive surface and NA signifies non-adhesive surface. All solutions were 0.1 mg/ml.

levels of attachment (~25%) whereas all other conditions, namely collagen-treated NAS, water-treated NAS, PL-treated NAS, BSA-treated AS and NAS, had less than 4 % (of control) attachment .

BSA has a net negative charge at physiological pH whereas PL carries a positive charge. These two molecules were utilized to attempt to distinguish non-specific charge interactions from receptor-specific attachment. BSA was a deterrent to hepatocyte attachment on all surfaces. PL supported as much adhesion as water alone on the AS and reduced adhesion from 4% to 0 % on the NAS. This behavior can be explained by one of two phenomenon: (1) the PL did not adhere to the surface and the surface behaved as it did when treated with water or (2) the PL adherence does not support the high levels of attachment promoted by collagen.

Morphology of the attached cells was assessed after 24 hours of incubation. Figure 2.10 shows the PSA per cell of the attached cells. Cultures on collagen-treated AS had a PSA of $1508 \pm 521\ \mu m^2$ and were comparable to the PSA of cells cultured on a collagen gel. All other attached cells remained round with a PSA of 300 to 500 μm^2 including those cells attached to the PL-treated and water-treated AS. Therefore, the only cells which exhibited spreading similar to the standard culture techniques were those cultured on the collagen-treated AS .

Figure 2.11 shows the total PSA of the attached cells on the surfaces. Average PSA per cell is multiplied by the number of attached cells and error bars represent the standard deviation in attachment. The total PSA is a more meaningful representation of cell surface area available for mass exchange and the results clearly indicate the benefits of utilizing collagen-treatment on the AS. The total PSA was an order of magnitude higher for collagen gel and collagen-treated AS as compared to all other surfaces ($1 \times 10^9\ \mu m^2$ versus $0.1 \times 10^9\ \mu m^2$).

To assess the potential toxic effects of AS and NAS on cellular function, sandwich cultures were performed under different conditions and albumin secretion was measured.

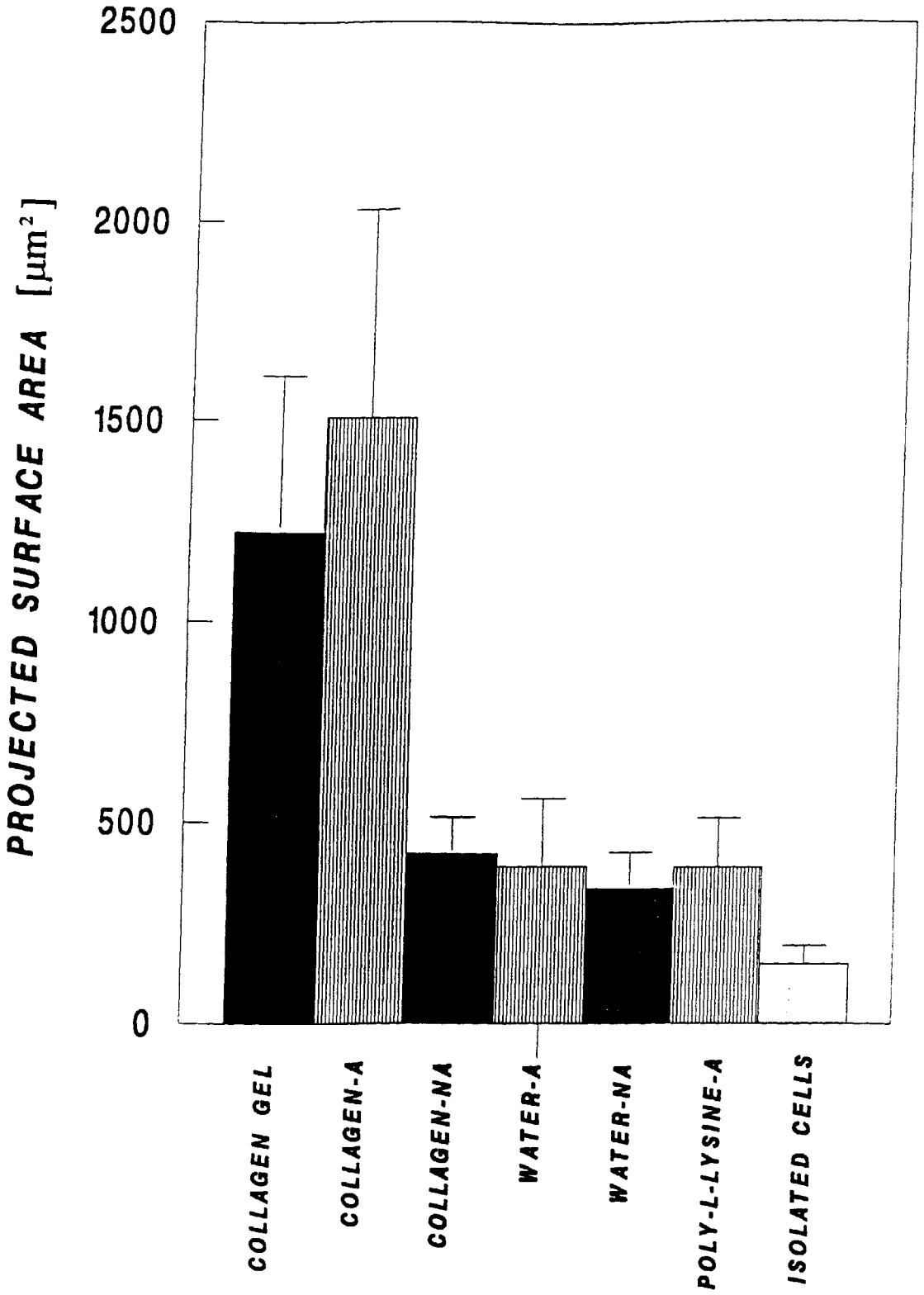

Figure 2.10. Projected surface area per cell of attached cells to various treated substrates. A signifies adhesive surface and NA signifies non-adhesive surface. All solutions were 0.1 mg/ml.

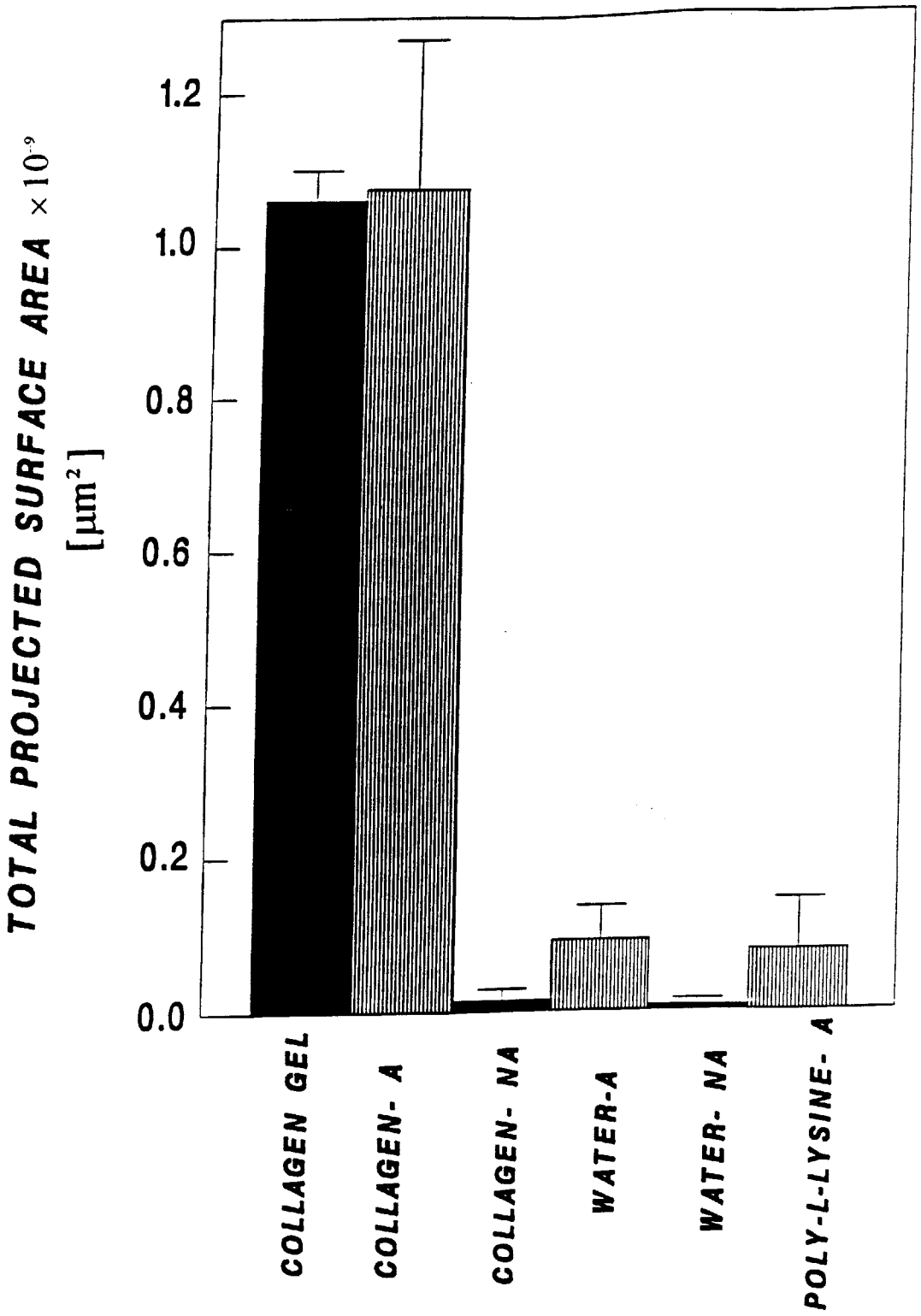

Figure 2.11. Total PSA per dish of attached cells on various treated substrates. Total PSA=Average PSA per cell × number of attached cells. A signifies adhesive surface and NA signifies non-adhesive surface. All solutions were 0.1 mg/ml.

AS were treated by immersion into a 0.5 mg/ml collagen gel solution. As previously mentioned, monomeric collagen polymerizes at physiological pH and osmolarity and this process is accelerated at elevated temperatures. Therefore, subsequent incubation of these surfaces yielded a thin collagen gel for hepatocytes to be seeded on. The hepatocytes were sandwiched after 24 hours with a standard collagen gel overlay and albumin secretion was compared to that of a standard sandwich culture. Figure 2.12 shows differentiated function of hepatocytes on AS as compared to the standard sandwich culture. Both culture conditions produced increasing albumin secretion which reached a plateau at 3.2 $\mu g/h/2\times 10^6$cells around day 10.

In contrast, to determine the toxic effects of NAS, standard sandwich cultures were incubated with medium previously incubated at 37 °C for 24 hours with a NAS. Cells could not be cultured directly on NAS because hepatocytes are anchorage-dependent cells. Figure 2.13 indicates comparable levels of albumin secretion for sandwich cultures incubated in standard media and media pre-incubated with NAS . Albumin secretion for both conditions plateaued at day 7 at 3 $\mu g/h/2\times 10^6$cells.

Hepatocyte-Banded Surface Interactions (Combined Adhesive (AS) and Non-adhesive Surfaces (NAS))

The selection of the polymers for the AS and NAS and the separate characterization of cell-biomaterial interactions was followed by combining both surfaces on a banded surface (Figure 2.3). Surfaces can be treated with collagen using a variety of application methods. Two methods investigated in this study were dipping and spin-coating. Another parameter to investigate was the concentration of the applied collagen solution. Attachment and spreading were investigated on banded surfaces and expressed as differential attachment. Differential attachment refers to the percent attachment on the AS region minus the percent attachment on the NAS region. Finally, long-term differentiated

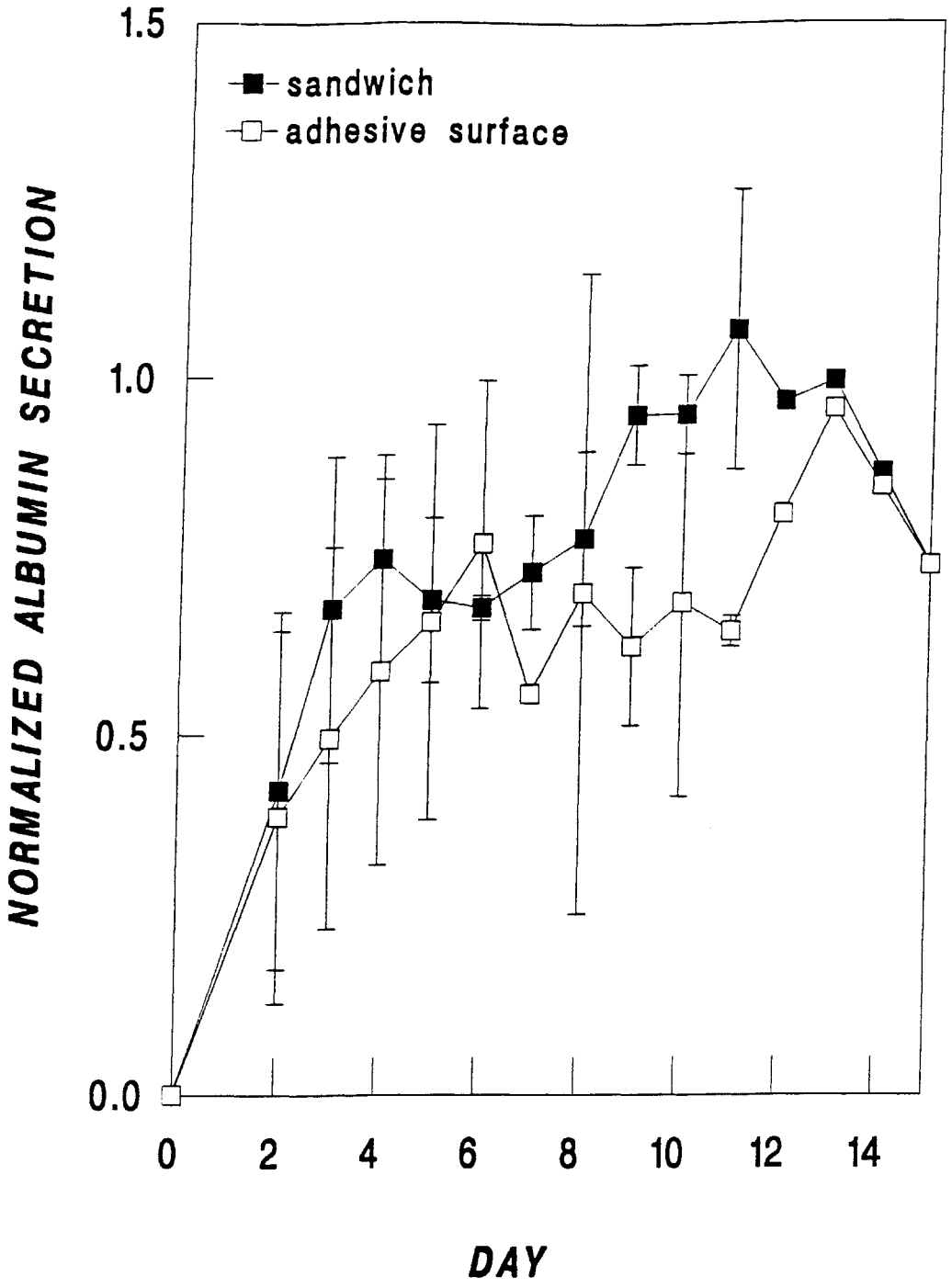

Figure 2.12. Normalized albumin secretion of hepatocytes seeded on treated adhesive surfaces as compared with sandwich culture. Adhesive surfaces were immersed in 0.5 mg/ml collagen gel solution and hepatocytes were overlayed with 1 mg/ml collagen gel. (A normalized value of 1.0 corresponds to 3.2 $\mu g / h / 2 \times 10^6$ cells.)

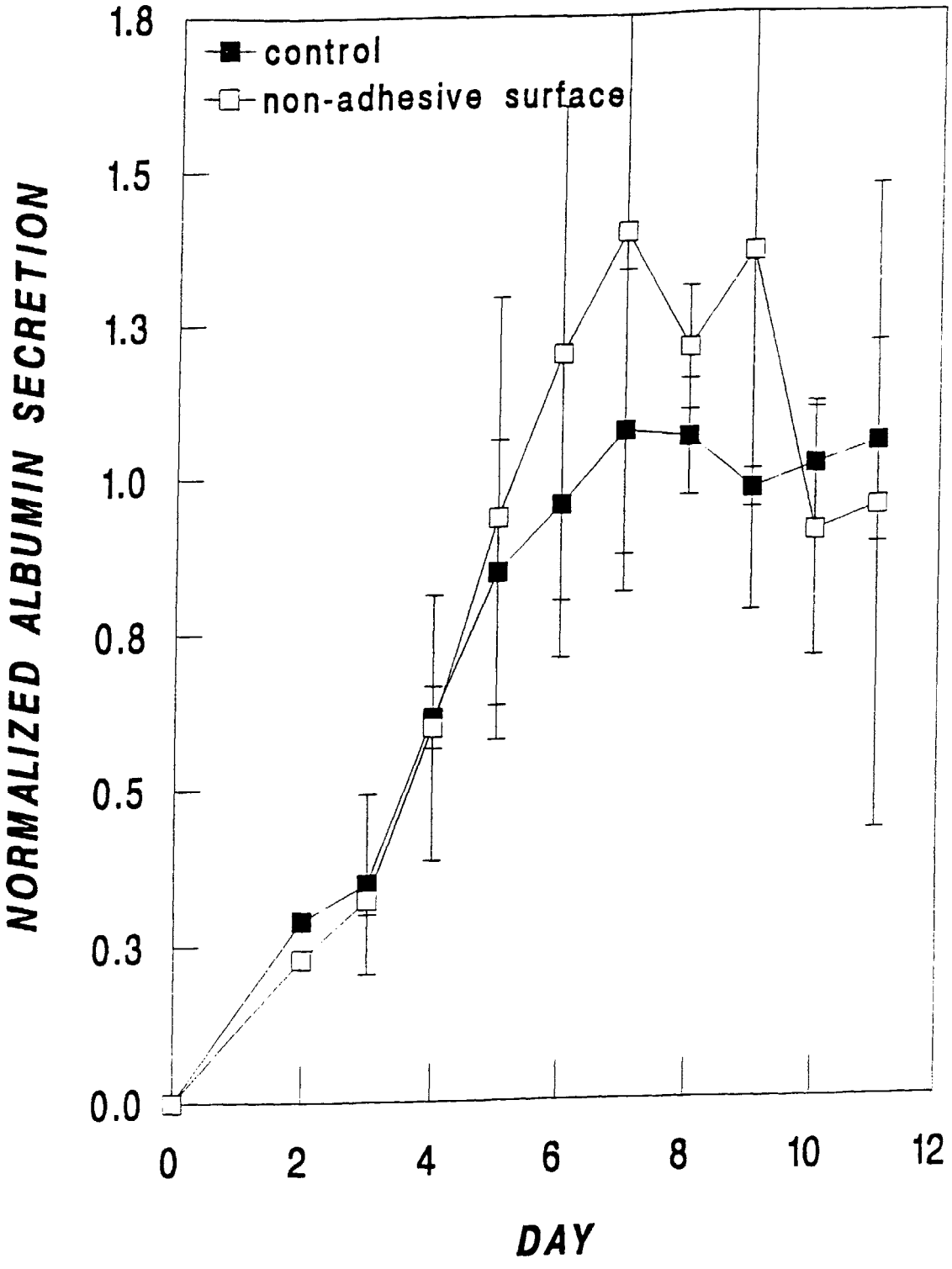

Figure 2.13. Normalized albumin secretion of hepatocytes in sandwich culture as compared to a sandwich culture whose media had been pre-incubated with a non-adhesive surface. (A normalized value of 1.0 corresponds to 3.0 $\mu g/h/2\times10^6$ cells.)

function of hepatocytes on the banded surface with a collagen gel overlay to create a sandwich culture was evaluated.

A comparison was made between immersion into collagen solutions versus spin-coating. Surfaces were immersed at a 90° angle at a controlled rate of 1 mm/s into a 300 ml bath of 0.1 mg/ml collagen solution. Spin-coating was performed by using 2 ml of 0.1 mg/ml collagen solution and a modified centrifuge spinning at 500 rpm for 25 seconds. Dipping yielded uniform non-selective cell adhesion to both regions of the surface whereas spin-coating yielded preferential attachment to the AS and a clear boundary between the two regions. Thus, spin-coating was chosen for the selective adhesion of hepatocytes in the rest of this study. However, it is noteworthy to mention that one could also vary the rate of dipping and presumably reach some speed at which the contact time of the collagen solution with the surface was reduced sufficiently to obtain diminished attachment on the NAS .

Having chosen spin-coating as the method of collagen solution application, the concentration of the collagen solution was investigated by varying the coating concentration between 2 mg/ml and 0.005 mg/ml. Figure 2.14 displays the percent of cells attached to both the AS and NAS regions of the banded surface as compared to a collagen gel control. The AS shows relatively constant attachment efficiency as the collagen solution concentration decreases until it reaches the lowest concentration of 0.005 mg/ml. The diminished attachment at lower concentrations is due to a patchy pattern of adhesion similar to that seen on the water-treated surface. Conversely, NAS show low levels of cell adhesion for most concentrations lower than 2 mg/ml whereafter cell adhesion increases. Subtracting these two curves to obtain differential attachment, a measure of patterning efficiency, yielded Figure 2.15. A plateau of maximal differential attachment is obtained between 0.01 to 1 mg/ml. Outside this optimal operating range, differential attachment decreases signifying non-optimal selective adhesion of hepatocytes. At higher concentration this appears to be due to increased binding on the NAS whereas at lower

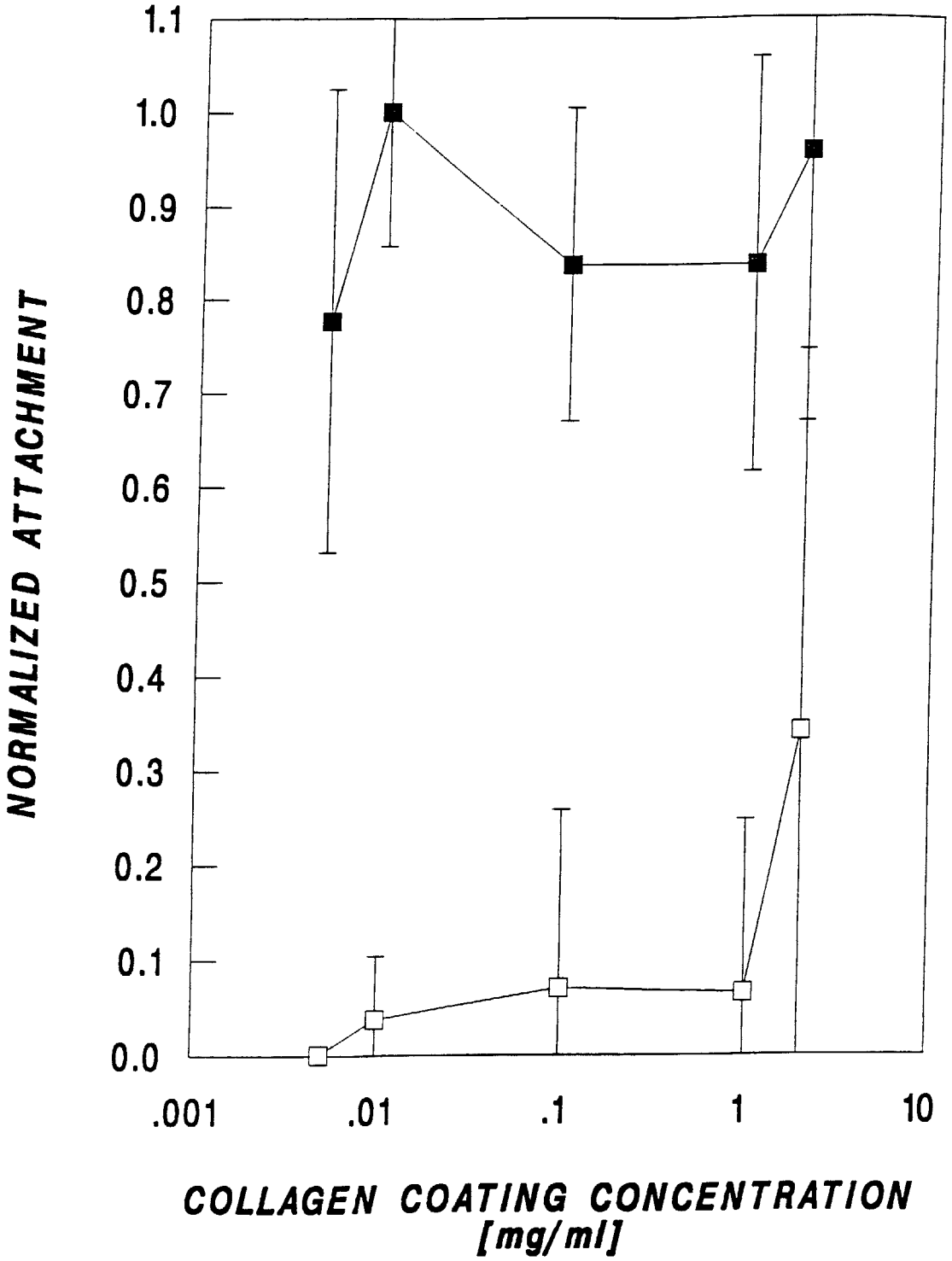

Figure 2.14. Normalized attachment of hepatocytes to adhesive and non-adhesive regions of a banded surface after spin-coating with various concentrations of collagen I solution. Attachment is expressed as percentage of cells which attached to a collagen gel and is then normalized to the maximum value for each experiment. (A normalized value of 1.0 corresponds to 75% attachment as compared to a collagen gel control.)

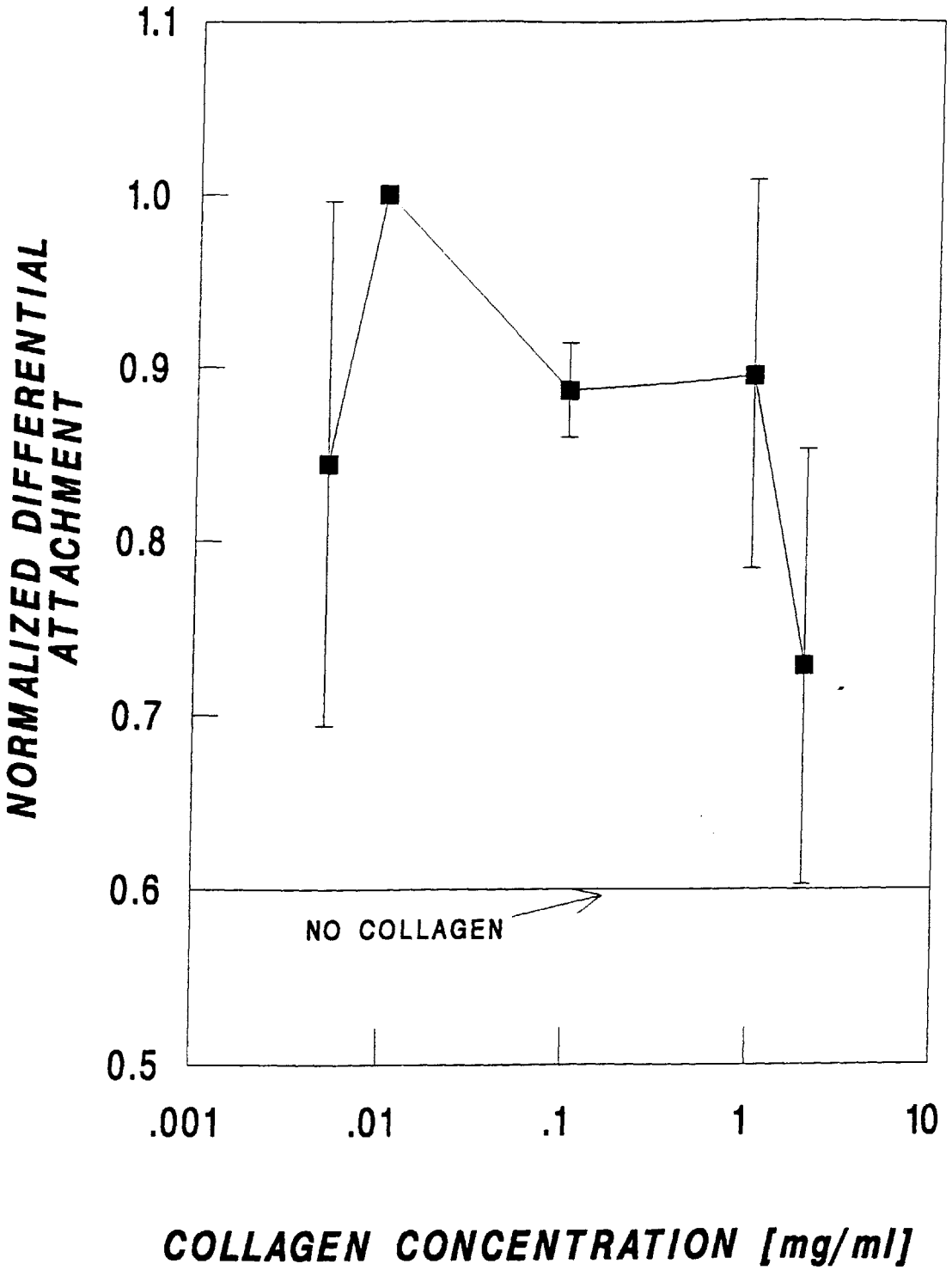

Figure 2.15. Normalized differential attachment of hepatocytes to adhesive and non-adhesive regions of a banded surface. Differential attachment = attachment on adhesive surface- attachment on non-adhesive surface. Each experiment was normalized to maximum percentage attachment for that experiment. (A normalized value of 1.0 corresponds to 72% attachment as compared to a collagen gel control.)

coating concentration this appears due to decreased binding to the AS. This qualitative pattern was reproduced in 2 experiments with 2 surfaces per experiment and 10 random fields on each region of the banded surface per surface. To obtain statistical significance of the trend observed in Figure 2.15, more experiments with a larger number of sampled fields is necessary.

The PSA of the attached cells on the AS surface was determined at 24 h as a measure of cell spreading. Figure 2.16 shows no significant effect of coating concentration on PSA per cell. PSA per cell were between 1000 to 1250 μm^2. Given the aforementioned attachment results and these spreading studies, a coating concentration of 0.1 mg/ml was chosen for subsequent experiments.

Figure 2.17 shows hepatocytes which have adhered to this surface after 24 h of culture. This is a typical field along the boundary of the two surface coatings. The cells maintain their characteristic polygonal morphology and do not spread or migrate onto the NAS. In addition, many are multi-nucleated (typical of hepatocytes in culture) and have well-defined boundaries. Clearly, the selective adsorption of collagen molecules seen in Figure 2.7 correlates with the resulting selective adhesion of hepatocytes in Figure 2.17.

To assess the differentiated function of these cells, a second layer of gel was applied at day 1 to mimic the sandwich culture configuration. Figure 2.18 shows the increase in albumin secretion until the plateau at ~2.2 μg/h/dish at day 12 as seen in the control sandwich culture.

2.4 DISCUSSION

A reproducible process for selective adhesion of hepatocytes to a solid substrate has been developed. The cells display normal morphology and differentiated function in

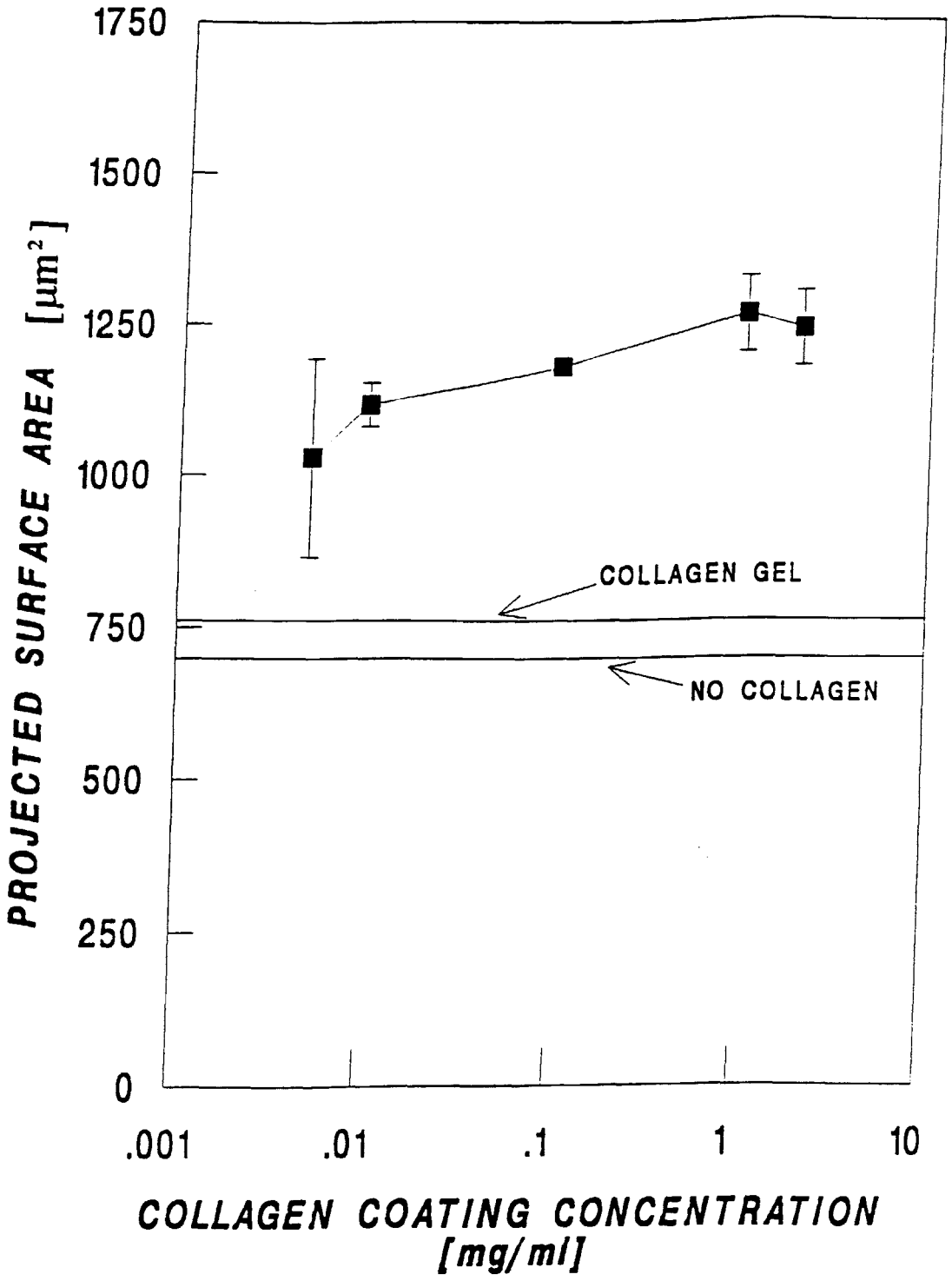

Figure 2.16. Projected surface area per cell of hepatocytes after 24 hours of culture on the adhesive region of banded surfaces that were spin-coated with various concentrations of collagen solution.

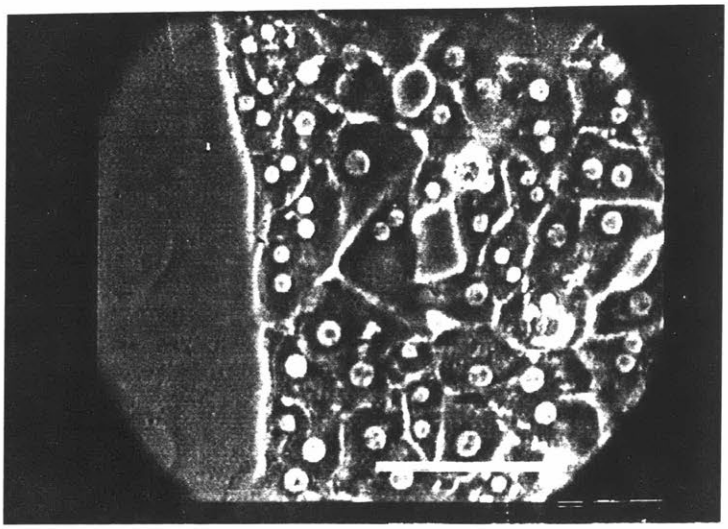

Figure 2.17. Selective adhesion of hepatocytes. A typical micrograph of the interface between adhesive and non-adhesive regions of a banded surface after 24 hours of culture. This substrate was treated with a 0.1 mg/ml collagen solution. Scale bar corresponds to 100 μm.

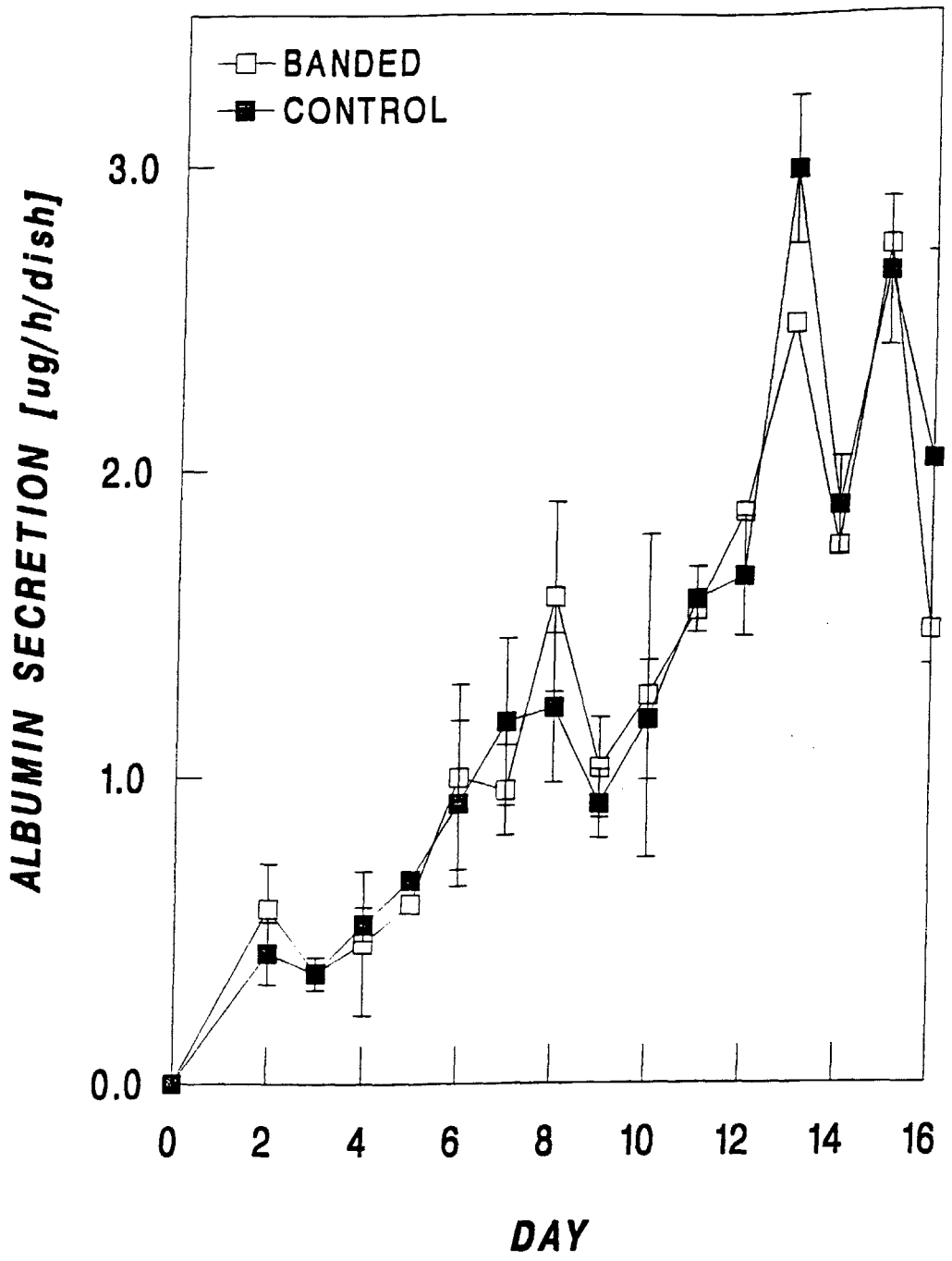

Figure 2.18. Albumin secretion of hepatocytes on a banded surface with a collagen gel overlay as compared to a sandwich culture. Hepatocytes on the banded surface were seeded at 3 million per P-60 dish (to account for only 46% adhesive surface) and 2 million per dish in control cultures. It is likely that less than 2 million cells adhered to the adhesive surface on the banded surface.

long-term culture conditions on the adhesive portion of the surface as compared to a stable, differentiated sandwich culture control. The adhesion may be a receptor-specific process as opposed to a non-specific charge interaction as demonstrated by the lack of selective adhesion mediated by positively and negatively charged molecules. This processing technique and the information gained from the characterization of the cell-biomaterial interaction will be central to the development of a microchannel device. This device may potentially have the capacity to function as an extracorporeal bioartificial liver device by efficiently performing liver-specific functions as plasmas fluid is perfused through the device. This approach to an extracorporeal device for hepatocytes has significant advantages over other conventional configurations such as microcarriers, hollow fibers, and monolayer cultures. As shown in Chapter III in more detail, the device would maintain cell exposure to low shear stresses and viscous pressure drop while maintaining a maximal diffusion path of 50-75 μm, thus creating the ability for very efficient nutrient transport.

The selective adhesion is achieved by exposing the hydrophilic, adhesive surface (AS) and the hydrophobic, non-adhesive surface (NAS) to an aqueous collagen solution, resulting in preferential collagen adsorption to the AS by simple wetting of the AS. In terms of the processing, spin-coating of the substrates was chosen over dipping because selective adhesion was not obtained by immersion of the surface in a collagen solution bath. One possible reason for the success of selective adhesion via spin-coating as compared to dipping is the time of contact between the collagen molecules in solution and the hydrophobic NAS. Time-dependent hydrophobic-hydrophobic bonding betwen the collagen molecules and the NAS may take place during the dipping process (120 seconds) as opposed to the 40 seconds of exposure in the spin-coating process. A schematic depicting the spin-coating process is shown in Figure 2.19 (Elliott, 1989). In this case, a 'static flood' dispense process was utilized meaning the coating solution was applied and allowed to spread to equilibrium before spinning began. During a typical spin-coating

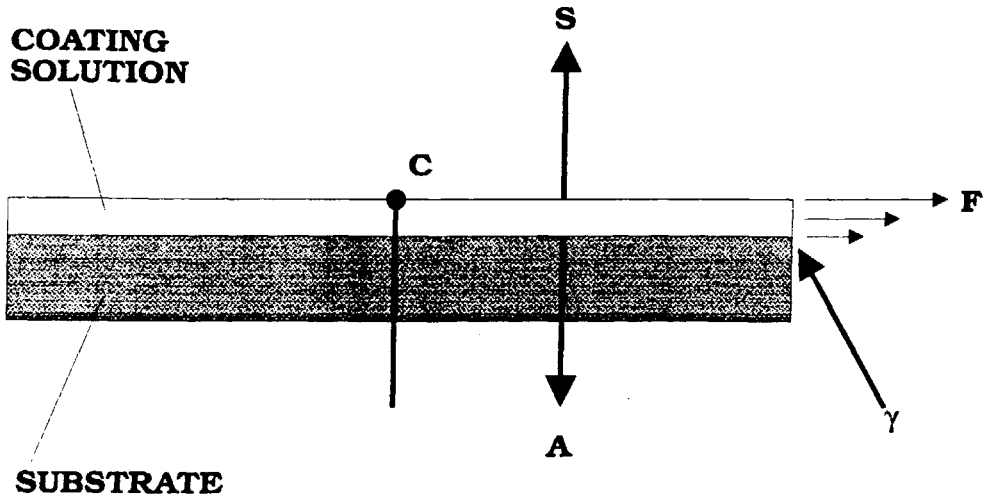

Figure 2.19. Schematic of spin-coating process and competing forces (Elliott, 1989). C indicates the center of rotation, F indicates centrifugal force, S corresponds to evaporating solvent, A indicates adhesive force between the solution and the substrate, and γ indicates the surface tension at the substrate edge.

process, a number of parameters affect the consistency, thickness, and texture of the coating: centrifugal force, F, solvent evaporation, S, solvent viscosity, ν, adhesive force, A, and surface tension at the wafer edge, γ. Initially, a wave of solution forms and moves outward radially until no excess solution remains to supply the wave propagation. Subsequent spinning causes scrubbing of the remaining coating in a spiral pattern. Uneven drying caused by excessive spin times may also cause striations approximately 400 nm high. In the case of banded surfaces, both the adhesive forces and the contact angle (angle through which surface tension forces are exerted) are different on the AS and NAS. The result is collagen adhesion to the AS with spiral-shaped edge effects on the NAS. Evidence of edge effects is seen in cell adhesion to the outlying areas of the non-attaching surface in a spiral tail pattern prior to agitation. However, the strength of binding seems to be low because the edge effects are eliminated immediately upon agitation (data not shown). Direct surface examination by AFM also showed striation patterns on the NAS regime which is not suprising; if the hydrophobic NAS surface dewets more quickly than the hydrophilic, AS, these striation patterns might be expected. Furthermore, their dimensions (10-100 nm) correlated well with those reported in the literature (Elliott, 1989). Limitations of this processing technique stem from the limits of resolution that may occur at smaller patterning widths. According to the AFM images, this limit is on the order of 5 μm. This value may have limited applications in patterns manufactured photolithographically as compared to those produced by adhesive masking since the profile of the interface may vary with the different processes. Finally, a number of independent variables exist for optimization: spinning speed, solution volume, spinning time, and temperature. These parameters were held constant for this study although at smaller patterning widths they may have a strong influence on the limit of resolution.

At the cellular level, the mechanism of the selective adhesion on collagen may be receptor-specific. For receptor-mediated attachment to occur, most investigators define a multi-step process including initiation of cell contact, propagation of adhesion through

receptor migration, and cell spreading (Hammer et al, 1989, Rubin et al., 1981, van Kooten et al., 1992). In this study, positively and negatively charged molecules at neutral pH (PL and BSA, respectively) were utilized to determine the effect of non-specific charge interactions. PL on the AS was the only experimental condition other than the water control which showed significant levels of attachment although the percentage attachment was much lower than that seen on the collagen-treated AS. This effect may have been due to either: (1) lack of adsorption of PL to the surface resulting in behavior of the surface like the water-treated AS or (2) PL adsorption mediating low, but significant, levels of attachment. We did not directly assay for the presence of PL on the surface, therefore it is impossible to specify one of the two phenomena. The specific mechanism, by which low, but significant, levels of attachment occurs is beyond the scope of this study. In contrast, BSA is known to have adhered to the surfaces as is evidenced by its effect in deturring attachment. For optimal attachment efficiency, a receptor-specific adhesion molecule was utilized; namely, native collagen I. Other adhesive molecules found in the extracellular matrix such as laminin and fibronectin may have also been used with success. In fact, laminin is reported to bind to the same integrin receptors as collagen of form $\alpha_1\beta_1$, $\alpha_2\beta_1$, and $\alpha_3\beta_1$ (Hynes, 1992, Gullberg et al., 1989). In this study, experiments were limited to the utilization of only one of the many known adhesive molecules. In addition, this study was limited to the use of serum-supplemented media. Proteins such as fibronectin and vitronectin which are present in serum are known to mediate cell adhesion. Other demonstrations of selective adhesion (Matsuda et al., 1992, Stenger et al., 1992) have used serum-supplemented media as well; nevertheless, this parameter needs to be investigated further for its effects on selective adhesion in our system.

Similar selective adhesion to that obtained in this study has been obtained by Matsuda et al. (1992) for neurocircuit applications by mediating endothelial cell attachment to a collagen-coated substrate. However, the process requires an incubation

period to obtain adsorption of collagen to nonionic hydrophobic sites as opposed to the process we have developed which requires less processing time and facilitates collagen adsorption to hydrophilic sites. Matsuda et al. (1992) did not quantitatively investigated morphology or sustained cell function in the patterned configuration. Furthermore, endothelial cells, which divide in culture, are utilized for the selective adhesion process and hepatocytes, which do not divide in culture, may respond to the substrates differently.

Some studies have reported selective cell adhesion of other cell types without the use of collagen coatings (Britland et al., 1992, Harris, 1973, and Stenger et al., 1992). However, hepatocytes, as anchorage-dependent cells, must attach and spread to function. Therefore, projected surface area, as a measure of cell spreading, was investigated after a washing step and 24 hours of culture on the various coated substrata. It is interesting to note that unwashed cells seeded on NAS displayed multicellular spheroid formation typical of that found in nonadherent environments (data not shown) (Koide et al, 1990). In general, cells seeded on collagen coated AS spread significantly more than cells on other surfaces and displayed the characteristic polygonal morphology. Studies on PSA in sandwich cultures and on dried collagen coatings (1 ng/cm^2) have shown a PSA of approximately 1500 μm^2 corresponds with phenotypic protein production in hepatocytes (Mooney et al., 1992, Rotem et al., 1992). Thus, hepatocytes on the collagen-coated AS which spread to approximately 1250 μm^2 are more likely to display sustained differentiated function than hepatocytes seeded on AS and NAS with any of the other coatings. For example, cells seeded on PL-coated AS remained rounded in this study suggesting a less compatible surface for preserving differentiated function. In contrast, Ben-Ze'ev et al. (1988) found that cells seeded on PL coated tissue culture plastic spread as much as those seeded on a collagen I coating. Since the coating concentration and data were not reported in their study, it is unclear whether the underlying tissue culture plastic may have mediated this effect.

Other investigators have examined hepatocyte interaction with a collagen coating of various concentrations in terms of spreading and function. Our PSA values can be compared to other studies based on an estimation of coating concentration. Spin-coating of a 0.1 mg/ml collagen I solution of approximate viscosity 0.008 centipoise at 500 rpm for 25 s should yield a film of less than 3.5 μm thickness [2] (Elliott, 1989). Given that the AS is approximately 46% of a 5.08 cm diameter disk, this corresponds to a coating concentration of less than 35 ng /cm^2. Furthermore, Rubin et al. (1981) correlated added collagen α_1(I) chains to bound chains in this regime and found approximately 40% of the protein bound to a tissue culture dish. This corresponds to a bound protein concentration on the order of less than 14 ng /cm^2. Mooney et al. (1992) reported a PSA of approximately 1500 μm^2 for a coating concentration of 1 ng/cm^2 which correlates well with the PSA measured in this study at approximately 1250 μm^2. This comparison is the result of a number of approximations because direct measurements of adsorbed collagen concentration were not performed. Immunochemical fluorescent staining was unsuccessfully attempted as a method of quantifying this parameter. Ultimately, radiolabelled protein should be employed in the quantification of the surface collagen concentration.

The literature has conflicting reports on the effect of varying surface coating concentration on spreading on collagen IV: Bissell et al. (1986) report a saturation effect of spreading at approximately 50 ng/cm^2 bound collagen IV whereas Mooney et al. (1992) report an increase in PSA of 2.7 fold between 1 and 50 ng/cm^2 of coated collagen IV and a 1.8 fold increase between 50 and 1000 ng/cm^2 of coated collagen IV. In this study, PSA was not found to vary significantly over almost 3 decades of coating concentration. If it is assumed that there is a saturation of spreading as a function of coating concentration, our data suggests either the curve saturates at much lower

[2] Assuming a kinematic viscosity close to water at room temperature of 8 centistokes, a spin-coat speed of 500 rpm and extrapolation from Figure 6.6 in Integrated Circuit Fabrication Technology (Elliott, 1989).

concentrations for collagen I than it does for collagen IV, or the curve saturates at high concentrations but our variations span a relatively flat domain.

In addition to variations in PSA seen on different dried collagen coatings, hepatocytes respond differently to the rigidity of the substrate in terms of gene expression and cell differentiation (Ben-Ze'ev et al., 1988, and Keese and Giaver, 1991). Reports of sustained differentiated function are predominantly correlated with gel cultures: sandwich gel configuration (Dunn et al., 1991), a high hepatocyte density on a single layer of collagen gel (Ben-Ze'ev et al., 1988), and the tumor derived Engelbreth-Holm-Swarm gel (Bissell et al., 1987). In this study, dried collagen was utilized rather than a gel for practical reasons associated with building the ultimate device. In the eventual assembly of a microchannel device, the influence of a rigid sandwich will be important. Dunn et al. (1991) suggest that a rigid underlying substratum with a gel overlay preserves hepatocyte differentiation as well as the sandwich culture containing collagen gel on both surfaces. Furthermore, data presented in this study showed stable albumin synthesis for an underlying dry collagen I coating with a gel overlay (Figure 2.19). It is still unclear whether a rigid sandwich will perform as well as the half-gel sandwich systems, nevertheless this investigation is beyond the scope of this work and was reserved for investigation in future studies.

Substrate rigidity and varying concentrations of extracellular matrix molecules clearly play a role in cell differentiation and function. In addition, the importance of extracellular matrix components is well-documented in the literature (Hughes and Stamatglou, 1987, Sawada et al., 1986). Evidence exists that suggests that hepatocyte differentiation as in the sandwich configuration is a byproduct of the physical construct of the sandwich system as opposed to its chemical composition which appears to regulate cell differentiation in the case of EHS single gel cultures. For example, albumin secretion by hepatocytes has been determined to be dependent on proline (Lee et al., 1992). Proline, an amino acid, is an important component of collagen and its depletion may

inhibit the secretion of extracellular matrix proteins by hepatocytes. Therefore, the maintenance of albumin secretion by hepatocytes in a sandwich configuration may be linked to the necessity of a continual refabrication of the extracellular matrix by the hepatocytes but not the composition of the physical structure itself. Thus, the preservation of albumin secretion in sandwich cultures may be due to a physical orientation of the hepatocytes rather than being a result of the chemical composition of the gel matrix. Additional evidence that the polarity and subsequent differentiation of the cells may be a result of a physical construct is our examination of the composition of the gel matrix. The concentration of a single component of the sandwich, collagen I gel, was varied from 0.5 to 3 mg/ml and no significant variations in albumin synthesis were noted. This suggests that the physical configuration of a sandwich may influence phenotypic hepatocyte behavior by a mechanism independent of molecular composition. It therefore seems possible that a rigid sandwich culture could preserve hepatocyte differentiation as well as a malleable gel sandwich. On the other hand, collagen gel sandwiches of lower concentrations could not be investigated due to the instability of the collagen I gel at less than 0.4 mg/ml; therefore, lower concentrations of collagen in a gel structure may have had some effect on albumin secretion.

In summary, the data presented show that a process for reproducible selective adhesion of hepatocytes has been developed. The extent of spreading and albumin secretion of hepatocytes on the adhesive surface correlate well with other studies on primary differentiated hepatocytes. In addition, there is some indication that in a rigid sandwich configuration, as would exist in a micropatterned device, hepatocytes will maintain their phenotypic expression. This process can now be applied to the further development of a micropatterned device which allow for long-term maintenance of differentiated functions, shear stress and viscous pressure drop near physiological levels, and efficient mass transport.

CHAPTER III

MODEL OF OXYGEN DISTRIBUTION AND VISCOUS PRESSURE DROP IN MICROCHANNELS

3.1. Introduction

The liver consumes 20-33% of the body's oxygen at basal conditions (Campra and Reynolds, 1988). Hepatocytes, comprising 75 % of the liver (by volume), are known to have a high metabolic rate; therefore, oxygen limitations in any bioreactor configuration utilizing these cells is of primary importance to the development of liver support devices (Yarmush et al., 1992B). In microchannels, proposed in our micropatterned device (see Figure 1.3), cells are continually taking up oxygen on both sides of every channel while the oxygen supply is limited by the flow rate of the incoming fluid. The achievable length of the channel for a given oxygen uptake rate by hepatocytes is therefore related to the flow rate. Increasing the flow rate will increase the achievable channel length; however, excessive shear stresses at the cell surface and viscous pressure drop along the channel will occur at high flow rates. Therefore, the optimization of the channel length and the flow rate must consider limitations due to both oxygen delivery and pressure drop. In this study, *in vivo* design constraints for the oxygen distribution and pressure drop are used to approximate characteristic dimensions for the design of the micropatterned device and the appropriate range of operating conditions.

3.2. Model for Oxygen Distribution

Figure 3.1A illustrates a side view of a typical microchannel and Figure 3.1B depicts the same channel from the top. Hepatocytes are assumed to be arranged in confluent arrays on either side of the channel. The channel height is dictated by the cells lining the periphery. Typical dimensions for channel width and height are also shown in Figure 3.1. Channel width is dependent on the pre-determined micropattern dimensions but remains fixed for a given channel .

Assuming that the velocity profile is fully developed, laminar plug flow traveling at the mean fluid velocity with negligible axial diffusion of oxygen, and that hepatocytes are modeled as a confluent array of cells which account for a constant oxygen uptake rate at the cell surface, the oxygen transport in the liquid flowing along the channel can be modeled as a combination of axial convection and radial diffusion. The dimensionless transport equation describing the oxygen distribution is as follows:

$$\frac{\partial \hat{c}}{\partial \hat{x}} = \frac{\partial^2 \hat{c}}{\partial \hat{y}^2} \tag{3.1}$$

where $\hat{c}$ is the dimensionless oxygen concentration, $\hat{x}$ is the dimensionless axial coordinate and $\hat{y}$ is the dimensionless radial coordinate. The boundary conditions are:

$$\frac{\partial \hat{c}}{\partial \hat{y}} = 0 \qquad \text{at} \quad \hat{y} = 0 \tag{3.2}$$

$$\hat{c} = 0 \qquad \text{at} \quad \hat{x} = 0 \tag{3.3}$$

$$\frac{\partial \hat{c}}{\partial \hat{y}} = -\frac{V_m \rho D_h}{D c_i} = R \qquad \text{at} \quad \hat{y} = \frac{L}{D_h} \tag{3.4}$$

where V_m is the maximal oxygen uptake rate, ρ is the cell density, D_h is the hydraulic diameter, D is the diffusivity of oxygen in liquid, and c_i is the inlet oxygen concentration.

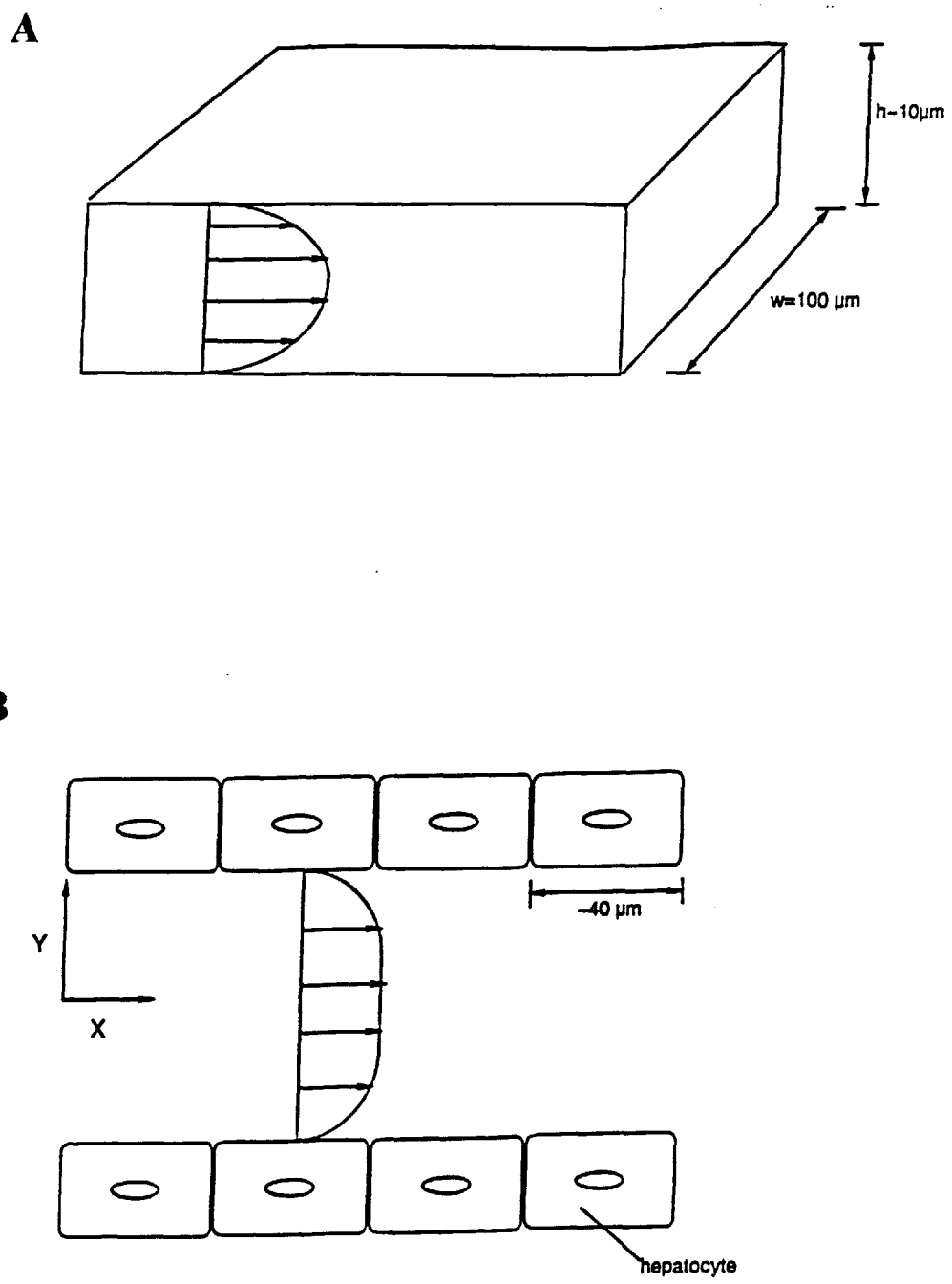

Figure 3.1. Illustration of a typical microchanel. A. Side view. B. Top view.

Equation (3.2) describes a symmetrical gradient about the center of the channel, Equation (3.3) describes an inlet oxygen concentration at the channel entrance, and Equation (3.4) describes a constant oxygen flux, R, at the cell surface. This last expression is a simplification of the Michaelis-Menten model of oxygen uptake rate:

$$V = \frac{V_m \rho P_{O_2}}{K_m + P_{O_2}} \tag{3.5}$$

where V is the local oxygen uptake rate, P_{O_2} is partial pressure of oxygen (proportional to concentration) and K_m is the P_{O_2} corresponding to half-maximal oxygen uptake rate. At partial pressures significantly greater than K_m the expression can be approximated by ρV_m as in Equation (3.4).

The dimensionless variables are defined as follows:

$$\hat{x} = \frac{x}{D_h\, Pe} \qquad\qquad \hat{y} = \frac{y}{D_h} \tag{3.6}$$

where x is non-dimensionalized with respect to hydraulic diameter (D_h) and Peclet number (Pe). The inclusion of the dimensionless Pe number, a measure of the relative magnitude of convective and diffusive effects, allows one to neglect axial diffusion for large Pe numbers. y is non-dimensionalized solely with respect to hydraulic diameter because no radial convective term exists in the axial mass transfer equation . In addition, oxygen concentration and fluid velocity are non-dimensionalized as follows:

$$\hat{c} = \frac{c - c_i}{c_i} \qquad\qquad \hat{u} = \frac{u}{u_m} \tag{3.7}$$

where oxygen concentration is non-dimensionalized such that its inlet value is 0 by subtracting inlet oxygen concentration from c prior to normalizing with respect to inlet concentration. Velocity, u , was normalized with respect to mean velocity. Because the model approximates the velocity profile as a constant at the mean velocity, u_m , $\hat{u}$

becomes 1 and therefore drops out of the transport equation. Finally, Peclet number and hydraulic diameter are defined below:

$$Pe = Re * Sc = \frac{u_m D_h}{D} \qquad D_h = \frac{4A}{P} = \frac{2wh}{w+h} \tag{3.8}$$

A is the cross-sectional channel area, P is the channel perimeter, w is the channel width, h is the channel height, Re ($= \frac{D_h u_m}{\nu}$) is the Reynolds number and Sc ($= \frac{\nu}{D}$) is the Schmidt number where ν is the kinematic vicosity. The analytical solution of Equations (3.1) to (3.4) is (Carslaw et al., 1960):

$$\hat{c} = R\left\{\left(\frac{\hat{x}}{L} + \frac{3\hat{y}^2 - L^2}{6L}\right) - \frac{2L}{\pi^2}\sum_{n=1}^{\infty}\left(\frac{-1^n}{n^2} e^{-\frac{n^2\pi^2\hat{x}}{L^2}} \cos\frac{n\pi\hat{y}}{L}\right)\right\}. \tag{3.9}$$

The partial pressure of oxygen can then be determined from the concentration and the solubility of oxygen in the liquid, k, as follows:

$$P_{O_2} = \frac{c}{k} \tag{3.10}$$

Constants used in the solution of Equation (3.9) are summarized in Table 3.1.

Table 3.1 Constants used in the solution of the transport equations

SYMBOL	DESCRIPTION	VALUE
c_i	initial O_2 concentration	71.4 nmol/ml
D	diffusivity of O_2 in liquid	2×10^{-5} cm^2/s [1]
k	solubility of O_2 in liquid	1.19 nmol/ ml/ mm Hg [2]
Sc	Schmidt number	350
μ	viscosity of media at 37°C	0.007 g/cm/s [3]
V_m	maximal oxygen uptake rate	0.36 nmol/s/ 10^6 cells [4]

[1](Yarmush et al., 1992A)
[2] ibid.
[3] (van Kooten et al., 1992)
[4](Rotem et al., 1992)

3.3. Model of Viscous Pressure Drop

Assuming that rectangular channel flow between two confluent layers of hepatocytes can be approximated by fully developed, laminar parallel-plate flow, as shown in Figure 3.1, the Navier-Stokes equation describes the momentum transport in the channels as follows:

$$0 = -\frac{\partial P}{\partial x} + \mu \frac{\partial^2 u}{\partial z^2} \tag{3.11}$$

where P is the hydrostatic pressure, μ is the viscosity of the fluid, u is the fluid velocity, x is the axial coordinate, and z is the vertical coordinate. The boundary conditions are:

$$u = 0 \qquad \text{at} \qquad z = 0 \tag{3.12}$$

$$\frac{\partial u}{\partial z} = 0 \qquad \text{at} \qquad z = h/2 \tag{3.13}$$

where h is channel height. Equation (3.12) describes the no-slip condition at the channel wall and Equation (3.13) describes a symmetrical velocity gradient about the center of the channel. Integrating Equation (3.11) yields an expression for the velocity profile:

$$u = -\frac{dP}{dx} \cdot \frac{1}{2\mu}(hy - y^2) \tag{3.14}$$

Integrating the velocity profile over the channel height and multiplying by width yields flow rate:

$$Q = -\frac{dP}{dx}\frac{h^3 w}{12\mu} \tag{3.15}$$

Finally, replacing dP/dx with $\Delta P/L_c$ results in the following expression for total pressure drop:

$$\Delta P = \frac{12\,\mu\,Q\,L_c}{w\,h^3} \tag{3.16}$$

The aforementioned solution is valid for a one-dimensional velocity profile in the z-direction, however, due to the shape of the channel a smaller velocity gradient exists in the y-direction as well. This is the gradient responsible for shear forces at the cell surface. The series solution to the two-dimensional velocity profile is (White,1974):

$$u(z,y) = \frac{48Q \sum_{j=1,3,5,\ldots}^{\infty} (-1)^{(j-1)/2} \left[1 - \frac{\cosh(j\pi y/h)}{\cosh(j\pi w/2h)}\right] \frac{\cos(j\pi z/h)}{j^3}}{\pi^5 wh\left[1 - \frac{192h}{\pi^5 w} \sum_{i=1,3,5\ldots}^{\infty} \frac{\tanh(i\pi w/2h)}{i^5}\right]} \tag{3.17}$$

where z is the vertical coordinate and y is the axial coordinate. The shear stress at the cell surface is therefore described by:

$$\tau = \mu \left.\frac{\partial u}{\partial y}\right|_{y=w/2} \tag{3.18}$$

where τ is the shear stress at the cell surface and $\frac{\partial u}{\partial y}$ can be approximated by the slope of the velocity profile at the cell surface.

3.4. Results

The maximum allowable channel length with no oxygen limitations to hepatocytes (i.e., critical length) was calculated using the oxygen distribution model. In the calculations, the inlet partial pressure was defined as 60 mm Hg (de Groot et al., 1988), and the lower limit of acceptable oxygen partial pressure as 5 mm Hg ($10 \times$ Km). The channel length where this partial pressure was achieved was mathematically defined as the critical channel length, L_c. The effect of various flow rates and channel geometries on the critical channel length was then investigated. Figure 3.2A displays the effect of flow rate on oxygen concentration along the center of the channel. As expected, increasing flow rates (proportional to Pe) resulted in proportional increases in critical channel length. In comparison, Figure 3.2B displays the oxygen distribution along the cell surface. Because of the two-dimensional gradient (i.e. oxygen profile in the radial direction), critical length defined at the cell surface is actually smaller than that at the center of the channel, although the flow rate dependence shows a similar trend. Further calculations utilized critical length defined by the partial pressure of oxygen at the cell surface because it is the more relevant parameter.

The influence of channel geometry on critical channel length was also investigated as shown in Figure 3.3. The sensitivity of L_c to height variations is relevant because this dimension will actually be dictated by the cell height. In the microchannel system, typical estimated values for channel height range between 5 and 10 μm. Figure 3.3A shows that a 100% decrease in height resulted only in a 13% decrease in L_c. Furthermore, variations in channel width (Figure 3.3B) produced even smaller changes in critical length.

In order to characterize the limitations imposed on the micropatterned device by the hydrostatic pressure drop, Equation (3.16) was solved using typical *in vivo* values. Hydrostatic pressure has been measured in vivo between 10 and 0 mm Hg (Nakata et al., 1960). By limiting the viscous pressure drop to 10 mm Hg, Equation (3.16) was used to

A

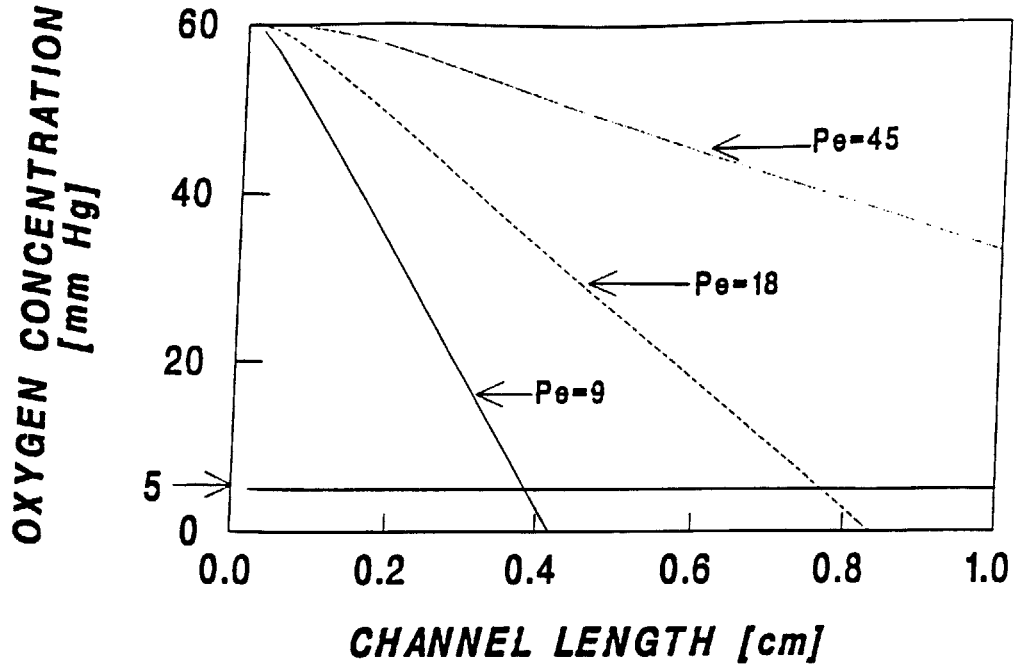

B

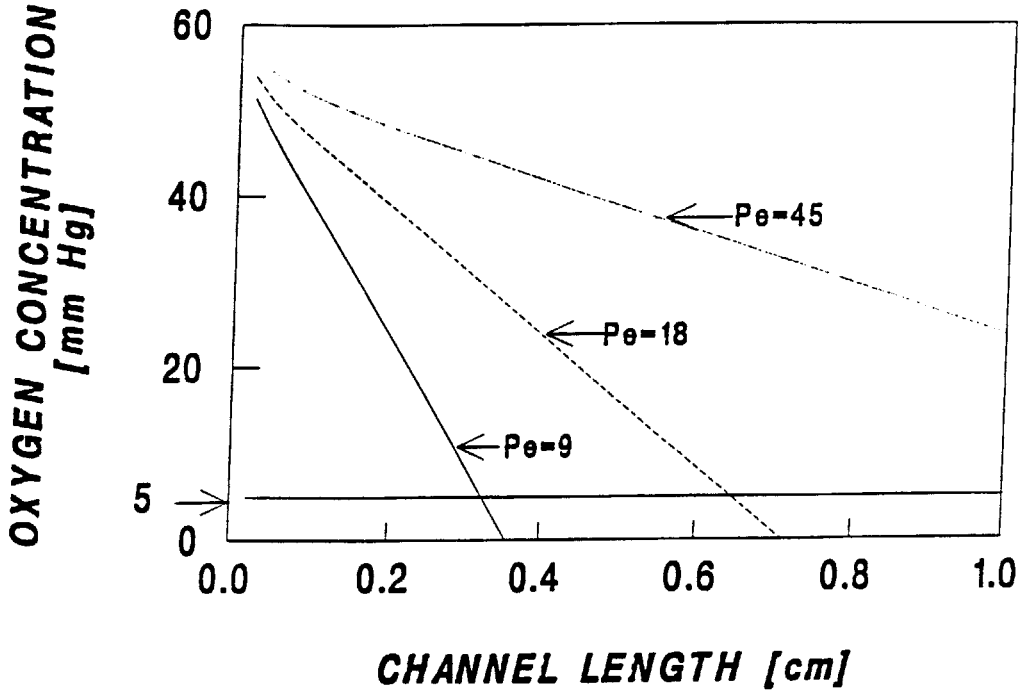

Figure 3.2. Results of oxygen distribution model. Effect of flow rate (proportional to Pe) on oxygen concentration at A. the center of channel and B. at cell surface. Channel dimensions are 100 μm × 10 μm.

A

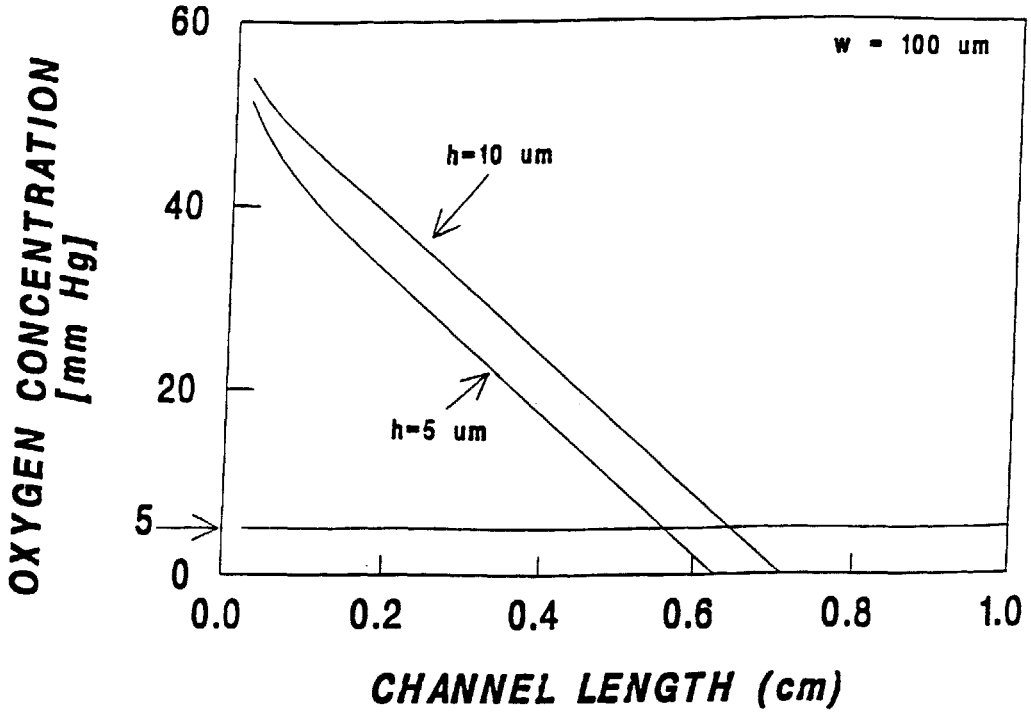

B

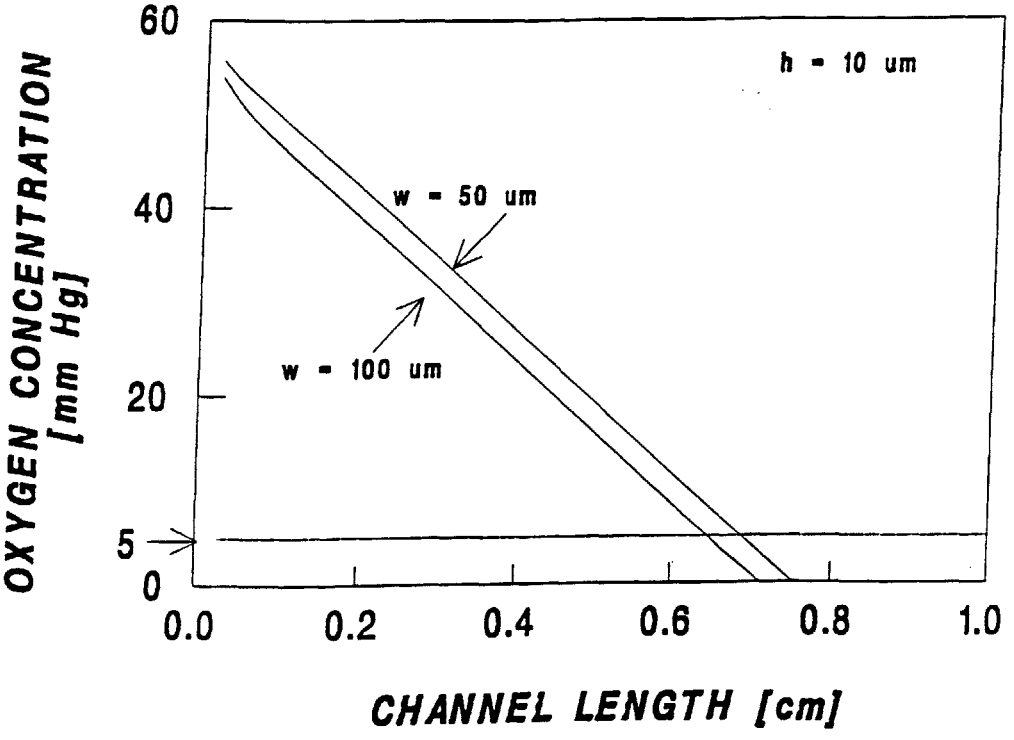

Figure 3.3. Results of oxygen distribution model. Effect of channel geometry on oxygen distribution at cell surface. A. Effect of changes in channel height. B. Effect of changes in channel width.

generate a relationship between the flow rate and the critical length (Figure 3.4). Combining the opposing limitations of hydrostatic pressure drop and oxygen concentration on the critical channel length and flow rate resulted in a limited set of operating constraints (Figure 3.5). The longest achievable channel length taking oxygen and pressure drop limitations into account was approximately 0.7 cm with an accompanying flow rate of approximately 2.2×10^{-6} ml/s in a 100 μm × 10 μm channel.

Furthermore, to assure that the flow rate of 2.2×10^{-6} ml/s will not result in deleterious shear stresses (Horbett et al., 1988, Truskey and Pirone, 1990, Kooten et al., 1992), Equation (3.18) was used to estimate the shear stress in a typical microchannel. Results showed that typical shear stresses for the flow in the range of 5-10 dynes/cm^2.

3.5. Discussion

A critical feature of the liver is its mass transport efficiency. Its geometric configuration enables the exchange of molecules in the perfused blood directly with every parenchymal cell. Our approach to ensuring efficiency of mass transport and prolonged *in vitro* cell differentiation is to build a micropatterned device. An assembly of typical microchannels would form a single plate in a multi-plate extracorporeal liver support device. The viability and differentiated function of the hepatocytes in such a device are essential to its successful operation; therefore, the supply of oxygen and the exposure to fluid stresses must be satisfactorily understood. This study analyzed the mass transfer and fluid dynamics of a typical microchannel and used this knowledge to estimate the approximate channel dimensions.

The mathematical models utilized in obtaining the operating conditions shown in Figure 3.5 required a number of assumptions. Oxygen uptake rate is treated as a constant at the maximal level (V_m) in Equation (3.4) whereas more accurate modeling should

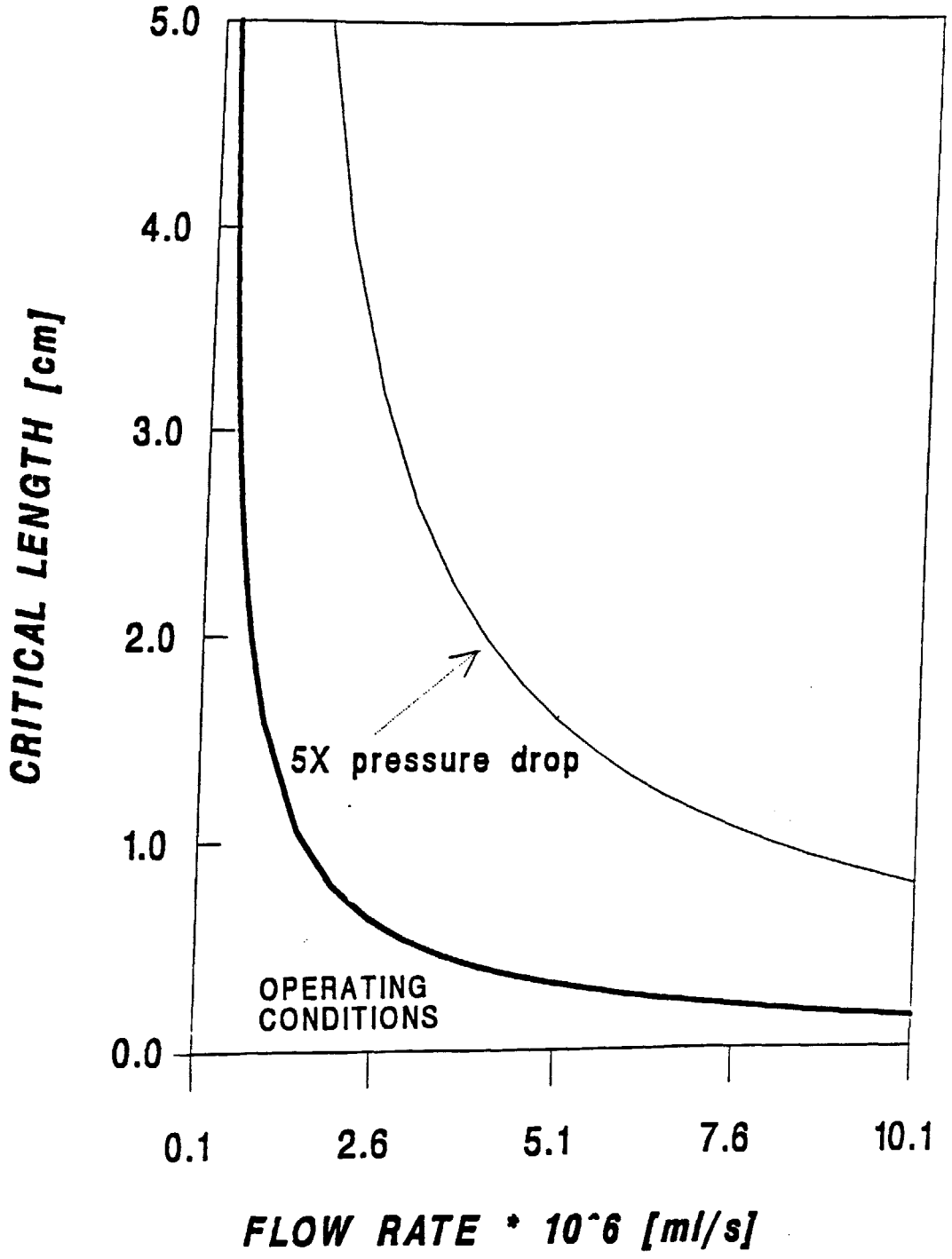

Figure 3.4. Results of viscous pressure drop model. Effect of increasing allowable viscous pressure drop from 10 mm Hg to 50 mm Hg.

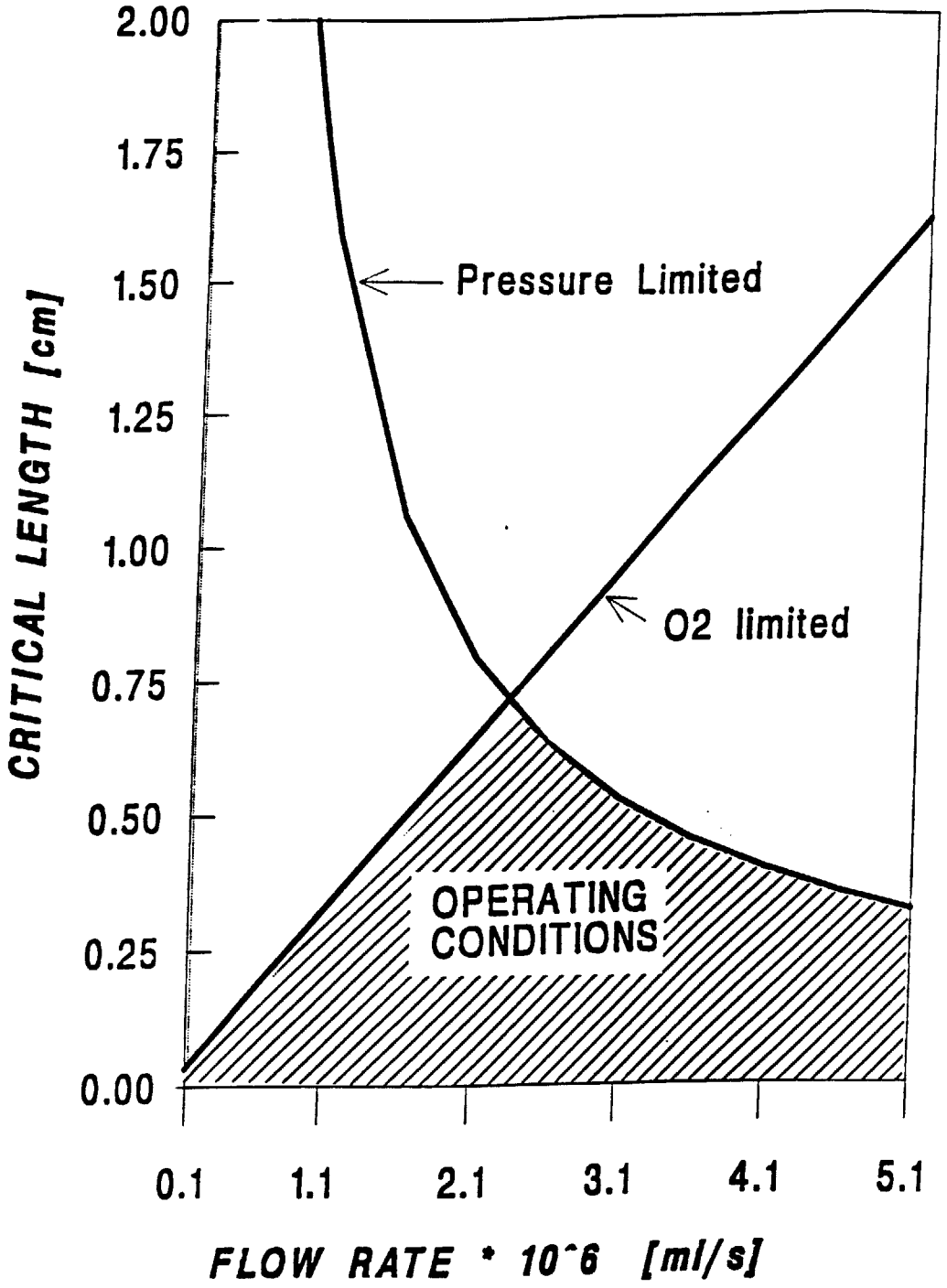

Figure 3.5 Combined operating conditions dictated by oxygen distribution and viscous pressure drop model. Channel dimensions are 100 μm × 10 μm. Viscous pressure drop is 10 mm Hg, inlet oxygen concentration is 60 mm Hg, and critical channel length is 5 mm Hg.

incorporate a Michaelis-Menten type of kinetics as specified in Equation (3.5). The unknown parameters V_m and K_m have been experimentally determined in isolated and cultured cells (de Groot et al., 1988; Rotem et al., 1992). In our microchannel system, where oxygen delivery should be maintained above the K_m of the cells to prevent hypoxia and necrosis, the oxygen limitations on the uptake kinetics can be neglected. Since the K_m of cultured cells is relatively low, 0.5 mm Hg, saturation occurs at very low oxygen partial pressures and it is therefore reasonable to approximate the oxygen uptake rate by a constant for a P_{O_2} greater than $10 \times K_m$, or 5 mm Hg.

Furthermore, the oxygen uptake rate model at the cell surface neglects any intracellular oxygen gradients. Rigorously, there are oxygen concentration variations on several length scales: the larger scale with dimensions on the order of cell diameter, and the smaller intracellular scale of variation associated with mitochondrial uptake (Clark and Clark, 1985). Since mitochondria are the true oxygen sinks, large gradients exist between the cell surface and the mitochondrial membrane. In addition, mitochondria are not randomly dispersed in the cytoplasm as one might expect, rather Jones (1984) reported on intracellular mitochondrial clustering with each cluster behaving like a larger oxygen sink. The variations in intracellular oxygen occur on the order of 2 μm (Jones, 1984); however, we are interested in the macroscopic delivery of oxygen to a population of cells along a channel with dimensions on the order of cm. Therefore, focusing on the larger scale variations of oxygen in the bulk fluid, as in our model, seems reasonable.

Our problem formulation also assumes confluent hepatocytes, implying the existence of a completely flat and smooth channel wall. This will not be the case in the proposed micropatterned device because the channel wall is composed of a series of spread cells with different geometries. There may be regions of reduced flow flow separation regions producing areas of less efficient transport. Since our interests lie in the lower bound on acceptable channel lengths, corresponding to the largest possible oxygen uptake in a microchannel device, overestimating oxygen uptake rate seems justified.

The oxygen distribution model also includes a number of approximations to the velocity profile and mass transport in the perfused fluid. In terms of mass transport, the axial diffusion is neglected. This approximations holds for large Pe where the axial coordinate is non-dimensionalized with Pe and therefore the convective term dominates by a factor of Pe. It should be noted that convective terms are dependent on 1/Pe whereas diffusive terms are related to $1/Pe^2$. The velocity profile is approximated as plug flow (flat velocity profile) with the value of the mean velocity to allow for the use of an analytical solution. Parameter variation can be readily examined with the use of such a simple, closed-loop solution. Finite difference (or other numerical) solutions can be performed for increased accuracy at the expense of lengthier computations. In addition, the velocity profile is assumed to be fully developed laminar flow with a constant fluid viscosity. Reynolds numbers are much less than one, therefore the flow is laminar. Fluid viscosity is assumed to be equivalent to that of tissue culture media at 37° C (van Kooten et al, 1992). Perfusing the microchannel with alternative fluids, will require manipulation of this constant. The fully developed approximation is analogous to neglecting the entrance length. Fay (1992), defines a laminar momentum entrance length as 0.063 x Re x D_h. The Schmidt number, a measure of the relative boundary layer thickness of momentum and mass transfer, is high (350); therefore, the momentum entrance effects dominate over the mass transport effects and the entrance length can be approximated as the momentum entrance length. A range of reasonable Reynolds numbers yield negligible momentum entrance lengths on the order of a few microns (i.e. less than a single cell).

In fully developed channel flow, the pressure gradient is a constant and the pressure drop is approximated by Equation (3.16). A more precise two-dimensional infinite series approximation can be found in White (1974); however, this expression yields minimal increased accuracy. The motivation for estimating the viscous pressure drop is the existence of a hydrostatic pressure drop (i.e. the blood pressure) in vivo. The possible effects of elevated hepatic vein pressures on liver function and structure have

been explored (Brauer et al., 1959) . In our microchannel system, hydrostatic pressure drop should be, at first, limited to physiological levels (10 mm Hg). After building the device, one can experimentally investigate whether this constraint can be relaxed.

Utilizing some reasonable approximations, and the flow rate and channel length obtained in Figure 3.5, a number of calculations can be performed to assess the feasibility of scale-up of a microchannel device. Asonuma et al. (1992), determined that as little as 12% (by weight) of the rat liver is sufficient for liver support of the animal. Therefore, assuming a cell diameter of approximately 40 μm, a channel length of 0.7 cm, and the necessity of 60 million cells per device (approximately 10% of the parenchymal cells in a 200g rat), a value of 350,000 channels per device is obtained. If one assumes each plate of the eventual device to be 20 cm wide, this would translate to 300 plates per device. Furthermore, the dead volume associated with such a device would be 2.5 ml with a device flow rate of 0.77 ml/s and a shear stress of 5-10 dynes/cm^2. These values seem reasonable in terms of practical implementation.

Finally, comparisons between the device flow rate and channel length to the in vivo sinusoidal volume flow rate and sinusoidal length can be made. A channel length of 0.7 cm favorable compares to the *in vivo* length of the rat sinusoid of approximately 0.04 cm while remaining within one order of magnitude (Yamamoto et al., 1985) . Similarly, for *in vivo* sinusoidal diameters of the order of the hydraulic diameter utilized in our calculations, volumetric flow rates have been measured to be approximately 0.1×10^{-6} ml/s as compared to microchannel flow rates of 2.2×10^{-6} ml/s (Koo et al., 1975). Therefore, flow rates are also maintained within one order of magnitude of in vivo values.

A comparison of micropatterning with several alternative bioartificial liver support technologies is shown in Table 3.2. Various approaches are evaluated on the basis of dead volume, diffusion path length, and perfusion path length. Dead volume is the fluid volume associated with a rat liver support device (excluding the volume of inlet and outlet lines) consisting of 60 million cells. Diffusion path length is the typical path length of

diffusion for a molecule being transported between the liquid phase and cell surface and perfusion path length is the typical length of perfusion of the entire device. Hepatocyte monolayer systems have large values associated with all of the aforementioned quantities, whereas hollow fiber devices have only about 10% of that dead volume. A variety of configurations have been utilized in hollow fiber-based support systems: extraluminal cell seeding, extraluminal microcarrier-attached cell seeding, and intraluminal collagen-gel entrapped cell seeding. Despite the relatively small dead volume, all of the hollow fiber approaches have significant limitations. Both extraluminal seeding approaches suffer from possible mass transport limitations due to the large diffusion and perfusion path lengths. In addition, the transport is difficult to control due to the large variations in interfiber distance and the difficulty in precisely controlling cell configuration with respect to the fiber surface. Intraluminal cell seeding suffers from mass transport limitations due to the

Table 3.2 Critical Design Parameters in Various Bioreactor Designs

APPROACH	DEAD VOLUME (ml)	DIFFUSION PATH LENGTH (μm)	PERFUSION PATH LENGTH (cm)
MICROPATTERNING[1]	1.3-2.5	25-50	0.5-0.7
MONOLAYERS[2]	75	500	10
MICROCARRIERS[3]	2.3	40	6
HOLLOW FIBERS[4]	5 - 7	400	10 - 20

[1] Assuming 100 μm x 10 μm x 0.7 cm or 50 μm x 10 μm x 0.5 cm channel and hepatocyte diameter is 40 μm.

[2] Assuming liquid thickness of 1 mm and 100% confluency.

[3] Assuming microcarrier diameter of 200 μm, 100% confluency, perfect bead packing and cartridge diameter of 1cm.

[4] Assuming extraluminal cell seeding, external fiber diameter of 760 μm, 75 fibers per cartridge, internal cartridge diameter of 2 cm, and even distribution of fibers within the cartridge. In practice, the interfiber distance and therefore the diffusion path length may vary greatly.

enormous cell density within the fiber. Given the avid oxygen uptake of hepatocytes, the cells in the center of the cell mass may suffer from hypoxia and necrosis. Evidence for this exists in the literature for both extraluminal (Wolf et al., 1975) and intraluminal (Nyberg et al., 1993) configurations. In contrast, microcarrier approaches have small diffusion path lengths. However, the high cell density requires a large flow rate to supply adequate nutrients to maintain cell viability. In a packed sphere configuration, this flow rate would be associated with large shear stresses due to the small voids between the spheres. Although this may be alleviated by increasing the cartridge diameter (and thereby reducing the fluid velocity for a given flow rate), there is a practical upper limit on the ratio of cartridge diameter to cartridge height because consistent perfusion is difficult to attain at higher aspect ratios. Finally, evaluation of the micropatterning approach yields reasonable values for dead volume (~ 2 ml), and diffusion (~35μm) and perfusion (~0.6 cm) path lengths. This approach utilizes the surface area of every cell for efficient transport with a small fluid volume and reasonable fluid dynamics while mimicking the hepatocyte's in vivo geometrical configuration. Furthermore, the diffusion and perfusion path lengths are independent variables dictated by the channel geometry and can be decreased significantly.

In summary, modeling of the oxygen profile and viscous pressure drop in a typical microchannel has been used to determine approximate channel dimensions and the associated flow rates. The resulting channel length of 0.7 cm at a flow rate of 2.2×10^{-6} ml/s for a 100 μm × 10 μm channel is reasonable in terms of practical implementation.

CHAPTER IV

CONCLUSIONS AND OUTLOOK

4.1 Conclusions

This work was completed in the context of developing a novel technology for a bioartificial liver. An experimental method was developed to obtain selective adhesion of hepatocytes. This method will have applications in micropatterning hepatocytes. In addition, a mathematical model was utilized to estimate a range of operating conditions under which this device may operate. These parameters will be critical in the design and construction of a micropatterned flow chamber.

The experimental portion of this work began by characterizing individual surface coatings in terms of their hepatocyte-surface interaction. Urethane epoxy, a hydrophilic, adhesive coating, mediated approximately 83% attachment[1] after immersion into a bath of 0.1 mg/ml collagen solution. In contrast, a hydrophobic, perflourinated, non-adhesive coating, had less than 4 % attachment. The differential adhesion was used to obtain large-scale patterning of hepatocytes on a glass substrate. The processing technique chosen was a spin-coating method utilizing a 0.1 mg/ ml collagen solution for 25 seconds of spinning at 500 rpm. This technique provided selective adsorption of collagen to the adhesive surface. Furthermore, hepatocytes adhesion correlated with the preferential collagen adsorption to the adhesive surface. Hepatocytes displayed the typical polygonal, multi-nucleated morphology. When overlayed with a top layer of collagen gel to mimic sandwich culture, albumin secretion was comparable to that produced by a stable, differentiated sandwich culture.

The modeling portion of this work focused on the oxygen uptake of hepatocytes, which are known to have a high metabolic rate, and the viscous pressure drop along the

[1]Attachment is defined as (cells adhered to a treated surface/ cells adhered to a collagen gel)

channel. The oxygen distribution as a function of flow rate and distance along a perfused microchannel was approximated. Critical channel length was defined at the point at which the oxygen concentration reached 5 mm Hg at the cell surface. The radial gradient (from the center to the cell surface) was found to be significant in terms of defining a critical length of the channel. In addition, changes in channel geometry by factors of 2 had very little effect on critical length. Since channel height ultimately is a function of the variable parameter, cell height, the latter result is encouraging. Similarly, by limiting the viscous pressure drop to the blood pressure drop across the liver *in vivo*, another range of channel length and corresponding flow rates can be approximated. In this case, critical channel length is defined at the axial distance at which 10 mm Hg viscous pressure drop occurs. The combination of both sets of operating constraints allowed the determination of an optimal channel length of 0.7 cm with a flow rate of 2.2×10^{-6} ml/s for a channel geometry of 100 μm × 10 μm. These values are reasonable in terms of practical implementation and can be utilized in the design of a micropatterned flow chamber.

In conclusion, experimental and mathematical methods have been utilized to further the development of a micropatterned, hepatocyte-based device.

4.2 Future Directions

A number of issues are associated with the design and construction of a micropatterned device. First, quantitation of the amount of adsorbed collagen associated with this technique, and the determination of the stability of the layer, are important for further characterization of the system. More importantly, the spin-coating process will be applied to the creation of micropatterns, or rows of hepatocytes on the order of 50-100 μm wide. Optimization of the dimensions of these patterns with respect to cell function may be performed due to the fact that the degree of cell-cell interaction (more on wider patterns) may be important in this respect. Furthermore, if these cells are to be sandwiched in a device, cell height as a function of time must be investigated. Hepatocytes spread

markedly over the first 24 hours, and if the spreading is to be arrested at a certain height, the time-dependence of this process must be elucidated. In addition, hepatocytes may not need two patterned surfaces to maintain the microchannel geometry. The importance of a patterned top layer is critical information; if an entirely adhesive top surface can be utilized, as opposed to a patterned one, technical issues associated with alignment will be simplified. The creation of the flow chamber itself will be done by screen printing a ~10 μm spacer around the periphery of the micropatterned surface. The loading of this device may involve seeding cells, allowing them to spread for some known time, and then compacting the device to the height of the spacer, expelling excess fluid and unattached cells.

After the construction of a micropatterned device is complete, many basic science questions can be answered. The mathematical model of oxygen distribution can be examined using optical oxygen sensors or vital dyes. The effect of various spatial gradients on hepatocyte heterogeneity, as related to that seen *in vivo* can be investigated. Gradients along the channel could easily be reversed by reversing the direction of flow. This would be useful in examining the induction of heterogeneity in hepatocytes along the channel. In addition, the geometry of the liver lobule could be mimicked more closely by creating a circular pattern with radial channels. This could be useful in investigating the effect of varying shear stresses along a channel. Finally, scale-up of the device could be performed. By seeding approximately 60 million cells, the effect of the device in a rat liver failure model or the effects of a regenerating liver on the micropatterned hepatocytes could be investiagted. Clearly, the creation of such a device has a great potential to answer many basic science questions as well as the potential to be a novel technology for bioartificial liver support.

REFERENCES

Albrecht-Bueller, G.. The Angular Distribution of Directional Changes of Guided 3T3 Cells. Journal of Cell Biology 80:53-60, 1979.

Arnaout, W.S., Moscioni, A.D., Barbour, R.L., and Demetriou, A.A.. Development of a Bioartificial Liver: Bilirubin Conjugation in Gunn Rats. Journal of Surgical Research 48: 379-382, 1990.

Asonuma, K., Gilbert, J.C., Stein, J.E., Takeda, T. and Vacanti, J.P.. Quantitation of Transplanted Hepatic Mass Necessary to Cure the Gunn Rat Model of Hyperbilirubinemia. Journal of Pediatric Surgery 27: 298-301, 1992.

Baier, H., and Bonhoeffer, F.. Axon Guidance by Gradients of a Target-Derived Component. Science 25: 472-475,1992.

Ben-Ze'ev, A., Robinson, G.S., Bucher, N.L.R., and Farmer, S.R.. Cell-cell and Cell-matrix Interactions Differentially Regulate the Expression of Hepatic and Cytoskeletal Genes in Primary Cultures of Rat Hepatocytes. Proceedings of National Academy of Science 85: 2161-2165, 1988.

Berthiaume, F., Toner, M., Tompkins, R., and Yarmush, M.L.. Tissue Engineering in Implantation Biology. Implantation Biology: the Response of the Host. Editor R.S.Greco, (CRC Press), in press, 1993.

Bissell, D.M., Arenson, D.M., Maher, J.J., and Roll, F.J.. Support of Cultured Hepatocytes by a Laminin-rich Gel: Evidence for a Functionally Significant Subendothelial Matrix in Normal Rat Liver. Journal of Clinical Investigation 79: 801-812, 1987.

Borel Rinkes, I.H.M., Toner, M., Sheehan, S.J., Tompkins, R.G., and Yarmush, M.L.. Long-Term Functional Recovery of Hepatocytes after Cryopreservation in a Three-Dimensional Culture Configuration. Cell Transplantation 1:281-293, 1992.

Brauer, R.W., Holloway, R.J., and Leong, G.F.. Changes in Liver Function and Structure due to Experimental Passive Congestion Under Controlled Hepatic Vein Pressures. American Journal of Physiology 197: 681-692, 1959.

Britland, S., Clark, P., Connolly, P., and Moores, G.. Micropatterned Substratum Adhesiveness: A Model for Morphogenetic Cues Controlling Cell Behavior. Experimental Cell Research 198: 124-129, 1992A.

Britland, S., Perez-Arnaud, E., Clark, P., McGinn, B., Connolly, P., and Moores, G.. Micropatterning Proteins and Synthetic Peptides on Solid Supports: A Novel Application for Microelectronics Fabrication Technology. Biotechnology Progress 8: 155-160, 1992B.

Brunner, G.. Differential specificity of substrate-attached lectins stimulating spreading of GH3-cells under serum-free, hormone-supplemented culture conditions. Cell and Tissue Research 224: 553-561, 1982.

Brunette, D.M.. Fibroblasts on Micromachined Substrata Orient Hierarchically to Grooves of Different Dimensions. Experimental Cell Research 164:11-26, 1986.

Bucher, N.L.R., Robinson, G.S., and Farmer, S.R.. Effects of Extracellular Matrix on Hepatocyte Growth and Gene Expression: Implications for Hepatic Regeneration and the Repair of Liver Injury. Seminars in Liver Disease 10: 11-19, 1990.

Cai, Z., Shi, Z., O'Shea, G.M., and Sun, A.M.. Microencapsulated Hepatocytes for Bioartifical Liver Support. Artificial Organs 12: 388-393, 1988.

Campra, J.L. and Reynolds, T.B.. The Liver Biology and Pathobiology. The Hepatic Circulation. Editors M. Arias et al., (Raven Press), pp. 911-930, 1988.

Carslaw, H.S., and Jaeger, J.C.. Conduction of Heat in Solids. (Oxford,2nd edition). pp.112, 1959.

Carter, S.B.. Haptotactic Islands: A method of Confining Single Cells To Study Individual Cell Reactions and Clone Formations. Experimental Cell Research 48: 189-193, 1967.

Carter, S.B.. Principles of Cell Motiility: The Direction of Cell Movement and Cancer Invasion. Nature 208: 1183-1187,1965.

Cima, L.G., Ingber, D.E., Vacanti, J.P., and Langer, R.. Hepatocyte Culture on Biodegradable Polymeric Substrates. Biotechnology and Bioengineering 38: 145-158, 1991.

Clark, A. Jr., and Clark, P.A.A.. Local Oxygen Gradients Near Isolated Mitochondria. Biophysical Journal 48: 931-938, 1985.

Cooper, A., Munden, H.R., and Brown, G.L.. The growth of mouse neuroblastoma cells in controlled orientations on thin films of silicon monoxide. Experimental Cell Research 103: 435-439,1976.

Corey, J.M., Wheeler, B.C., and Brewer, G.J.. Compliance of Hippocampal Neurons to Patterned Substrate Networks. Journal of Neuroscience Research 30: 300-307, 1991.

de Groot, H., Littauer, A., and Noll, T.. Metabolic and Pathological Aspects of Hypoxia in Liver Cells. Oxygen Sensing in Tissues , Editor H. Acker, (Springer-Verlag),1988.

Demetriou, A.A., Chowdury N.M., Michalski, S., Whiting, J., Schechner, R., Feldman, D., Levenson, S.M., anc Chowdury, J.R.. New Method of Hepatocyte Transplantation and Extracorporeal Liver Support. Annals of Surgery: 259-270, 1986A.

Demetriou, A.A., Whiting, J.F., Feldman, D, Levenson, S.M., Chowdury, N.R, Moscioni, A.D., Kram, M., and Chowdury, J.R.. Replacement of Liver Function in Rats by Transplantation of Microcarrier-Attached Hepatocytes. Science 233:1190-1192, 1986B.

DiPersio, C.M., Jackson, D.A., and Zaret, K.S.. The Extracellular Matrix Coordinately Modulates Liver Transcription Factors and Hepatocyte Morphology. Molecular and Cellular Biology 11: 4405-4414, 1991.

Dixit, V., Darvasi, R., Arthur, M., Brezina, M., Lewin, K., and Gitnick, G.. Restoration of Liver Function in Gunn Rats without Immunosuppression Using Transplanted Microencapsulated Hepatocytes. Hepatology 12:1342-1349, 1990.

Dow, J.A.T., Clark, P., Connolly, P., Curtis, A.S.G., and Wilkinson, C.D.W.. Novel Methods For the Guidance and Monitoring of Single Cells and Simple Networks in Culture. Journal of Cell Science Supplement 8: 55-79,1987.

Dunn, G.A.. Contact Guidance of Cultured Tissue Cells: a Survey of Potentially Relevant Properties of the Substratum. Cell Behaviour. Edited by R. Bellairs, A. Curtis, G. Dunn. (Cambridge University Press), pp. 247-280,1982.

Dunn, G.A., and Brown, A.F.. Alignment of Fibroblasts on Grooved Surfaces Described By a Simple Geometric Transformation. Journal of Cell Science. 83: 313-340, 1986.

Dunn, J.C.Y., Tompkins, R.G., and Yarmush, M.L.. Long-term In Vitro Function of Adult Hepatocytes in a Collagen Sandwich Configuration. Biotechnology Progress 7:237-245, 1991.

Elliott, D.J.. Integrated Circuit Fabrication Technology. (McGraw-Hill, 2nd edition). pp. 179-196, 1989.

Elsdale, T., and Bard, J.. Collagen Substrata for Studies on Cell Behavior. Journal of Cell Biology 54: 626-637, 1972.

Fay, James. Introduction to Fluid Mechanics. (M.I.T., in press), pp. 184, 1992

Foy, B.D., Lee, J., Morgan, J., Toner, M., Tompkins, R., and Yarmush M.L.. Optimization of Hepatocyte Attachment to Microcarriers: Importance of Oxygen. Biotechnology and Bioengineering. in press, 1993.

Freedman, D.H.. If He Only Had a Brain (Masuo Aizawa). Discover August : 54-60,1992.

Gail, M.H., and Boone, C.W.. Cell-substratum Adhesivity. Experimental Cell Research 70: 33-40, 1972.

Guguen-Guillouzo, C., Clement, B, Baffet, G., Beaumont, C., Morel-Chany, E., Glaise, D., and Guillouzo, A.. Maintenance and Reversibility of Active Albumin Secretion by Adult Rat Hepatocytes Co-cultured With Another Liver Epithelial Cell Type. Experimental Cell Research 173: 47-54, 1983.

Gullberg, D., Terracio, L., Borg, T.K., and Rubin, K.. Identification of Integrin-like Matrix Receptors with Affinity for Interstitial Collagens. The Journal of Biological Chemistry 264: 12686-12694, 1989.

Gundersen, R.W.. Sensory Neurite Growth Cone Guidance by Substrate Adsorbed Nerve Growth Factor. Journal of Neuroscience Research 13:199-212, 1985.

Gundersen, R.W.. Response of Sensory Neurites and Growth Cones to patterned Substrata of Laminin and Fibronectin in Vitro. Developmental Biology 121: 423-431, 1987.

Guyton, A.C.. Textbook of Medical Physiology. (WB Saunders), pp. 835, 1986.

Hager, J.C., Carman, R., Porter, L.E., Stoller, R., Leduc, E.H., Galletti, P.M., and Calabresi, P.. Neonatal Hepatocyte Culture on Artificial Capillaries: A Model for Drug Metabolism and the Artificial Liver. ASAIO 6: 26-35, 1983.

Hager, J.C.. A Prototype For A Hybrid Artificial Liver. Transactions ASAIO 24:250-253, 1978.

Hammarback, J.A., Palm, S.L., Furcht, L.T., and Letourneau, P.C..Guidance of Neurite Outgrowth by Pathways of Substratum-Adsorbed Laminin. Journal of Neuroscience Research 13: 213-220,1985.

Hammarback, J.A., and Letourneau, P.C.. Neurite Extension across Regions of Low Cell-Substratum Adhesivity: Implications for the Guidepost Hyothesis of Axonal Pathfinding. Developmental Biology 117: 655-662, 1986.

Hammarback, J.A., McCarthy, J.B., Palm, S.L., Furcht, L.T., and Letourneau, P.C.. Growth Cone Guidance by Substrate-Bound Laminin Pathways Is Correlated with Neuron-to-Pathway Adhesivity. Developmental Biology 126: 29-39,1988.

Hammer, D.A. and Lauffenburger, D.A.. A Dynamical Model for Receptor-Mediated Cell Adhesion to Surfaces in Viscous Shear Flow. Cell Biophysics 14: 139-150, 1989.

Harris, A.. Behavior of Cultured Cells on Substrata of Variable Adhesiveness. Experimental Cell Research 77: 285-297,1973.

Horbett, T.A., Waldburger, J.J., Ratner, B.D., Hoffman, A.S.. Cell Adhesion to a Series of Hydrophilic-hydrophobic Copolymers Studied With a Spinning Disc Apparatus. Journal of Biomedical Materials Research 22: 383-404, 1988.

Hughes, R.C. and Stamatoglou, S.C.. Adhesive Interactions and the Metabolic Activity of Hepatocytes. Journal of Cell Science Supplement 8: 273-291, 1987.

Hynes, R.O.. Integrins: Versatility, Modulation, and Signaling in Cell Adhesion. Cell 69: 11-25, 1992.

Ireland, G.W., Doppin-Hepenstal, P., Jordan, P., and O'Neill, C.. Effect of Patterned Surfaces of Adhesive Islands on the Shape, Cytoskeleton, Adhesion and Behaviour of Swiss Mouse 3T3 Fibroblasts. Journal of Cell Science Supplement 8: 19-33, 1987.

Isom, H.C., Secott, T., Georgoff, I., Woodworth, C., and Mumaw, J.. Maintenance of Differentiated Rat Hepatocytes In Primary Culture. Proceedings of National Academy of Sciences USA 82: 3252-3256, 1985.

Jauregui, H.O., Naik, S., Driscoll, J.L., Solomon, B.A., and Galletti, P.M.. Adult Rat Hepatocyte Cultures As the Cellular Component of an Artificial Hybrid Liver. Biomaterials in Artificial Organs. Editors J.P.Paul, J.D.S. Gaylor, J.M.Courtney, and T. Gilchrest, (Macmillan Press), 1984.

Jauregui, H.O., and Gann, K.L.. Mammalian Hepatocytes as a Foundation for Treatment in Human Liver Failure. Journal of Cellular Biochemistry 45:359-365, 1991.

Jones, D.P. Effect of Mitochondrial Clustering on O2 Supply in Hepatocytes. Cell Physiology 16: C83-C89, 1984.

Kasai, S., Oikaw, I., Asakawa, H., Yamamoto, T., Sawa, M., Sakata, H., Kondoh, K., Munakata, T., Mito, M., and Tanzawa, H.. Evaluation of an Artificial Liver Support Device Using Isolated Hepatocytes. Progress in Artificial Organs, Vol. 2. Editors K. Atsumi, M. Maekawa, K. and Ota, (ISAO Press No. 204), Cleveland, 1984.

Keese, C.R.and Giaever, I.. Substrate Mechanics and Cell Spreading. Experimental Cell Research 195: 528-532, 1991.

Klebe, R.J.. Cytoscribing: A Method for Micropositioning Cells and the Construction of Two- and Three- Dimensional Synthetic Tissues. Experimental Cell Research 179: 362-373, 1988.

Kleinfeld, D., Kahler, K.H., and Hockberger, P.E.. Controlled Outgrowth of Dissociated Neurons and Patterned Substrates. The Journal of Neuroscience 8: 4098-4120, 1988.

Koide, N., Sakguchi, K., Koide, Y., Asano, K., Kawaguchi, M., Matsushima, H., Takenami, T., Shinji, T., Mor, M., and Tsuji, T.. Formation of Multicellular Spheroids Composed of Adult Rat Hepatocytes in Dishes with Positively Charged Surfaces and under Other Nonadherent Environments. Experimental Cell Research 186: 227-235, 1990.

Koo, A. Liang, I.Y.S., and Cheng, K.K.. The Terminal Hepatic Microcirculation in the Rat. Quarterly Journal of Experimental Physiology 60: 261-266, 1975.

Kreamer, B.L., Staecker, J.L., Sawada, N., Sattler, G.L., Hsia, M.T.S., and Pitot, H. Use of a Low-speed, Iso-density Percoll Centrifugation Method to Increase Viability of Isolated Rat Hepatocytes Preparations. In Vitro Cellular and Developmental Biology 22: 201-211, 1986.

Lee, J., Morgan, J.R., and Tompkins, R.G.. The Importance of Proline on Long-Term Hepatocyte Function in a Collagen Gel Sandwich Configuration: Regulation of Protein Secretion. Biotechnology and Bioengineering 40: 298-305, 1992.

Letourneau, P.. Cell-to Substratum Adhesion and Guidance of Axonal Elongation. Developmental Biology 44: 92-101, 1975.

Margulis, M.S., Erukhimov, E.A., Andreiman, L.A., and Viksna, L.M.. Temporary Organ Substitution by Hemoperfusion Through A Suspension of Active Donor Hepatocytes In a Total Complex Of Intensive Therapy In Patients With Acute Hepatic Insufficiency. Resuscitation 18: 85-94, 1989.

Matas, A.J., Surtherland, D.E.R., Steffes, M.W., Mauer, S.M., Lowe, A., Simmons, R.L., and Najarian, J.S.. Hepatocellular Transplantation for Metabolic Deficiencies: Decrease of Plasma Bilirubin in Gunn Rats. Science 192: 892-894, 1976.

Matsuda, T., Sugawara, T., and Inoue, K.. Two-dimensional Cell Manipulation Technology. ASAIO Journal 38: M243-M247, 1992.

Matsuda, T., Inoue, K., and Sugawara, T.. Development of Micropatterning Technology for Cultured Cells. Transactions of ASAIO 36: M559-M562, 1990.

Matsumura, K.N., Guevara, G.R., Huston, H., Hamilton, W.L., Rikimaru, M., Yamasaki, G., and Matsumura, M.S.. Hybrid Bioartificial Liver in Hepatic Failure: Preliminary Clinical Report. Surgery: 99-103, 1992.

Mito, M., Kusano, M., Onishi, T., Saito, T., and Ebata, H.. Hepatocellular transplantation--Morphological Study on Hepatocytes Transplanted into Rat Spleen. Transplantation 28: 499-505, 1979.

Miura, Y., Akimoto, T., Kanazawa, H., and Yagi, K.. Synthesis and Secretion of Protein by Hepatocytes Entrapped within Calcium Alginate. Artificial Organs 10(6): 460-465, 1986.

Mooney, D., Hansen, L., Vacanti, J., Langer, R., Farmer, S., Inger, D.. Switching From Differentiation to Growth in Hepatocytes: Control by Extracellular Matrix. Journal of Cellular Physiology 151: 497-505, 1992.

Nakata, K, Leong, G.F., Brauer, R.W.. Direct Measurement of Blood Pressures in Minute Vessels of the Liver. American Journal of Physiology 6: 1181-1188, 1960.

Neuzil, D.F., Rozga, J., Moscioni, A.D., Ro M., Hakim, R., Arnaout, W.S., and Demetriou A.A.. Use of a Novel Bioartificial Liver In a Patient With Acute Liver Insufficiency. Surgery 113: 340-343, 1993.

Nyberg, S.L., Shatford, R.A., Hu,W., Payne, W.D., and Cerra F.B.. Hepatocyte Culture Systems For Artificial Liver Support: Implications for Critical Care Medicine (Bioartificial Liver Support). Critical Care Medicine 20:1157-1168, 1992.

Nyberg, S.L., Shatford, R.A., Peshwa, M.V., White, J.G., Cerra, F.B., and Hu, W.. Evaluation of a Hepatocyte-Entrapment Hollow Fiber Bioreactor: A Potential Bioartificial Liver. Biotechnology and Bioengineering 41:194-203, 1993.

Olumide, F., Eliashiv, A., Kralios, N., Norton, L., and Eiseman, B.. Hepatic Support With Hepatocyte Suspensions In A Permeable Membrane Dialyzer. Surgery 82: 599-606, 1977.

Rotem, A., Toner, M., Tomkins, R.G., Yarmush, M.L.. Oxygen Uptake Rates in Cultured Hepatocytes. Biotechnology and Bioengineering 40: 1286-1291, 1992.

Rovensky, Y.A., Slavnaja, I.L., and Vasiliev, J.M.. Behavior of Fibroblast-like Cells On Grooved Surfaces. Experimental Cell Research 65: 193-201,1971.

Rozga, J., Williams, F., Ro, M., Neuzil, D., Giorgio, T.D., Backfisch, G., Moscioni, A.D., Hakim, R., and Demetriou, A.A.. Development of a Bioartificial Liver: Properties and Function of a Hollow-fiber Module Inoculated with Liver Cells. Hepatology 17:258-265, 1993.

Rubin, K. and Hook, M.. Substrate Adhesion of Rat Hepatocytes: Mechanism of Attachment to Collagen Substrates. Cell 24: 463-470, 1981.

Sawada. M., Tomomura, A., Sattler, C.A., Sattler, G.L., Kleinman, H.K., and Pitot, H.C.. Extracellular Matrix Components Influence DNA Synthesis of Rat Hepatocytes in Primary Culture. Experimental Cell Research 167: 458-470, 1986.

Sawada, N., Tomomura, A., Sattler, C.A., Sattler, G.L., Kleinman, H.K., and Pitot, H.C.. Effects of Extracellular Matrix Components on the Growth and Differentiation of Cultured Rat Hepatocytes. In Vitro Cellular and Developmental Biology. 23: 267-273, 1987.

Seglen, P.O.. Preparation of Isolated Rat Liver Cells. Methods Biol. 13:29-83, 1976.

Shatford, R.A., Nyberg, S.L., Meier, S.J., White, J.G., Payne,W.D., Hu, W., and Cerra, F.B.. Hepatocyte Function in a Hollow Fiber Bioreactor: A Potential Bioartificial Liver. Journal of Surgical Research 53: 549-557, 1992.

Shatford, R.A., Nyberg, S.L., Payne, W.D., Hu, W., and Cerra, F.B.. A Hepatocye Bioreactor as a Potential Bioartificial Liver: Demonstration of Prolonged Tissue-Specific Functions. Surgical Forum 42: 54-60, 1991.

Shnyra, A., Bocharov, A., Bochkova, N., and Spirov, V.. Large-Scale Production and Cultivation of Hepatocytes on Biosilin Microcarriers. Artificial Organs 14: 421-428, 1990.

Shnyra, A., Bocharov, A., Bochkova, N., and Spirov, V.. Bioartificial Liver Using Hepatocytes on Biosilon Microcarriers: Treatment of Chemically Induced Acute Hepatic Failure in Rats. Artificial Organs 15:189-197, 1991.

Stenger, D.A., Georger, J.H., Dulcey, C.S., Hickman, J.J., Rudolph, A.S., Nielsen, T.B., McCort, S.M., and Calvert J.M.. Coplanar Molecular Assemblies of Amino- and Perfluorinated Alkylsilanes: Characterization and Geometric Definition of Mammalian Cell Adhesion and Growth. Journal of the American Chemical Society 114: 8435-8442, 1992.

Sussman, N.L., Chong, M.G., Koussayer, T., He, D., Shang, T.A., Whisennand, H.H., and Kelly, J.H.. Reversal of Fulminant Hepatic Failure Using an Extracorporeal Liver Assist Device. Hepatology 16:60-65, 1992.

Sussman, N., and Kelly, J.H.. Improved Liver Function Following Treatment with an Extracorporeal Liver Assist Device. Artificial Organs 17: 27-30, 1993.

Takahashi, M., Matsue, H., Matsushita, M. Sato, K., Nishikawa, M., Koike, M., Noto, H., Nakajima, Y., Uchino, J., Komai, T., and Hashimura, E.. Does a Porcine Hepatocyte

Hybrid Artificial Liver Prolong the Survival Time of Anhepatic Rabbits? ASAIO Journal 38: M468-M472, 1992.

Truskey, G.A. and Pirone, J.S.. The Effect of Fluid Shear Stress Upon Cell Adhesion to Fibronectin-treated Surfaces. Journal of Biomedical Materials Research 24: 1333-1353, 1990.

Turner, D.C., Lawton, J., Dollenmeier, P., Ehrismann, R., and Chiquet, M.. Guidance of Myogenic Cell Migration by Oriented Deposits of Fibronectin. Developmental Biology 95: 497-504, 1983.

Uchino, J., Tsuburaya, T., Kumagai, F., Hase, T., Hamada, T., Komai, T., Funatsu, A., Hashimura, E., Nakamura, K., and Kon, T.. A Hybrid Bioartificial Liver Composed of Multiplated Hepatocyte Monolayers. ASAIO Transactions 34: 972-977, 1988.

Vacanti, J.P., Morse, M.A., Saltzman, W.M., Domb, A.J., Perez-Atayde, A., and Langer, R.. Selective Cell Transplantation Using Bioabsorbable Artificial Polymers as Matrices. Journal of Pedriatric Surgery 23: 3-9, 1988.

Vanholder, R., and Ringoir, S.. Bioartificial Pancreas and Liver: A Review. The International Journal of Artificial Organs. 14:398-402, 1991.

van Kooten, T.G., Schakenraad, J.M., Van der Mei, H.C, and Busscher, H.J.. Development and Use of a Parallel-plate Flow Chamber For Studying Cellular Adhesion to Solid Surfaces. Journal of Biomedical Materials Research 26: 725-738, 1992.

Weiss, P.. Experiments on Cell and Axon Orientation In Vitro: the Role of Colloidal Exudates in Tissue Organization. Journal of Experimental Zoology 100: 353-386, 1945.

White, F. Viscous Fluid Flow. (McGraw-Hill). pp. 123, 1974.

Wolf, C.F.W., and Munkelt, B.E.. Bilirubin Conjugation by an Artificial Liver Composed of Cultured Cells and Synthetic Capillaries. Transactions ASAIO 21:16-27, 1975.

Yamamoto, K., Sherman, I., Phillips, M.J., and Fisher, M.M.. Three-Dimensional Observations of the Hepatic Arterial Terminations in Rat, Hamster and Human Liver by Scanning Electron Microscopy of Microvascular Casts. Hepatology 5: 452-456, 1985.

Yanagi, K., Ookawa, K., Mizuno, S., and Ohshima, N.. Performance of a New Hybrid Artificial Liver Support System Using Hepatocytes Entrapped Within a Hydrogel. ASAIO Transactions 35: 570-572, 1989.

Yarmush , M. L., Toner, M., Dunn, J.C.Y., Rotem, A., Hubel, A., and Tompkins, R.G.. Hepatic Tissue Engineering: Development of Critical Technologies. Annals of the New York Academy of Sciences 665: 238-252, 1992A.

Yarmush, M.L., Dunn, J.C.Y., and Tompkins, R.G.. Assessment of Artificial Liver Support Technology. Cell Transplantation 1: 323-341, 1992B.